

NAVAL POSTGRADUATE SCHOOL  
Monterey, California

AD-A238 699



DTIC  
ELECTE  
JUL 16 1991  
S B D

**THESIS**

OBSERVATIONS AND MODELING OF  
CURRENTS WITHIN THE MONTEREY BAY  
DURING MAY 1988

by

Kim A. Koehler

June 1990

Thesis Advisor:

Steven R. Ramp

Approved for public release; distribution unlimited.

91-04924



91 7 12 053

Unclassified

security classification of this page

## REPORT DOCUMENTATION PAGE

1a Report Security Classification <b>Unclassified</b>			1b Restrictive Markings		
2a Security Classification Authority			3 Distribution Availability of Report		
2b Declassification/Downgrading Schedule			Approved for public release; distribution is unlimited.		
4 Performing Organization Report Number(s)			5 Monitoring Organization Report Number(s)		
6a Name of Performing Organization <b>Naval Postgraduate School</b>		6b Office Symbol (if applicable) <b>35</b>	7a Name of Monitoring Organization <b>Naval Postgraduate School</b>		
6c Address (city, state, and ZIP code) <b>Monterey, CA 93943-5000</b>			7b Address (city, state, and ZIP code) <b>Monterey, CA 93943-5000</b>		
8a Name of Funding/Sponsoring Organization		8b Office Symbol (if applicable)	9 Procurement Instrument Identification Number		
8c Address (city, state, and ZIP code)			10 Source of Funding Numbers		
			Program Element No	Project No	Task No
			Work Unit Accession No		
11 Title (include security classification) <b>OBSERVATIONS AND MODELING OF CURRENTS WITHIN THE MONTEREY BAY DURING MAY 1988</b>					
12 Personal Author(s) <b>Kim A. Koehler</b>					
13a Type of Report <b>Master's Thesis</b>		13b Time Covered From To		14 Date of Report (year, month, day) <b>June 1990</b>	
15 Page Count <b>121</b>					
16 Supplementary Notation The views expressed in this thesis are those of the author and do not reflect the official policy or position of the Department of Defense or the U.S. Government.					
17 Cosati Codes			18 Subject Terms (continue on reverse if necessary and identify by block number)		
Field	Group	Subgroup	Monterey Bay, Currents, Observations, Modeling, Upwelling.		
19 Abstract (continue on reverse if necessary and identify by block number)					
<p>The last week of April and first week of May 1988 along the central California coast were characterized as a period of strong coastal upwelling produced by moderate to strong northwesterly winds present throughout the period. A product of this upwelling event was the manifestation of a southward geostrophic jet which extended to a distance of approximately 50 km from the coast.</p> <p>During the period from 08 to 11 May 1988, a hydrographic survey consisting of 17 stations each occupied four to five times was conducted within the Monterey Bay. Internal waves, with amplitudes of up to 30 m were present throughout the period and effectively masked the mean signal, implying that averaging is essential to avoid aliasing. The CTD data were averaged to estimate the mean field during this time frame. ADCP data, also acquired during this period, were also averaged. The mean flow field and dynamic topography implied anticyclonic surface flow with cyclonic flow at 200 m depth, both roughly centered over the axis of the Monterey Submarine Canyon near the mouth of the Bay. Flow at depth appeared to be Canyon "trapped." Surface current speeds were on the order of 10 to 15 cm s<sup>-1</sup> with somewhat slower speeds at depth of approximately 10 cm s<sup>-1</sup>. ADCP derived mean flows compared favorably with geostrophic mean flows in all areas except one, the deep outflow region along the northern wall of the Canyon. Calculated standard errors were smaller than the mean signal for both data sets. The smaller standard errors calculated for the ADCP data implied that this method resolved the mean signal better than did the geostrophic calculations.</p> <p>Application of the geostrophic mean field to the open boundary of a two layer, primitive equation numerical ocean model yielded flows similar to those described above. The inclusion of linear bottom friction was shown to be particularly important in limiting deep flow to the confines of the Canyon. Wind stress forcing experiments indicated that a strong wind field may influence surface circulation in the Bay.</p> <p>Mean flow fields compared favorably with results of Klinck's (1989) three-level model of geostrophic adjustment of flow over a "narrow" submarine canyon. Interactions between the coastal upwelling geostrophic jet and the Monterey Submarine Canyon is believed to have been a major mechanism responsible for producing the observed mean flow.</p>					
20 Distribution Availability of Abstract			21 Abstract Security Classification		
<input checked="" type="checkbox"/> unclassified unlimited <input type="checkbox"/> same as report <input type="checkbox"/> DTIC users			Unclassified		
22a Name of Responsible Individual <b>Steven R. Ramp</b>			22b Telephone (include Area code) <b>(408)646-3162</b>		22c Office Symbol <b>68Ra</b>

DD FORM 1473,84 MAR

83 APR edition may be used until exhausted  
All other editions are obsolete

security classification of this page

Unclassified

Approved for public release; distribution is unlimited.

Observations and Modeling of  
Currents within the Monterey Bay  
During May 1988

by

Kim A. Koehler  
Lieutenant Commander, United States Navy  
B.S., Kutztown State College, 1978

Submitted in partial fulfillment of the  
requirements for the degree of

MASTER OF SCIENCE IN METEOROLOGY AND PHYSICAL  
OCEANOGRAPHY

from the

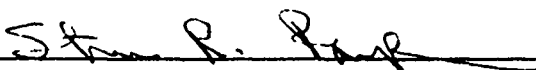
NAVAL POSTGRADUATE SCHOOL  
June 1990

Author:

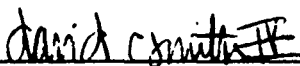


Kim A. Koehler

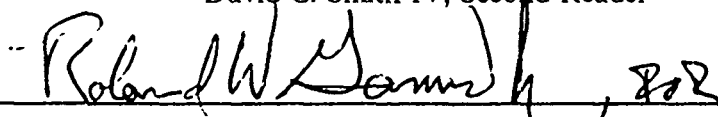
Approved by:



Steven R. Ramp, Thesis Advisor



David C. Smith IV, Second Reader



Curtis A. Collins, Chairman,  
Department of Oceanography

## ABSTRACT

The last week of April and first week of May 1988 along the central California coast were characterized as a period of strong coastal upwelling produced by moderate to strong northwesterly winds present throughout the period. A product of this upwelling event was the manifestation of a southward geostrophic jet which extended to a distance of approximately 50 km from the coast.

During the period from 08 to 11 May 1988, a hydrographic survey consisting of 17 stations each occupied four to five times was conducted within the Monterey Bay. Internal waves, with amplitudes of up to 30 m were present throughout the period and effectively masked the mean signal, implying that averaging is essential to avoid aliasing. The CTD data were averaged to estimate the mean field during this time frame. ADCP data, also acquired during this period, were also averaged. The mean flow field and dynamic topography implied anticyclonic surface flow with cyclonic flow at 200 m depth, both roughly centered over the axis of the Monterey Submarine Canyon near the mouth of the Bay. Flow at depth appeared to be Canyon "trapped." Surface current speeds were on the order of 10 to 15 cm  $s^{-1}$  with somewhat slower speeds at depth of approximately 10 cm  $s^{-1}$ . ADCP derived mean flows compared favorably with geostrophic mean flows in all areas except one, the deep outflow region along the northern wall of the Canyon. Calculated standard errors were smaller than the mean signal for both data sets. The smaller standard errors calculated for the ADCP data implied that this method resolved the mean signal better than did the geostrophic calculations.

Application of the geostrophic mean field to the open boundary of a two layer, primitive equation numerical ocean model yielded flows similar to those described above. The inclusion of linear bottom friction was shown to be particularly important in limiting deep flow to the confines of the Canyon. Wind stress forcing experiments indicated that a strong wind field may influence surface circulation in the Bay.

Mean flow fields compared favorably with results of Klinck's (1989) three-level model of geostrophic adjustment of flow over a "narrow" submarine canyon. Interactions between the coastal upwelling geostrophic jet and the Monterey Submarine Canyon is believed to have been a major mechanism responsible for producing the observed mean flow.



By _____	
Distribution/ _____	
Availability Codes	
Dist	Avail and/or Special
A-1	

## TABLE OF CONTENTS

I. INTRODUCTION .....	1
A. THE MONTEREY BAY AND VICINITY .....	1
1. Dimensions .....	1
2. Currents of the Central California Coast .....	1
a. The California Current .....	2
b. The California Undercurrent and Davidson Current .....	4
B. SYNOPSIS OF PREVIOUS MONTEREY BAY STUDIES .....	8
1. Direct Observations .....	8
a. Early Studies .....	8
b. Surface Current Studies .....	9
c. Flow at Mid-Depths .....	10
d. Deep Flow Studies .....	11
e. Internal Waves .....	13
2. Numerical Studies of Monterey Bay .....	14
a. Tidal Models .....	14
b. Mean Flow Models .....	15
C. PURPOSE OF STUDY .....	25
II. DATA ACQUISITION AND PROCESSING .....	27
A. COLLECTION .....	27
1. May 1988 NPS Student Cruise .....	27
2. Other Supporting Data .....	27
B. PROCESSING .....	29
1. Neil Brown Instrument Systems (NBIS) Mark IIIB CTD Probe .....	29
2. Acoustic Doppler Current Profiler (ADCP) .....	30
III. METHODS AND RESULTS .....	33
A. INTERNAL WAVE FIELD .....	33
1. Methods .....	33
2. Results .....	33

B. MEAN TEMPERATURE, SALINITY, DENSITY, AND GEOSTROPHIC FLOW .....	38
1. Method .....	38
2. Results .....	40
a. Mean Property Cross Sections, Geostrophic Flow, and Mass Transport .....	40
C. MEAN FLOW FROM ADCP DATA .....	50
1. Method .....	50
2. Results .....	52
a. ADCP Velocities Obtained During Successive Passes of Line 1 ...	52
b. Mean ADCP Velocities and Standard Errors .....	54
c. Comparison of Mean ADCP and Geostrophic Velocities .....	54
D. DESCRIPTION OF NOAA AVHRR SATELLITE IMAGERY .....	55
E. METEOROLOGICAL SYNOPSIS .....	56
1. The Period Prior to Data Acquisition (25 April - 08 May 1988) .....	56
2. Synoptic Situation During the Period 08 - 11 May 1988 .....	59
3. The Monterey Bay Aquarium Wind Field .....	59
F. SUMMARY OF MEAN CURRENT FLOW .....	59
G. NUMERICAL OCEAN MODELING OF THE MONTEREY BAY CIRCULATION .....	60
1. Model Description .....	60
a. Dynamics .....	60
b. Boundary Conditions and Domain .....	61
2. Initialization Methods .....	61
a. Methods of Model Forcing .....	61
3. Results of Experiments .....	65
IV. DISCUSSION .....	74
A. COASTAL PROCESSES .....	74
B. INTERNAL WAVES .....	75
C. CIRCULATION .....	76
D. MEAN FLOW MODELING .....	78
V. CONCLUSIONS AND RECOMMENDATIONS .....	81
A. CONCLUSIONS .....	81

B. RECOMMENDATIONS FOR FUTURE STUDIES .....	82
1. Currents .....	82
2. Numerical Studies .....	83
APPENDIX A. MEAN GEOSTROPHIC VELOCITIES .....	84
APPENDIX B. MEAN ACOUSTIC DOPPLER CURRENT PROFILER (ADCP) VELOCITIES .....	90
APPENDIX C. MONTEREY BAY MODEL BOUNDARY CONDITIONS ...	95
APPENDIX D. MEAN BRUNT-VAISALA FREQUENCIES AND ROSSBY RADI .....	100
REFERENCES .....	103
INITIAL DISTRIBUTION LIST .....	108

## LIST OF TABLES

Table 1.	SUMMARY OF NPS NEAR-BOTTOM CANYON CURRENT STUDIES. ....	12
Table 2.	NBIS MARK IIIB CTD MANUFACTURER SPECIFICATIONS ...	30
Table 3.	SUMMARY OF LINE 1 MEAN VELOCITIES .....	55
Table 4.	SUMMARY OF MONTEREY BAY NUMERICAL MODEL SIMULATIONS .....	65
Table 5.	COMPARISON OF MODEL OUTPUT AND LINE 2 GEOSTROPHIC MEAN .....	71



## LIST OF FIGURES

Figure 1. The Monterey Bay .....	2
Figure 2. Bottom topography of the Monterey Bay Submarine Canyon and vicinity	3
Figure 3. Long-term mean sea level atmospheric pressure over the north Pacific ..	5
Figure 4. Long term average wind stress (top) and wind stress curl (bottom) along the California coast .....	7
Figure 5. Surface density analysis and drogue trajectories (21-22 Aug 1972) .....	10
Figure 6. Monthly-mean isotherm topographies (m) .....	11
Figure 7. Current meter station locations occupied by Shepard .....	14
Figure 8. Along-axis current velocity vs. time in the Monterey Canyon .....	15
Figure 9. Time series of temperature distributions near the canyon head .....	16
Figure 10. Conceptual model (top) of temperature distributions (bottom) near the edge of the Monterey Canyon .....	17
Figure 11. Garcia's one layer cavity model .....	18
Figure 12. Bruner's two-layer, baroclinic model output #1 .....	19
Figure 13. Bruner's two-layer, baroclinic model output #2 .....	20
Figure 14. Bruner's two-layer, baroclinic model output #3 .....	21
Figure 15. Geostrophic velocity adjustment over a submarine canyon .....	24
Figure 16. CTD stations occupied during May 1988 NPS student cruise .....	28
Figure 17. CTD sampling interval overlayed on observed surface tidal heights ....	29
Figure 18. Scattergram of initial salinity difference for STMAY88 .....	31
Figure 19. Isotherm variance along Line 1 .....	34
Figure 20. Isotherm depth versus observed surface tidal heights .....	35
Figure 21. Acquired MBA ocean and atmospheric data 21 April - 20 June 1988 ..	37
Figure 22. Effective tides .....	39
Figure 23. Line 1 mean temperature, salinity, and density cross sections .....	41
Figure 24. Line 1 mean geostrophic flow field and standard error .....	42
Figure 25. Line 2 mean temperature, salinity, and density cross sections .....	46
Figure 26. Line 2 mean geostrophic flow field and standard error .....	47
Figure 27. Mean temperature fields .....	48
Figure 28. Mean dynamic height fields .....	49
Figure 29. Line 1 ADCP averaging scheme .....	51

Figure 30. Line 1 mean ADCP velocities and standard error .....	53
Figure 31. NOAA AVHRR satellite imagery from 2336 Z 04 May 1988 .....	57
Figure 32. NOAA AVHRR satellite imagery from 2247 Z 08 May 1988 .....	58
Figure 33. Numerical model bathymetry (top) and spatial domain (bottom) .....	62
Figure 34. Cross sections of model inputs .....	63
Figure 35. Monterey Bay model output from run No. 1 .....	66
Figure 36. Monterey Bay model output from run No. 2 .....	67
Figure 37. Monterey Bay model output from run No. 3 .....	68
Figure 38. Monterey Bay model output from run No. 4 .....	69
Figure 39. Monterey Bay model output from run No. 5 .....	70
Figure 40. Pt. Sur geostrophic velocity cross-section .....	75
Figure 41. Run 2 (left) and run 4 (right) height anomalies. ....	80

## ACKNOWLEDGEMENTS

I would first like to thank my advisor, Prof. Steven Ramp, for providing much insight into the many aspects and problems inherent in collecting, processing, and making sense out of acquired oceanographic data. Next, I would like to thank my second reader, Prof. David Smith IV, for his patience in leading me through the multi-faceted world of numerical ocean modeling. Together, they made me discover the fact that research can, and should be, fun and exciting. I would finally like to thank Mr. Paul Jessen for the numerous hours he spent in processing the data sets used in this study and Ms. Arlene Bird for her computer programming and mainframe manipulation assistance.

## **I. INTRODUCTION**

### **A. THE MONTEREY BAY AND VICINITY**

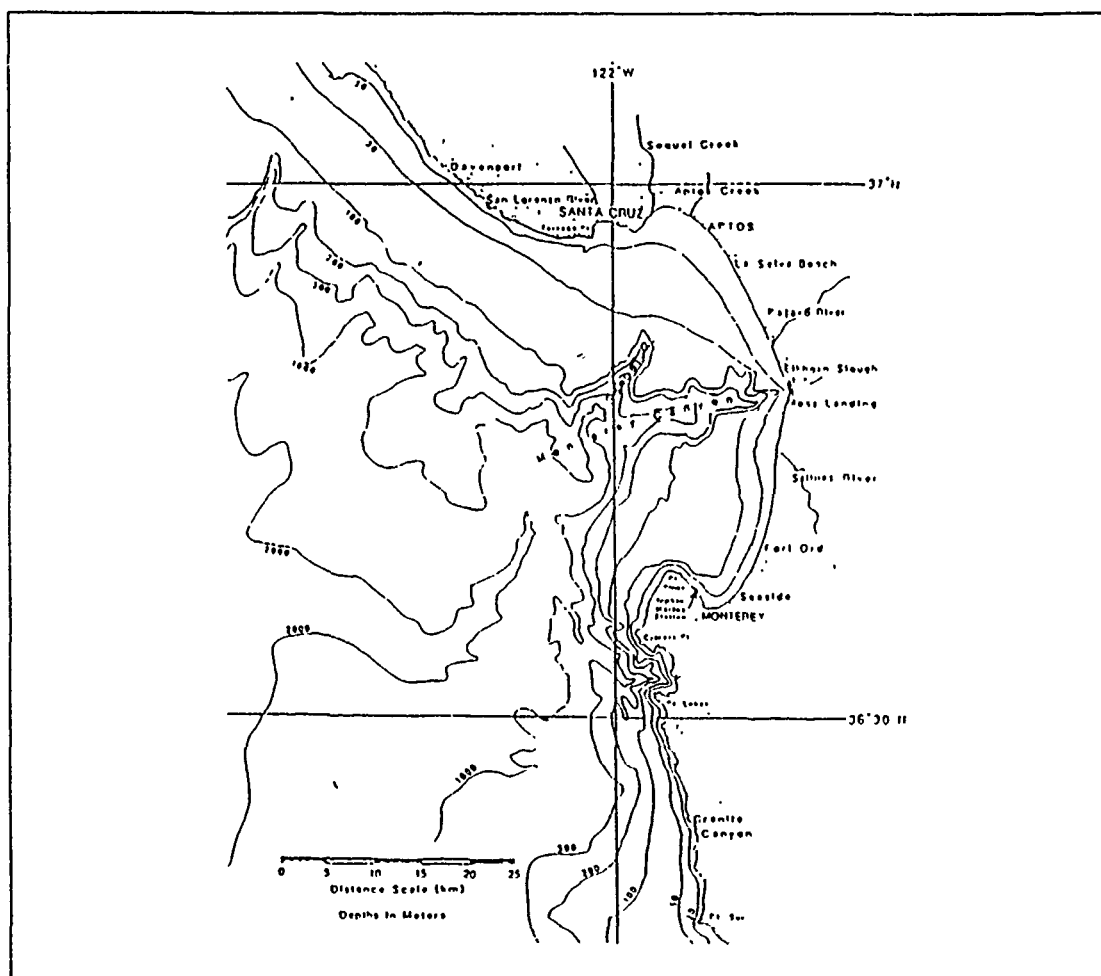
#### **1. Dimensions**

The Monterey Bay, located on the central California coast, is basically oriented north-south with the city of Santa Cruz located on the northern shore, Moss Landing to the east, and the Monterey Peninsula situated on the southern shore. To the west, the bay is open to the sea. A line drawn between Santa Cruz and the Monterey Peninsula measures 37 km, and Moss Landing lies approximately 20 km east of this line. The bay contains two bights (Breaker and Broenkow, 1989), one situated along the northern coast between Santa Cruz and Aptos, the other between the Monterey Peninsula and Fort Ord (Figure 1 on page 2). The area of the bay is approximately 550 km<sup>2</sup> constituting a volume of approximately 420 km<sup>3</sup> (Martin, 1964).

Monterey Bay is essentially a shallow water bay (less than 100 m deep) split into northern and southern shelf regions by the Monterey Submarine Canyon. This canyon is the largest bathymetric feature on the west coast, comparable in shape and relief to the Grand Canyon of the Colorado (Shepard, 1966). The canyon's axis runs roughly east-west within the bay, originating near the surface at the canyon head near Moss Landing where it is 5 km in width, then widens to 15 km, rapidly deepens to 1500 to 2000 m and begins to meander past the mouth of the bay, northwest of the Monterey Peninsula. The two largest tributaries entering the Monterey Canyon are the Soquel and Carmel Canyons, the former intersecting the axis near the center of the bay from the northeast and the latter entering it from the south just seaward of the Monterey Peninsula. Past the entrance to the bay, the axis runs southwest for 20 km, then heads seaward around a large fan feature to the north and continues deepening to over 3000 m. The relief of this feature is truly dramatic (Figure 2 on page 3).

#### **2. Currents of the Central California Coast**

Because circulation within the bay is undoubtedly affected by the flow offshore (Breaker and Broenkow, 1989), a brief description of major current systems in the vicinity of the California coast, and their generation mechanisms, is provided. The three major currents influencing the California coast are the California Current (CC), the California Undercurrent (CUC), and the Davidson Current. These names are usually applied to features existing in the long term or climatological sense (Hickey, 1979).



### a. *The California Current*

The California Current refers to the broad, diffuse, equatorward wind driven flow of the eastern boundary of the North Pacific Subtropical anticyclonic gyre. This current dominates (in the mean) the eastern Pacific flow and extends south from the North Pacific to approximately 25° N, where it turns to the southwest. This relatively fresh (Pacific Subarctic Water) current is usually strongest within a few hundred kilometers of the coast. The western boundary, of interest in this study, has arbitrarily been set at 1000 km from shore. Mean velocities range from 1 to 10 cm s<sup>-1</sup>, typical for most eastern boundary currents. Of more interest to this study are the CUC and the Davidson current, both located in the near shore regions, typically east of the CC (Illickey, 1979).

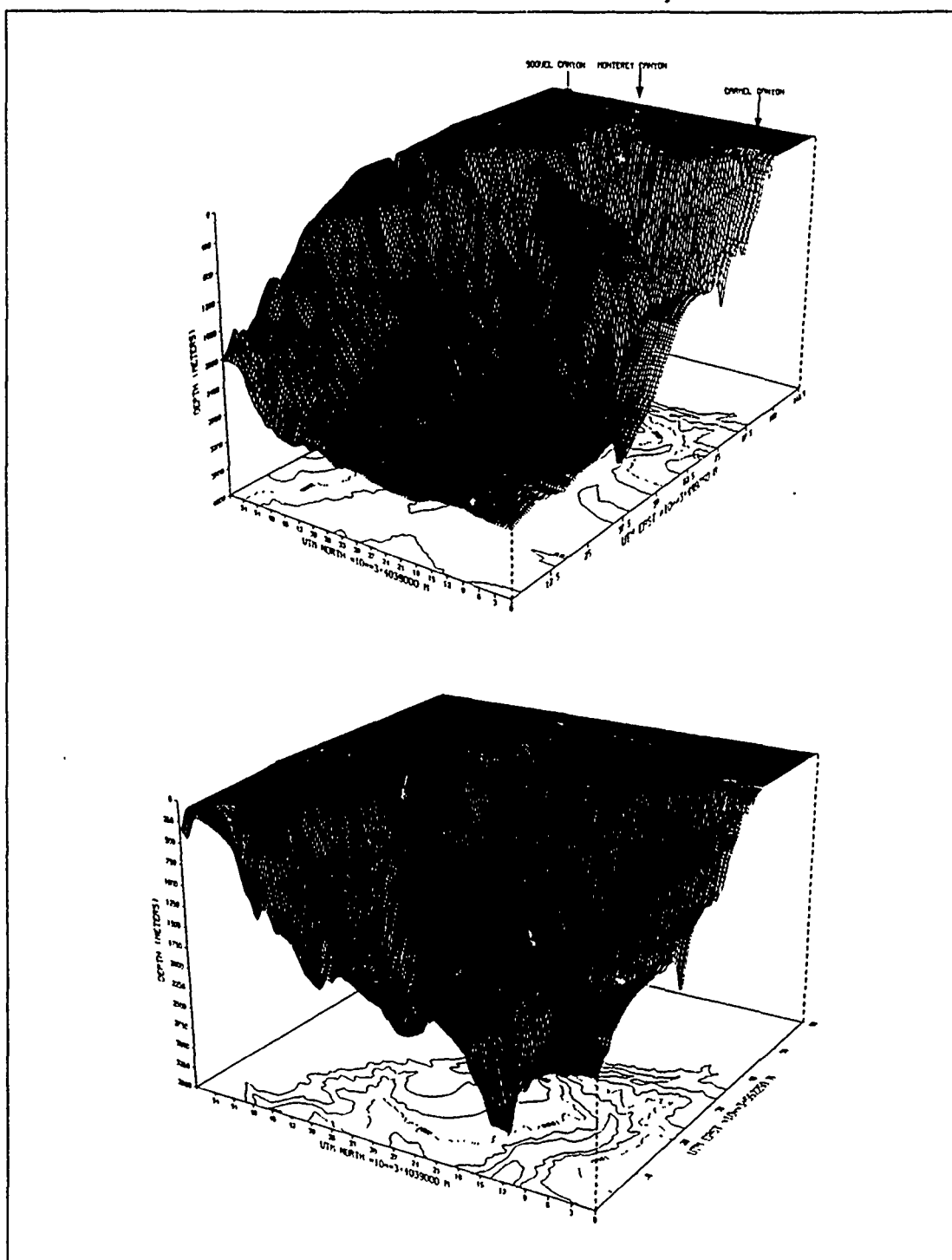


Figure 2. Bottom topography of the Monterey Bay Submarine Canyon and vicinity: Top figure extends seaward to 112 km, bottom to 60 km (figures derived from NOAA/NOS 250 m resolution gridded data).

*b. The California Undercurrent and Davidson Current*

The CUC is the mean poleward flowing current with mean core velocities of  $10 \text{ cm s}^{-1}$  that is typically found along the continental slope at depths ranging from 100 to 300 m. The Davidson Current refers to the northward flowing surface current found along the coast with velocities on the order of  $10 \text{ cm s}^{-1}$  and a width of approximately 80 km (McCreary et al., 1987).

Prevailing winds out of the northwest, generated by a quasi-stationary atmospheric high pressure system (Figure 3 on page 5) over the north central Pacific, are present year round over the California coast. The North Pacific High typically strengthens during the summer months while the thermal low pressure over the California coast, particularly in the central valley, deepens as the land warms. The combined effects of these phenomena results in a tighter atmospheric pressure gradient producing strong northwesterly winds along the California coast during the summer months (Huyer, 1983). Halliwell and Allen (1987) observed that high pressure frequently builds northeast across California after the passage of an atmospheric cyclone and its associated cold front generating periods of strong northwest winds and upwelling events along the coast. They also noted that wind maxima tended to propagate northward along the coast. Chelton (1984) noted that the spatial structure of the wind stress field is highly coherent in the alongshore direction and that the magnitude varies seasonally with the maximum intensity in May (Figure 4 on page 7). Since the strongest components are found approximately 200 km offshore, a positive wind stress curl ( $\text{curl } \tau$ ) is present year round in the nearshore regions (Nelson, 1977). These winds, through the Ekman transport, produce near shore upwelling resulting in dynamic height fields which slope downward towards the coast. The result is a geostrophically balanced surface jet which flows in the direction of the wind (i.e. equatorward) and a poleward undercurrent (the CUC) at approximately 100 to 300 m in depth. Hickey (1979) observed that this surface flow is strongest along the Pacific northwest coast during the spring with maximum flow typically located within the internal Rossby radius of deformation, between 5 and 25 km from the coast, and noted that variations in width, location, and strength can occur quite rapidly (on the order of days) in response to local changes in wind stress ( $\tau$ ). She also observed that during periods of weak northerly or southerly winds, this surface jet either weakens or disappears altogether. Hickey (1979) finally noted that the dynamics of the nearshore southward flow observed off the California coast are likely similar to the flows noted along the Pacific northwest coast.

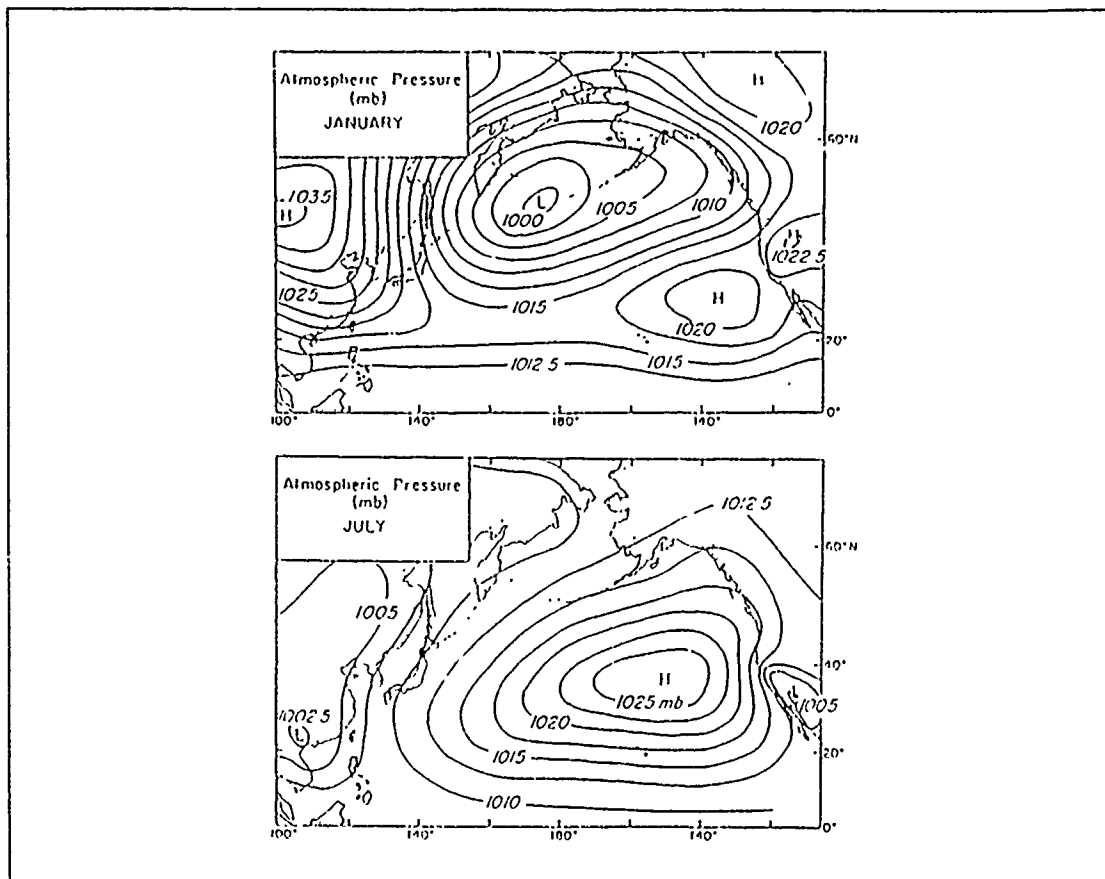


Figure 3. Long-term mean sea level atmospheric pressure over the North Pacific: Top figure is for January, bottom figure is for July (Source: Huyer, 1983).

During the summer, observed currents along the coast are in general agreement with Ekman transport theory but during the winter poleward flow (the Davidson Current) occurs along the coast, against the surface wind stress (McCreary et al., 1987). McCreary et al. (1987) cite four possible mechanisms, along with pros and cons of each, which might explain the appearance of the Davidson current, namely;

- Poleward propagation of coastally trapped waves.
- Relaxation of local winds. Sustained northwesterly winds produce a poleward pressure gradient. When these winds relax, a poleward current will be driven by this pressure gradient. This theory is consistent with the appearance of the Davidson Current during the winter, when mean equatorward surface wind stress decreases.



- Positive wind stress curl. Sverdrup (1947) surmised that the vertically integrated transport in the meridional direction ( $M_y$ ) is proportional to the vertical component of the curl of the wind stress, or:

$$M_y = \frac{\partial \psi}{\partial x} = \int_{-H}^0 v dz \quad (1)$$

$$M_y = \frac{1}{\beta} (\vec{k} \cdot \nabla \times \vec{\tau}) = \frac{1}{\beta} \times \left( \frac{\partial \tau_y}{\partial x} - \frac{\partial \tau_x}{\partial y} \right) \quad (2)$$

where  $\beta = \partial f / \partial y$  is the meridional change in the Coriolis parameter ( $f$ ),  $\psi$  is the stream function ( $\partial \psi / \partial x > 0$  implies northward flow), and  $\tau_x$  and  $\tau_y$  are the x and y components of the wind stress respectively. Thus, positive curl  $\tau$  should drive a poleward current, according to Sverdrup theory. The problem with this mechanism however, is the fact the Davidson Current is usually found during the winter months, a time period when curl  $\tau$  is typically the weakest.

- Thermohaline forcing. The north-south density gradient between subtropical and polar regions creates lower dynamic heights over the poles and relatively higher dynamic heights in the equatorial region. This situation drives a mid-ocean eastward geostrophic current which should turn cyclonically (poleward) when it encounters an eastern boundary such as the California coast. They argue that this mechanism is likely to be responsible for driving the Leeuwin Current off western Australia; however, since wintertime sea-surface topography off the California coast differs significantly from that observed off the west Australian coast, (i.e. dynamic heights bend toward the equator vice the pole off California), this mechanism appears to play a role which is subordinate to wind forcing in this area.

Using both wind stress curl and curl free wind stress as inputs into a coastal model, McCreary, et al. (1987), concluded that positive wind stress curl was the most likely mechanism responsible for driving the Davidson Current during the winter. During the summer months the along shore wind stress ( $\tau_y$ ) is strong enough to negate the effects of Sverdrup transport and therefore dominates the surface flow field. Hickey (1979) states that oceanic responses to sign changes in curl  $\tau$  would be slow, i.e. on the order of two to three months.

Chelton (1984), through the averaging of 23 years of hydrographic data acquired through the CalCOFI program, found the surface flow field to be closely coupled to the wind field. Analysis of the derived dynamic height fields at the surface and at 150 dbar relative to 500 dbar at Monterey (station 67.57) showed surface flow to be southward from February to June and from August to November with poleward flow from November to February and again in June to July. Subsurface flow (CUC) towards the north was present year round except for weak southward flow in April and May. Further south, at Point Conception, no reversal in the CUC was noted, and thus Chelton concluded that subsurface convergence must be taking place somewhere between Pt Con-

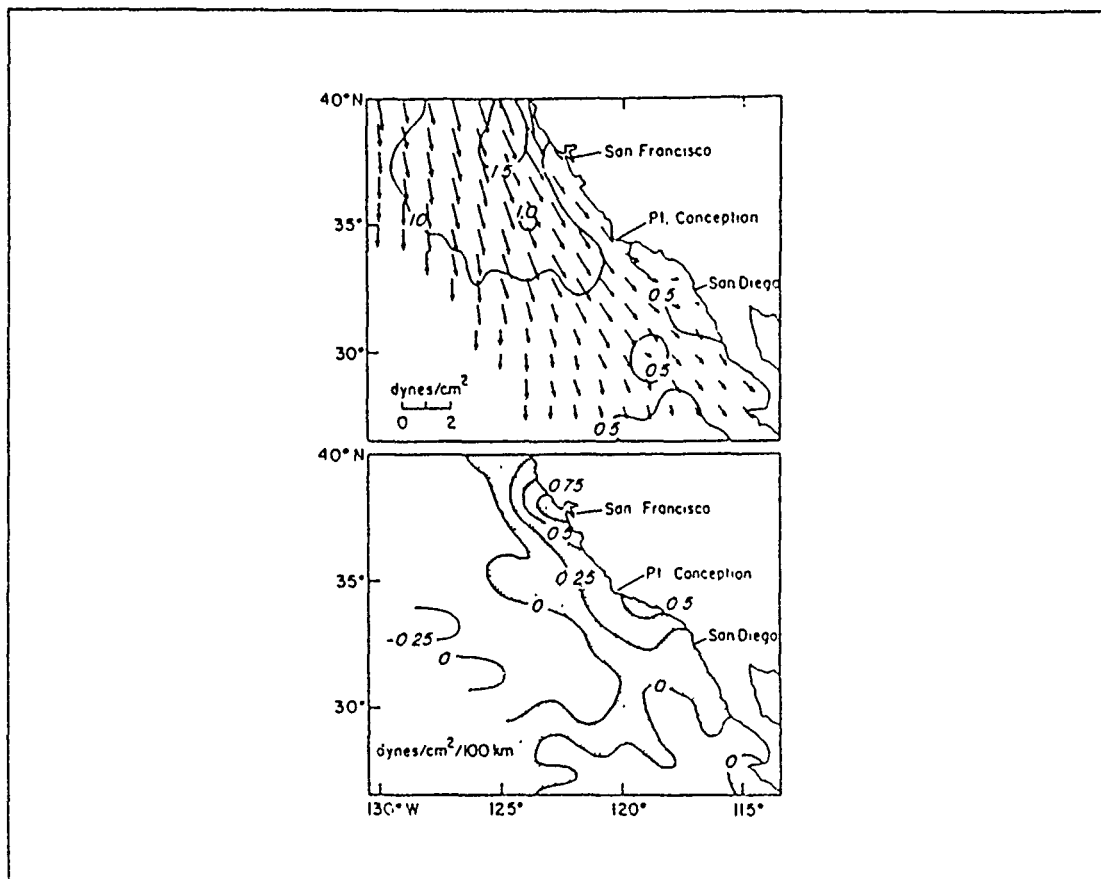


Figure 4. Long term average wind stress (top) and wind stress curl (bottom) along the California coast: Averages were obtained from 100 years of ship observations. The shaded region corresponds to positive wind stress curl (Source: Nelson, 1977).

ception and Pt. Sur, although the CalCOFI grid spacing was too coarse to resolve this convergence. In general, Chelton (1984) concludes that his findings support the general description of an equatorward CC, a poleward flowing CUC, and a coastal surface current whose direction of flow is seasonally dependent.

In summary, since coastal circulation undoubtedly influences, and possibly drives, flow within the Monterey Bay, full knowledge of the near shore processes which take place along the central California coast is crucial prior to attempting to understand flow patterns within the bay itself. For instance, surface flow within the Monterey Bay during winter, when the Davidson Current is present, more than likely differs from flow patterns within the bay during spring upwelling periods when the southward geostrophic jet is present. Also, deep flow within the Monterey Bay Submarine Canyon is probably

influenced to some extent by the CUC, although the effects of this current on circulation within the bay does not appear to be very well understood at present.

## **B. SYNOPSIS OF PREVIOUS MONTEREY BAY STUDIES**

### **1. Direct Observations**

Numerous studies have been conducted to ascertain the characteristics of the circulation within Monterey Bay utilizing a wide variety of methods including current meters, drift bottles, drogues, hydrographic data, thermistors, satellite imagery, aircraft observations, and sediment and nutrient distributions. Breaker and Broenkow (1989) provide an excellent in-depth summary of past research conducted in the bay, including comments relating these works to their own findings. Highlights of some of these major studies are provided.

#### *a. Early Studies*

One of the earliest studies of flow patterns within Monterey Bay was conducted by Bigelow and Leslie (1930) using hydrographic data obtained throughout the bay over the period 30 June to 24 July 1928. They observed higher sea surface temperatures over the shelf areas of the bay and somewhat depressed temperatures over the canyon implying that local heating played a major role during the summer months. Analysis of the cross sectional temperature field also led them to believe that upwelling from within the canyon occurred and subsequently spread out into the shelf regions of the bay. Dynamic height analysis (0 dbar referenced to 500 dbar) revealed the presence of high dynamic heights near the center of the canyon implying anticyclonic flow. They concluded that circulation within Monterey Bay varies greatly and is dramatically influenced by week to week changes in small scale local events (heating, land-sea breeze, winds, canyon upwelling, etc.).

Skogsberg (1936), through analysis of hydrographic data acquired between 1929 and 1933 in the southern portion of Monterey Bay, concluded that three separate cycles occurred annually. The first he described as a "cold water" or upwelling phase which lasted from February through November, a "warm water phase" attributed to light winds and onshore movement of warm oceanic waters from August through November, and finally, a "low thermal gradient phase" which lasted from December to February and coincided with the manifestation of the northward flowing Davidson Current. He emphasized the highly variable nature of flow within the bay stating instances where coastal flow was northward through the bay and other instances where it was southward. Through these thermal studies, Skogsberg finally noted that temperature trends at lower

levels were quite often opposite to those encountered at shallower depths suggesting that flows may, at times, be independent and opposite at separate levels within the bay.

*b. Surface Current Studies*

Utilizing nutrient displacement and mass fields, Lasley (1977) concluded that surface flow within the bay is predominantly to the north, frequently entering the bay around Pt. Pinos and exiting near Pt. Santa Cruz. Utilizing property distributions assimilated over a 27-month time span, Smethie (1973), and Broenkow and Smethie (1978), also inferred surface flow within the bay to be northward the majority of the time, in agreement with Lasley. They expected northward flow during the fall and winter; however, in light of the northwesterly winds present during the spring and summer, prevailing northward surface flow within the Monterey Bay was contrary to their expectations during this time frame. Current meter data acquired by Engineering Science, Inc. (ESI, 1978) in the area southwest of the Salinas River at depths of 9 and 30 m over the period from January 1976 to January 1977, indicated a northward flow 65% of the time and southward flow 35% of the time. Reise (1973), using drift-bottles over a 14 month period in 1963 and 1964 in the southern bight, and Moomy (1973), employing drogues over a two day period in August 1972, both determined surface flow within the bay to be generally cyclonic in nature (Figure 5 on page 10).

Pirie and Stellar (1974) inferred surface flow within the Monterey Bay and vicinity through sediment distribution, obtained from visual satellite imagery and aircraft observations. Their flow patterns suggested large current variability but seasonal trends indicated northward flow along the coast from October through February, with southward flow predominating from March through July. Northward flow appears to correlate well with the classic Davidson Current regime from October through February, with southward flow occurring during the typical coastal upwelling period. Breaker and Broenkow (1989), using AVHRR imagery taken during the upwelling spring transition in March 1980 observed cold, upwelled water extending along the entire central California coast from a strong thermal front at Pt. Pinos. During this event, sea surface temperatures at Granite Canyon (located between the Monterey Peninsula and Pt. Sur, see Figure 1 on page 2) dropped 4°C over a six day period (Breaker and Mooers, 1986). Coincident with this event, current direction was observed to reverse from north to south in the vicinity of Pt. Sur (Wickham et al., 1987). Other satellite imagery reviewed by Breaker and Broenkow (1989) suggest instances of warm water intrusions entering the bay from the open sea. They concluded that during strong upwelling events, cold water was often advected across the entrance of the bay, then south towards Pt. Sur, forming

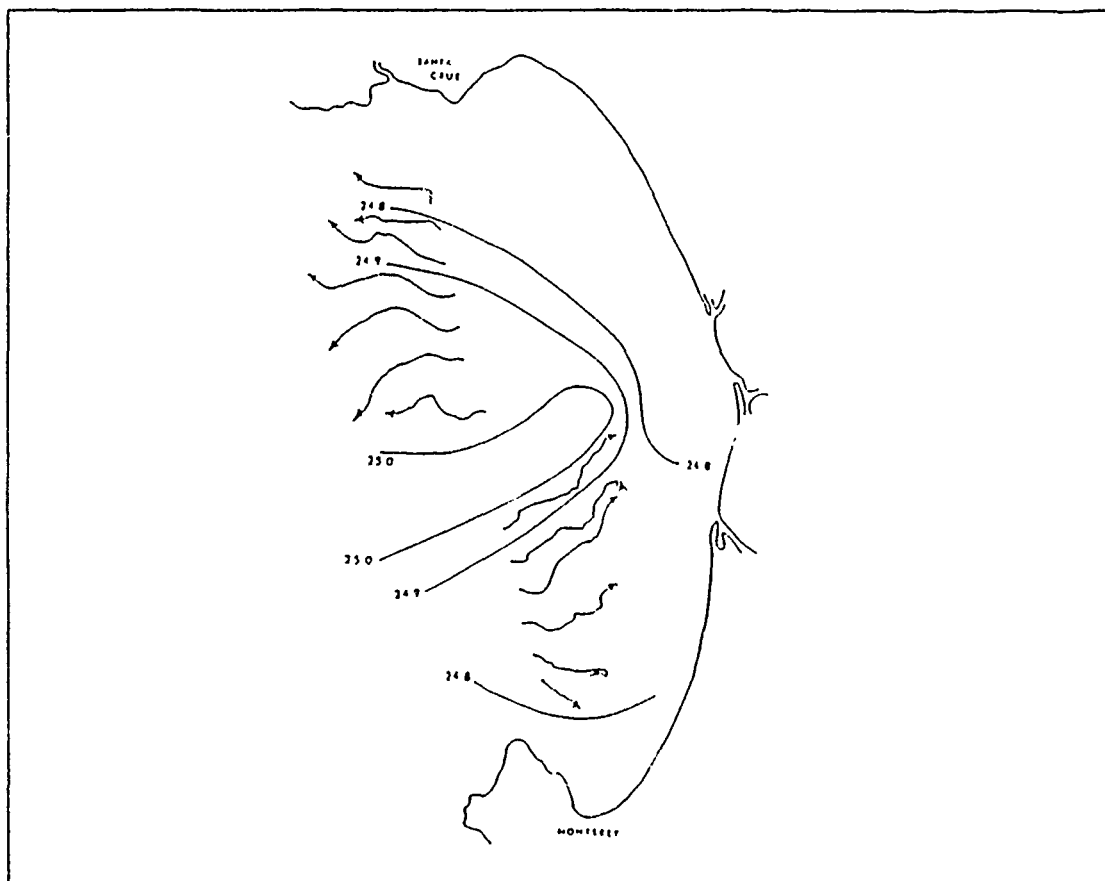


Figure 5. Surface density analysis and drogue trajectories (21-22 Aug 1972): Note inferred cyclonic circulation (Source: Moomy, 1973).

a continuous cold frontal feature. Another common characteristic found in satellite images was that generally warmer waters were found inside the bay providing support to Bigelow and Leslie's (1930) findings that local heating plays a large role in modifying water masses within the bay and coastal upwelling occurs on an infrequent basis within the bay itself (Breaker and Brøenkow, 1989).

#### *c. Flow at Mid-Depths*

Flow at intermediate depths (30 to 120 m) was investigated by Lammers (1971), using data acquired from Skogsberg, 1929-1933; Bolin et al., 1951-1955; and the CalCOFI program, 1954-1967 to construct a gridded temperature field over Monterey Bay. Geostrophic flow patterns were then implied through analysis of monthly-mean isotherm topographies (Figure 6 on page 11). The study concluded that, in the mean, a warm core anticyclonic feature within the thermocline persisted over the center of the

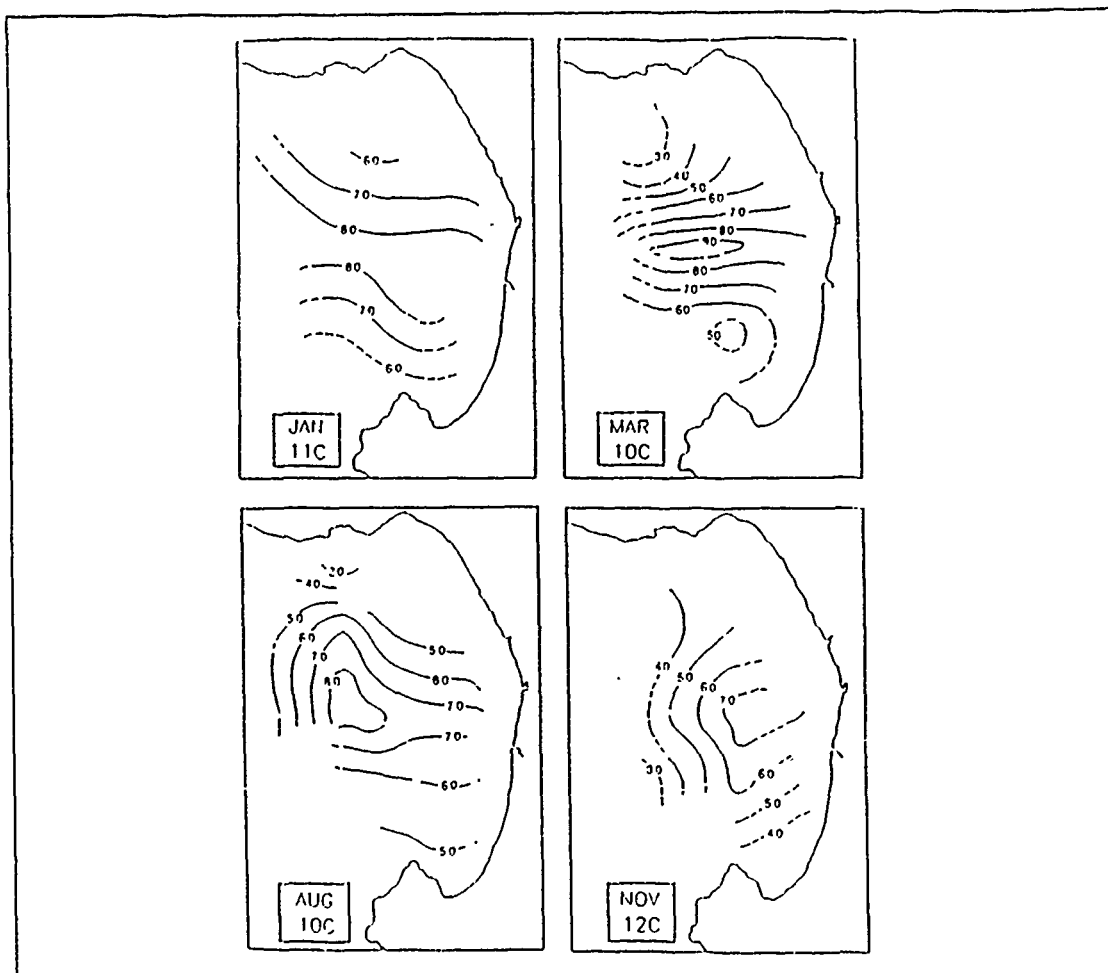


Figure 6. Monthly-mean isotherm topographies (m): Figures were obtained from 30 years of data and show a highly developed thermal high situated over central Monterey Bay (Source: Adapted from Lammers, 1971).

bay and tended to intensify during the winter. This warm core feature is in contrast to Bigelow and Leslie's (1930) findings of slightly depressed temperatures over the canyon during a one week period in summer but is in agreement with Lammers' inferred anticyclonic circulation. One possible mechanism thought to be responsible for this feature is momentum and heat transfer from the northward flowing CUC (Breaker and Broenkow, 1989).

#### *d. Deep Flow Studies*

A series of deep flow studies were undertaken from 1965 to 1975 by students at the Naval Postgraduate School (NPS). These studies were primarily conducted near the canyon head at depths ranging from 91 to 485 m (Table 1 on page 12) and were

**Table 1. SUMMARY OF NPS NEAR-BOTTOM CANYON CURRENT STUDIES.**

Reference	Bottom Depth(s)	Duration	Comments
Gatje and Pizinger, 1965	130 m	77 observations on nine different days	Currents tended to follow the canyon axis. Downcanyon flow was associated with incoming tide and upcanyon flow with outgoing tide.
Dooley, 1968	104-165m	5-162 h	Flows were predominantly in direction of canyon axis. Reversals in flow direction showed a strong semidiurnal component. Sudden increases or bursts in current speed also were noted. Spectral analysis revealed 6 and 4 h peaks in addition to semidiurnal component.
Njus, 1968	150-202 m	168 h	Current direction was generally along the canyon axis. Reversals in current direction occurred primarily at high and low tide. Spectral peaks occurred at 12.5, 6, and 4 h.
Caster, 1969	91-366 m	3-171 h	Cross-canyon flow was frequently observed. Flow at an adjacent shelf location showed weaker tidal oscillations and generally slower speeds.
Hollister, 1975	485 m	262-371 h	Flow at 30 m above bottom was predominantly along canyon axis and apparently tidally driven. Strong cross-canyon flow was observed at 60 m above bottom and was poorly correlated with flow at 30 m.

Source: Adapted from Breaker and Broenkow, 1989.

primarily of short duration ranging from a day (Gatje and Pizinger, 1965) to approximately two weeks (Hollister, 1975). Most current meter depths ranged from 5 to 16 m above the bottom (Hollister's study used meters placed 30 and 60 m above the bottom). Data acquired near the canyon head revealed predominantly along-axis flow with semidiurnal periods. Castor (1969) and Hollister (1975), on the other hand, observed

frequent cross-canyon flow in the deeper, wider areas of the canyon. The spectral analyses done by Dooley (1968) and Njus (1968) indicated super-tidal periods at 6 and 4 h in addition to the expected semidiurnal period. Gatje and Pizinger (1965) correlated downcanyon flow with the surface flood tide and upcanyon flow with the ebbing tide.

Shepard (1979) conducted extensive research on flows in numerous submarine canyons, including the Monterey Canyon. His work in the Monterey Submarine Canyon was at much greater depths (up to 1445 m) than those undertaken by NPS (Figure 7 on page 14). Of the nine records obtained, five showed virtually no directional correlation with the canyon axis, unique among all of the canyons investigated. One suggestion for the cause of this lack of directional control was related to the meandering of the axis along with flows into and out of canyon tributaries. Another interesting aspect noted by Shepard (1979) was that, unlike other California stations, the net flow was upcanyon in 6 out of the 9 records. Shepard stated that current direction and surface tides were not always coherent (Figure 8 on page 15), at times in phase with the tidal cycle, at other times out of phase. By observing discrepancies noted when time-velocity plots of different stations were overlayed (in particular stations 34 (at 357 m) and 35 (at 384 m) and stations 58 (at 1061 m) and 59 (at 1445 m) (see Figure 7 on page 14)), then shifting the profiles in time to match the observed up and down-canyon flows, Shepard concluded that internal wave patterns were propagating upcanyon between stations at shallower depths but downcanyon between stations at greater depths.

*e. Internal Waves*

Almost every study done in Monterey Bay cites evidence indicative of internal waves. Shea and Broenkow (1982) investigated the occurrence of semidiurnal internal waves using hydrographic and thermistor data and resolved internal waves with heights of 50 to 120 m (Figure 9 on page 16). Spectral and cross-spectral analysis of 7 days of surface tidal heights and thermistor data acquired near the canyon head suggested that these waves have a semidiurnal periodicity but lag the tides by about 7 h at the semidiurnal period. They cited the Monterey Submarine Canyon topography as the probable generation mechanism. As the semidiurnal long wave field approaches the shoaler and narrower canyon head, the period remains constant and the amplitudes increase as the wave energy becomes focused, as small amplitude wave theory predicts, and assumes the characteristics of an internal tidal bore. At high internal tides they found evidence that denser water from below the main thermocline within the canyon moved up and onto the shelves and then became pinched off as the internal tides fell (Figure 10 on page 17). Baroclinic tidal currents were also investigated by Broenkow



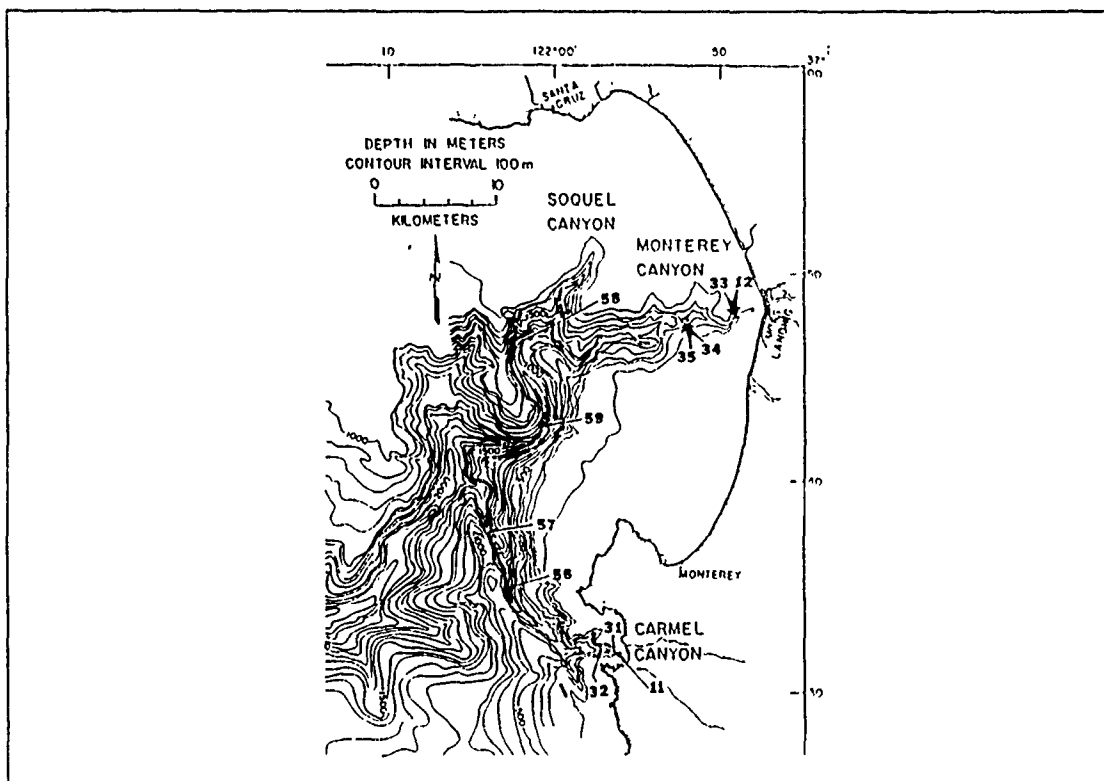


Figure 7. Current meter station locations occupied by Shepard: Results from station 59 are presented in Figure 8 on page 15. Time-velocity plots from stations 34, 35, 58, and 59 were used to imply internal wave propagation (Source: Shepard, 1979).

and McKain (1972) who found that tidal amplitudes generally decreased seaward from the canyon head and noted that the baroclinic and the barotropic tides were generally not in phase.

## 2. Numerical Studies of Monterey Bay

### a. Tidal Models

Schomaker (1933) used an implicit, two-dimensional (1 km grid) program with realistic topography to model homogenous barotropic tidal forcing in the bay. Resulting height fields showed the clear progression of the tides into the bay; however, the inferred currents into and out of the bay associated with these heights were relatively weak. Consequently, other effects, such as wind forcing and offshore currents, were determined to dominate the flow field, rather than barotropic tidal influences.

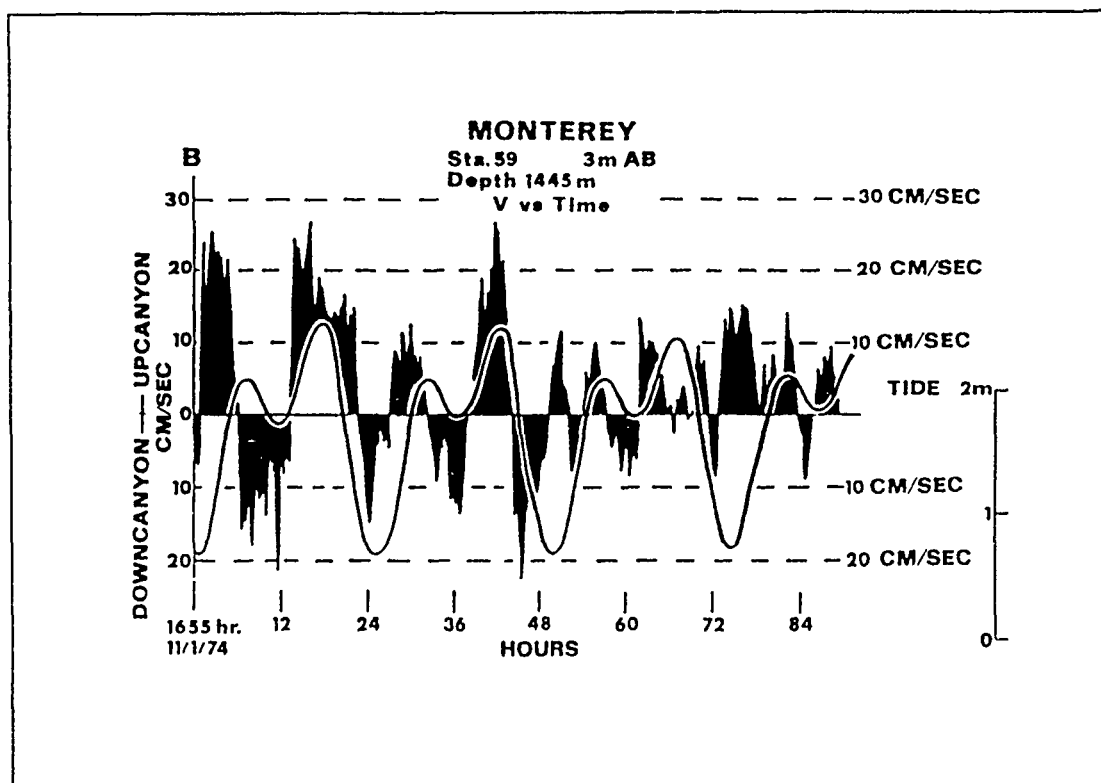


Figure 8. Along-axis current velocity vs. time in the Monterey Canyon: Figures show the incoherence between tidal height (smooth line) and current velocities (shaded). Current meter locations are on the previous figure (Source: Shepard, 1979).

#### b. Mean Flow Models

Using a one-layer barotropic numerical cavity flow model, with boundaries representative of the bay, Garcia (1971) attempted the first numerical study of the bay. The model was forced by momentum transfer (frictional shear) from northward flow adjacent (west of) to the cavity and included the effects of bottom topography (smoothed version of actual topography), friction, and the Coriolis force. Model outputs were in the form of mass transport stream functions. The results of this model led to the conclusion that the presence of a submarine canyon can induce a closed circulation within the bay and that the  $\beta$ -effect is negligible (Figure 11 on page 18). He also noted that the effects of bottom friction on the flow were negligible within the canyon itself but significantly influenced flow in the shallower regions. The most important result obtained from this model was the fact that the rotational nature of flow within the bay was changed by suppressing or adding the bottom topography of the Monterey

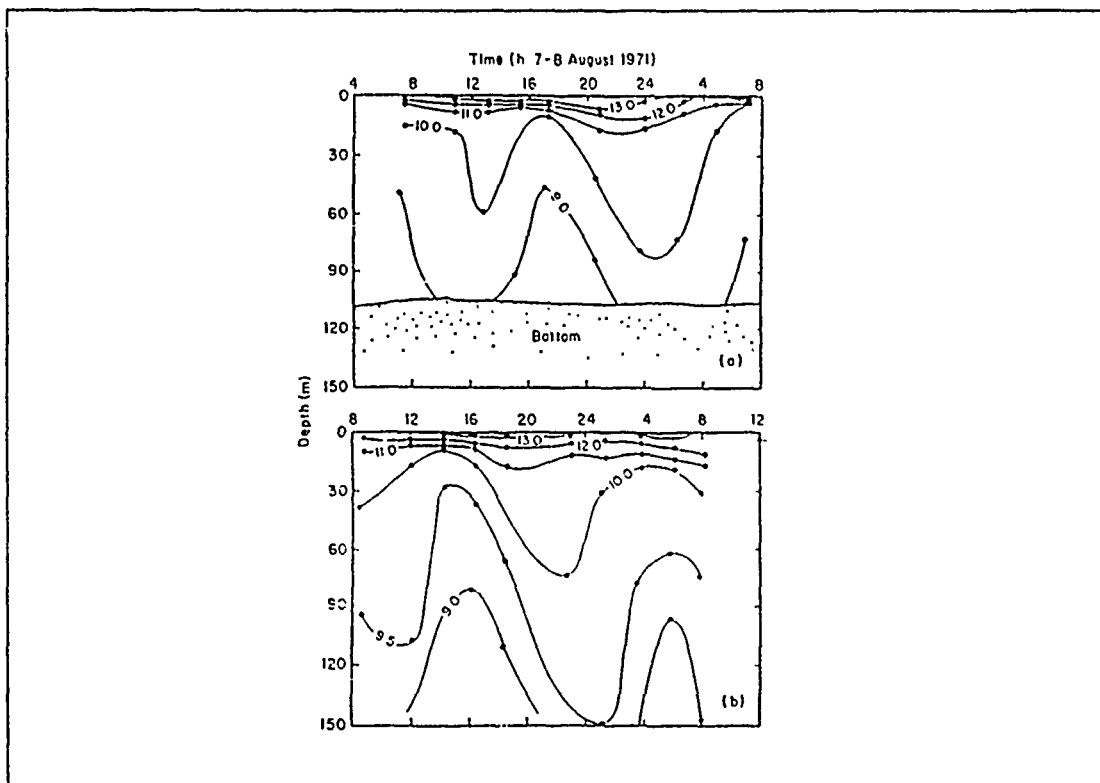


Figure 9. Time series of temperature distributions near the canyon head: Data were collected 1 km (top) and 4 km (bottom) west of the canyon head and imply internal wave heights of 50 to 120 m. Isotherms in °C (Source: Shea and Broenkow, 1982).

Submarine Canyon. For cavity flow without canyon topography, the northward mass transport stream simply entered the bay from the south and exited to the north resulting in cyclonically curved flow stemming from Coriolis force considerations. When canyon topography was added, momentum transfer, through shear stress from the north flow adjacent to the cavity, drove an anticyclonic gyre which effectively filled the Monterey Bay (Figure 11 on page 18).

Using output from a two layer, semi-implicit, primitive equation model and forcing across a north-south oriented boundary, Bruner (1988), showed that the upper layer was insensitive to bottom topography and to lower layer boundary forcing for velocities less than  $5 \text{ cm s}^{-1}$ . When lower layer flow was increased above  $5 \text{ cm s}^{-1}$ , the upper layer basically mirrored the lower. The lower layer was, of course, highly sensitive to bottom topography. Also, when the inflow width was decreased along the northern boundary, and southern boundary outflow was increased, the surface flow changed dra-

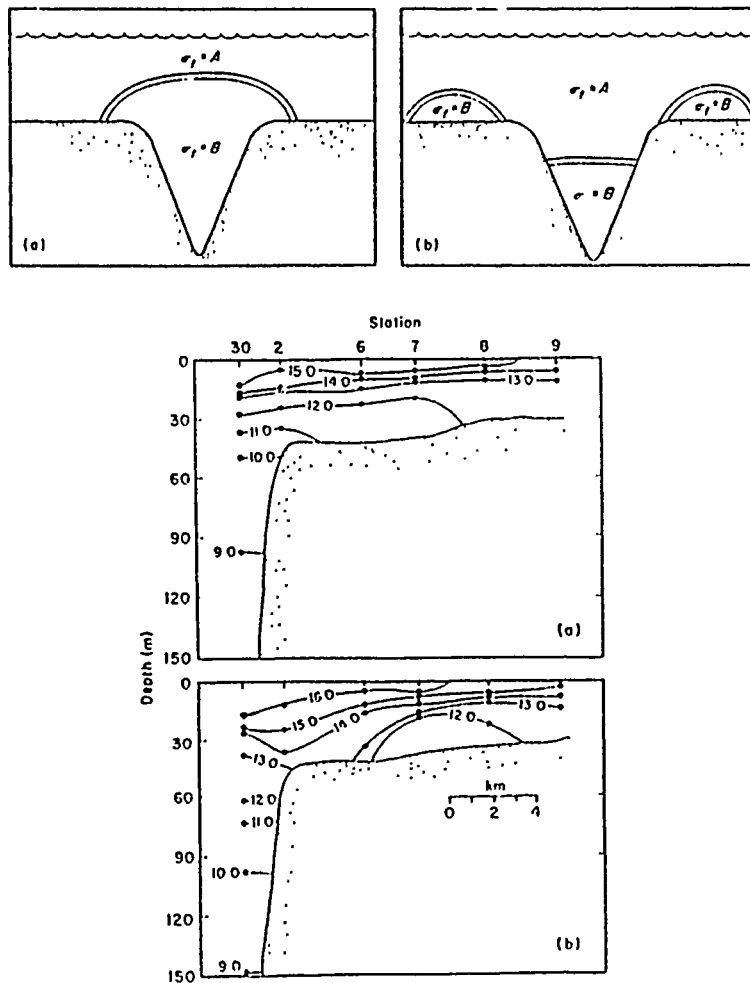


Figure 10. Conceptual model (top) of temperature distributions (bottom) near the edge of the Monterey Canyon: Top figures show the simple 2-level model used by Shea and Broenkow (1982) to describe how denser water from within the canyon is lifted out of the canyon at high internal tide (a), then pinched off onto the shelves during low internal tide (b). Bottom figures show actual temperature cross sections along the shelf during high internal tides (a) and low internal tides (b) (Source: Shea and Broenkow, 1982).

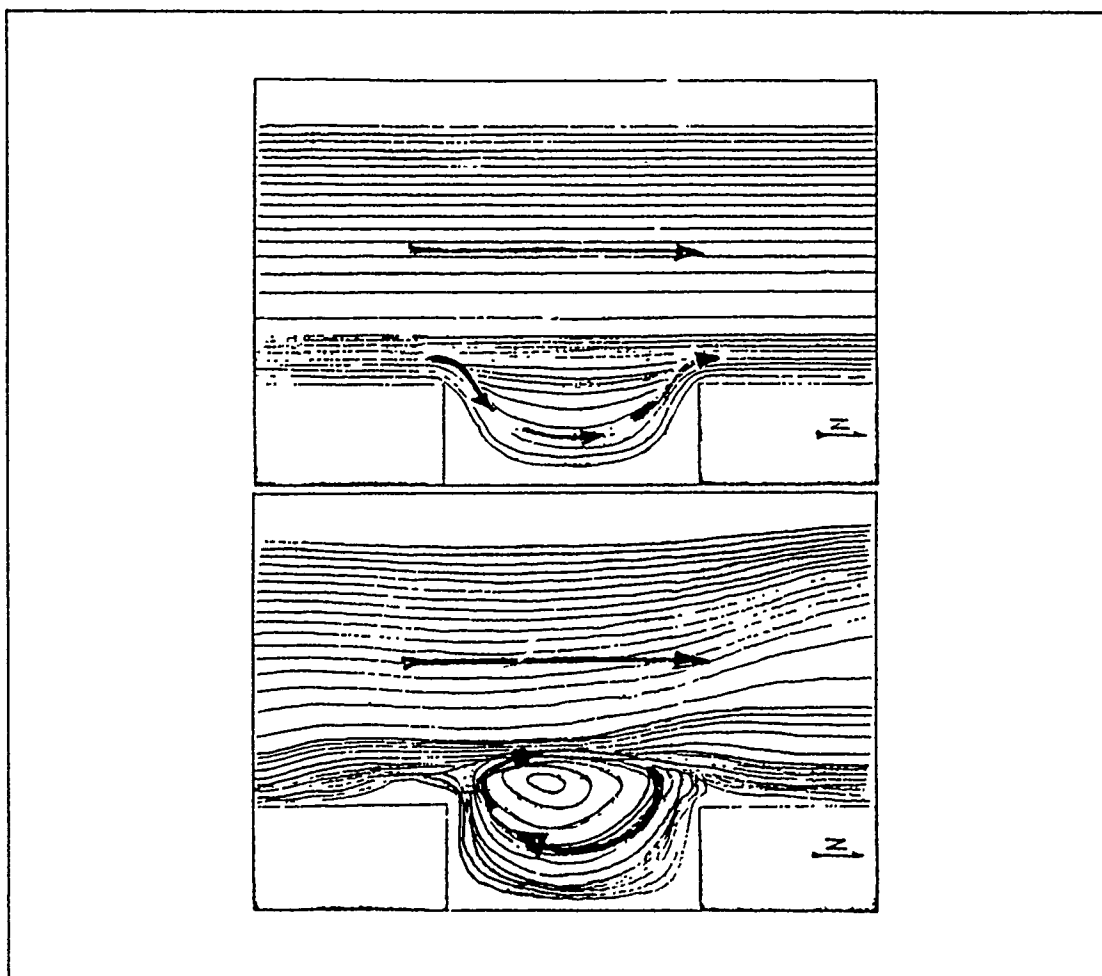


Figure 11. Garcia's one layer cavity model: Top figure represents model output with no canyon topography; bottom figure shows output with topographic effects included. Contours are volume transport stream functions with velocity arrows overlaid (Source: Garcia, 1971).

matically from cyclonic over the inner bay to totally anticyclonic flow while the lower layer flow was inhibited from entering the bay and turned, instead, almost immediately to the south of the bay where it exited (compare Figure 12 on page 19 and Figure 13 on page 20). Model outputs also showed that flow within the bay was highly sensitive to vertical shear. When no shear was present between the layers (barotropic case) the bottom layer had a great effect on the surface layer. However, when vertical shear was included (baroclinic case) the layers were essentially decoupled. Finally, Bruner noted that, when inflow was forced over the southern boundary simulating inflow of the Davidson Current, model runs depicted cyclonic circulation within the bay (Figure 14

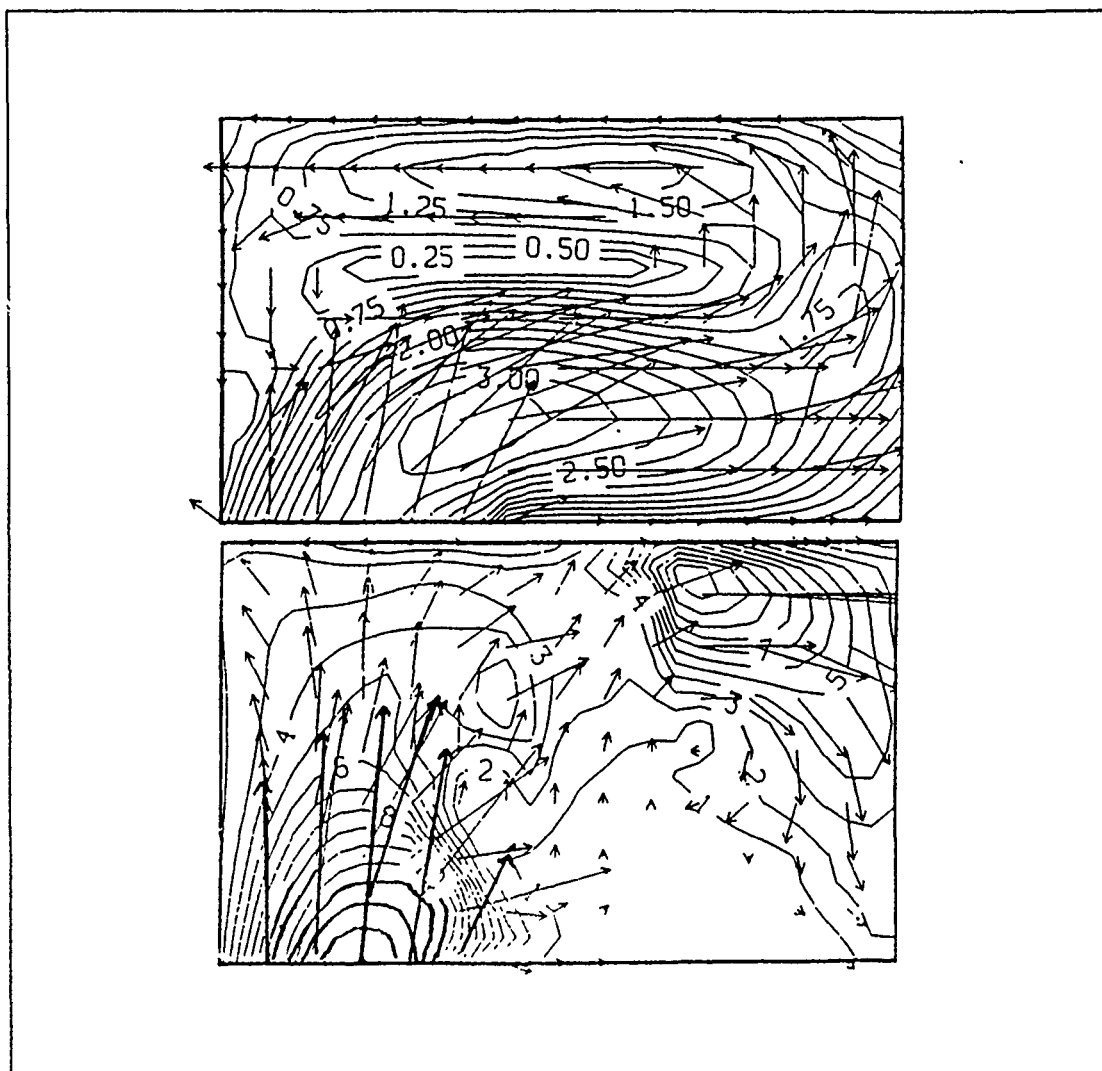


Figure 12. Bruner's two-layer, baroclinic model output #1: Surface flow (top) and lower layer flow (bottom) with forced inflow on the northern boundary and outflow over the southern boundary. North is to the left. Isotachs are overlaid with velocity vectors (Source: Bruner, 1988).

on page 21). These results contradict Garcia's barotropic model outputs, which predicted anticyclonic circulation within the confines of the bay from an adjacent northward flow. Boundary forcing in both Garcia's and Bruner's models was purely hypothetical, intended solely to test model responses (and the physics involved) to various flow scenarios.

Two final model studies, although not conducted exclusively for Monterey Bay, are mentioned here because of their obvious relevance. Both models, the first

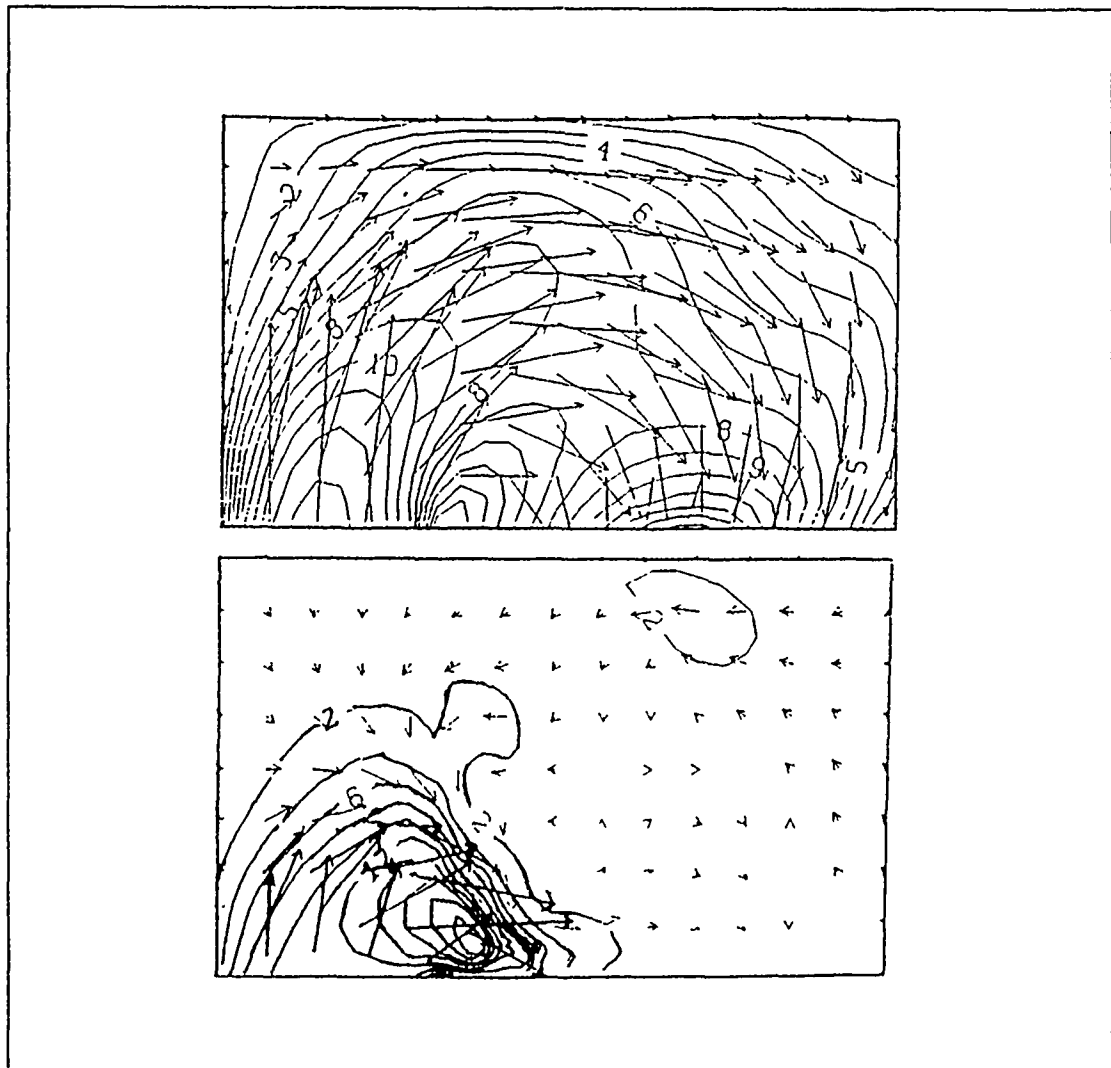


Figure 13. Bruner's two layer, baroclinic model output #2: The same as in Figure 12 on page 19 except that inflow area was constricted and outflow area was widened. North is to the left (Source: Bruner, 1988).

solved analytically and the second numerically, attempt to represent the adjustment process that takes place when a geostrophically balanced flow over a shelf encounters a submarine canyon, and are from Klinck (1988 and 1989).

In the first model, Klinck (1988) initially solved the shallow water equations by the Laplace Transform method for a two layer fluid on an  $f$ -plane, and then applied the boundary conditions of a flat bottom ocean intersected by an infinitely long rectangular trench. He then applied the initial condition of an arbitrarily wide flow in the upper layer perpendicular to the canyon with no initial flow within the canyon itself.

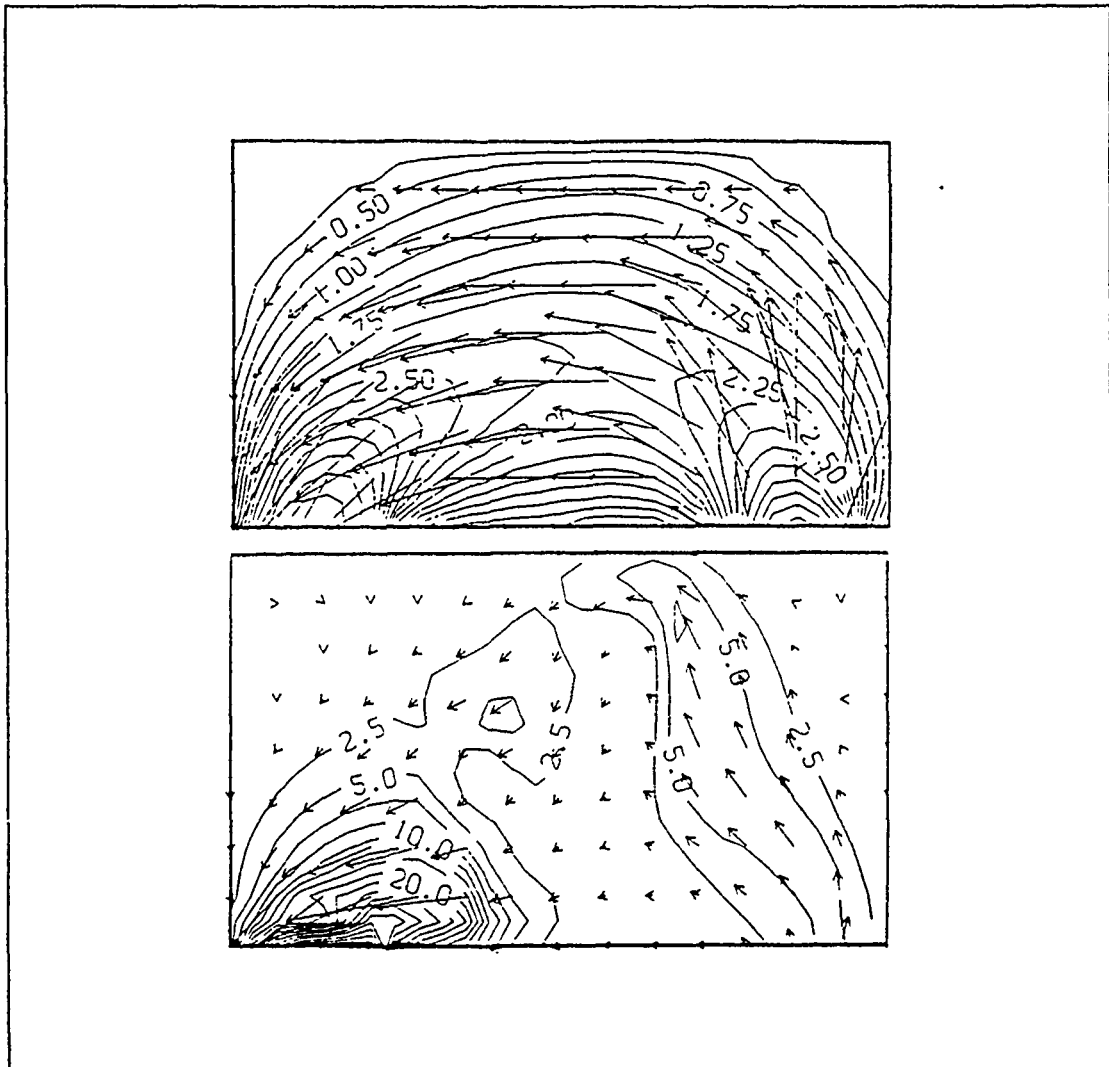


Figure 14. Bruner's two-layer, baroclinic model output #3: Surface flow (top) and lower layer flow (bottom) with forced inflow on the southern boundary, outflow over the northern boundary. North is to the left (Source: Bruner, 1988).

The solution to this problem yielded standing wave motion over the canyon with waves radiating from either side. In the absence of friction, these waves would continue to oscillate indefinitely as standing gravity modes. Results also showed that, in the steady state, there was no net flow across the canyon, implying that submarine canyons may inhibit barotropic geostrophic flow. For shelf currents on the order of the external Rossby radius of deformation ( $R_{d0}$ ), these oscillations have periods on the order of 0.1 to 1.0 times the local inertial frequency. For "narrow" canyons (defined in this case as



a canyon whose width is less than one half of the smaller of either the width of the current or  $R_{d0}$ ), Klinck showed that these oscillations would have periods on the order of 0.2 times the inertia period. He notes that these frequency ranges are observed in most canyons. Breaker and Broenkow (1989), citing this work, calculated a period of 4 h for Monterey Bay and noted the close agreement with Dooley (1968) and Njus' (1968) observed 4 h periods. They concluded that both inertial and non-linear effects associated with the interactions of the internal baroclinic tides and steep topography are both possibly at work in generating supertidal oscillations in Monterey Bay.

Klinck (1989) conducted further experiments on the geostrophic adjustment process, this time utilizing a three layer numerical model (Figure 15 on page 24) where both the internal and external modes can act (the two top layers modeled shelf flow, the third layer modeled flow within the canyon). As he states, the importance of using a three layer, stratified fluid is the fact that pressure gradients at the bottom of the upper layers will now influence the fluid within the canyon and that, "...density redistribution can cancel the effect of a surface slope such that there is a steady geostrophic flow," results which were not possible in his original model. In addition to the coastal current width, canyon width, and  $R_{d0}$ , the first internal Rossby radius of deformation ( $R_{d1}$ ) now becomes another important controlling factor in the geostrophic adjustment process. Klinck initialized this model in much the same way as his barotropic model, i.e. geostrophically balanced, steady, barotropic  $10 \text{ cm s}^{-1}$  flow over an infinitely wide flat bottom in the positive x direction (this would be the same as looking shoreward at a cross section of Monterey Bay from sea with an initial shelf current flowing equatorward along the coast) which crosses a rectangular canyon at right angles. Flow in the canyon was initially at rest. A 50 km wide current was used and runs were made using varying canyon widths including 200 and 10 km. In the 200 km wide case, the induced disturbance at the canyon walls are independent of each other (Figure 15 on page 24). Flow over the shelf decays away from the wall on the order of the current width, while flow within the canyon decays away from the wall on the order of  $R_{d1}$  for the internal mode and on the order of the current width for the external mode. Also, the largest density gradients are located within the canyon which, as Klinck points out, indicates that the strongest currents are along the walls of the canyon and are bottom trapped. He explains these results in terms of vortex stretching, stating;

During adjustment, the water in the canyon is pushed down the initial pressure gradient which causes upwelling at places where the surface elevation in the initial state was lowest and downwelling where it was highest. Upwelling stretches the vortex tubes in the canyon creating cyclonic vorticity at the edges of the canyon. The mass redistribution reduces the slope of the free surface creating cyclonic (anticyclonic) vorticity in level 1 on the shelf side of the canyon wall in places where the free surface rises (falls). The isopycnal surface over the canyon near the wall rises sharply compressing vortex tubes creating anticyclonic vorticity right at the wall.

In the narrow canyon case (10 km wide), the external mode is inhibited because the width is now smaller than any of the decay scales ( $R_{do}$ , or  $R_{dl}$ ). Isopycnals within the canyon create vortex stretching (positive vorticity) resulting in a topographically trapped cyclone within the canyon and vortex compaction (negative vorticity) which results in anticyclonic rotation in the fluid above the canyon. Finally, Klinck noted that as the canyon width continued to be shortened (narrowed), it ceased to have much of a perturbing effect on shelf flow when it reached approximately one half of  $R_{dl}$ . Limitations, however, should be kept in mind when applying these model results to Monterey Bay. First, the Monterey Bay Submarine Canyon is roughly triangular in shape (in plan view and in its vertical cross-section); second, the shelf region north and south of the bay is relatively narrow (approximately 6 km to the north and only 2 to 3 km to the south), and; finally, the canyon is located in a bay and does not simply extend seaward across a coastal shelf.

Typical values of the first internal Rossby Radius ( $R_{dl}$ ) were calculated for the Monterey Bay using the relationship:

$$R_{dl} = \frac{(gH_e)^{1/2}}{f}, \quad (3)$$

where  $H_e$ , the equivalent depth, is:

$$H_e = \frac{N^2 H^2}{g n^2 \pi^2}, \quad (4)$$

and  $N$ , the Brunt-Vaisala frequency, is defined as:

$$N^2 = -\frac{g}{\rho_0} \frac{\partial \rho}{\partial z}. \quad (5)$$

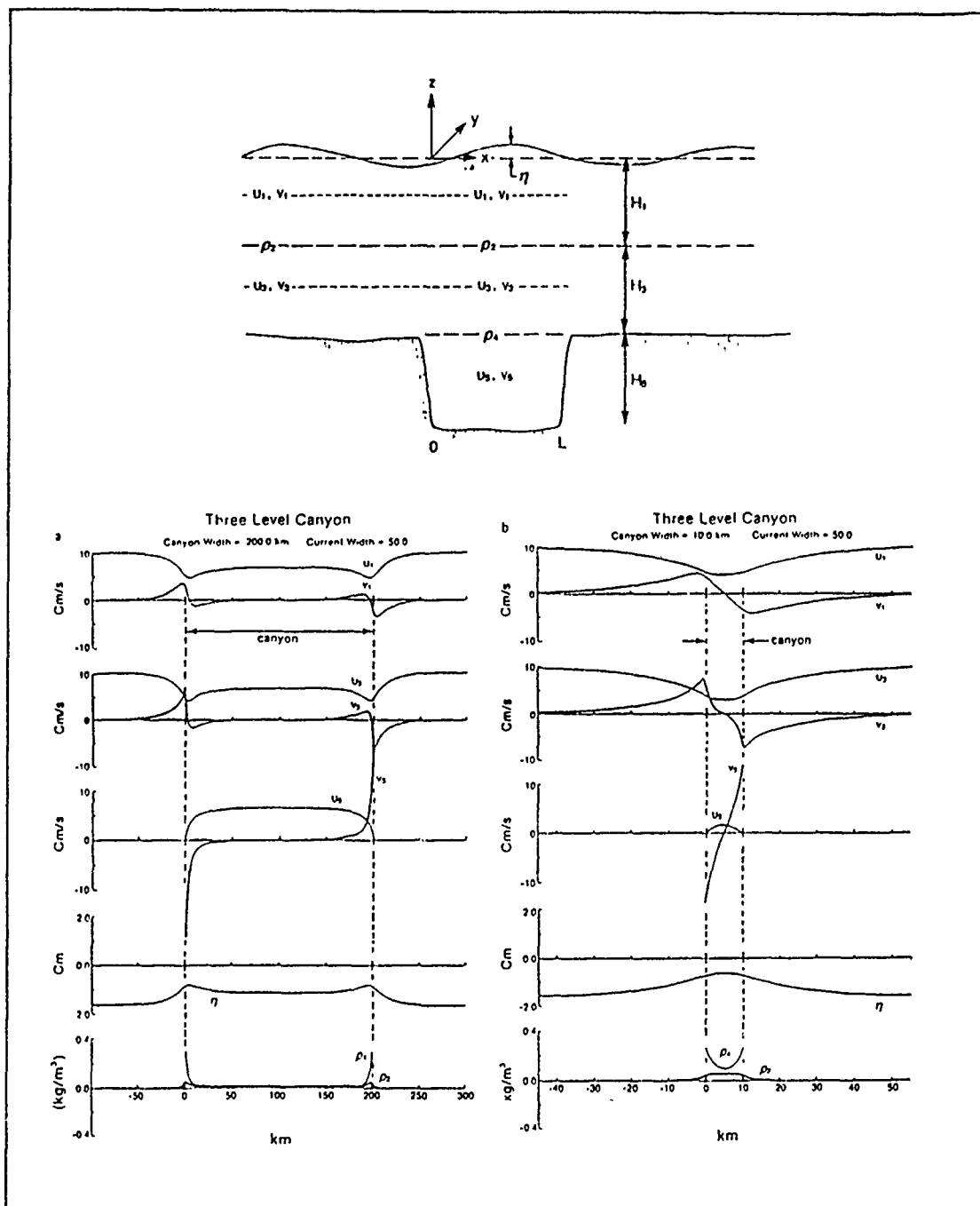


Figure 15. Geostrophic velocity adjustment over a submarine canyon: Side view of Klinck's 3-level canyon model (top). Bottom figures show cross canyon (x-direction) outputs forced by a 50 km wide current over 200 km (bottom-left) and 10 km (bottom-right) wide canyons (Source: Klinck, 1989).

Substituting equation (4) into equation (3), and solving for the first internal mode ( $n = 1$ ) yields:

$$R_{d1} = \frac{\bar{N}H}{\pi f} . \quad (6)$$

Brunt-Vaisala frequencies were obtained through 2 m finite differencing techniques and averaged throughout the water column to obtain values for  $\bar{N}$ , which ranged from approximately  $11 \times 10^{-3}$  Hz over the shelf area (very stable) to  $4 \times 10^{-3}$  Hz over the canyon axis (Appendix D). Values for  $R_{d1}$ , obtained from equation (6), ranged from 2 km over the shelf regions to 15 km over the axis of Monterey Bay (Appendix D). Canyon widths range from approximately 10 to 15 km at the mouth of the canyon, 7 to 9 km across the center, and 2 to 3 km near the head of the canyon. Calculated values of  $R_{d0}$ , obtained using the relationship:

$$R_{d0} = \frac{(gH)^{1/2}}{f} , \quad (7)$$

ranged from 200 km over the shelf regions to 1000 km near the center of the bay (Appendix D). These values are in close agreement with results obtained by Breaker and Broenkow (1989) through the averaging of 3 months of hydrographic data. Thus the Monterey Canyon could be defined as "narrow" in both the barotropic and baroclinic sense, although portions of the bay do approach the width scale of  $R_{d1}$ .

### C. PURPOSE OF STUDY

In light of recent sewage and agricultural run off problems experienced within the Monterey Bay, a solid grasp of the mean circulation is essential. This study attempts to quantify the mean flow field experienced within the bay over a four day period in May 1988 (upwelling period) using conductivity, temperature, and depth (CTD) data, acoustic Doppler current profiler (ADCP) measurements, current meter data acquired by the Monterey Bay Aquarium, and available NOAA-11 Advanced Very High Resolution Radiometer (AVHRR) satellite sea surface temperature imagery. Phase relationships between the tides and the baroclinic flow field, along with suggested internal wave fields in the Monterey Submarine Canyon, are also examined.

Finally, the circulation response within the bay to forcing by the observed mean flow determined from the CTD and ADCP data will be examined using an updated version of the baroclinic model used by Bruner (1988). Wind data, acquired both before and

during the period of this study, will also be used to force this model, a factor not previously considered.

## **II. DATA ACQUISITION AND PROCESSING**

### **A. COLLECTION**

#### **1. May 1988 NPS Student Cruise**

The vast majority of the data utilized in this study were acquired during the second half of an NPS student cruise conducted within the Monterey Bay during the period 08 to 11 May 1988 onboard the Research Vessel Point Sur, homeported at Moss Landing, California. Two cross-sections were run perpendicular to bottom topography, the first running roughly north-south across the mouth of the bay and, the second, roughly parallel but inshore of the first. Each line contained CTD stations which were sampled around the clock (Figure 16 on page 28). The seaward section intersected the mouth of the Monterey Submarine Canyon with station 7 situated directly over the axis (hereafter referred to as "Line 1"), while the landward section crossed the Monterey Canyon axis at station 13 and the axis of the Soquel Canyon at station 15 (hereafter referred to as "Line 2"). The first cross-section contained 10 CTD stations, each sampled a total of five times, while the shoreward Line acquired data from 7 hydrographic stations, each sampled four times, resulting in the overall collection of 78 CTD casts at 17 stations throughout the period. The cruise was designed, in part, to determine the mean currents. Thus, to negate the effects of the tidal motions in the water column, each station was occupied at approximately 15.5 hour intervals, resulting in exactly a 125% phase shift of the semidiurnal tidal cycle each time the station was sampled (Figure 17 on page 29). Each station was therefore occupied on all phases of the surface tide.

In addition to hydrographic data, the ADCP was operated continuously for each line throughout the duration of the cruise. The RV Point Sur is outfitted with an RD Instruments DR0150 ADCP which utilizes a four beam JANUS array operating at a frequency of 150 kHz. Beams are aligned fore and aft, and port and starboard, of the RV Point Sur. Raw data were acquired in 128 four meter bins averaged over a three minute ensemble interval. The ship's position was recorded from Loran-C at the end of each ensemble.

#### **2. Other Supporting Data**

Cloud free NOAA-11 AVHRR satellite imagery was obtained from 4, 8, and 11 May 1988 and processed at the Naval Oceanographic and Atmospheric Research Lab-

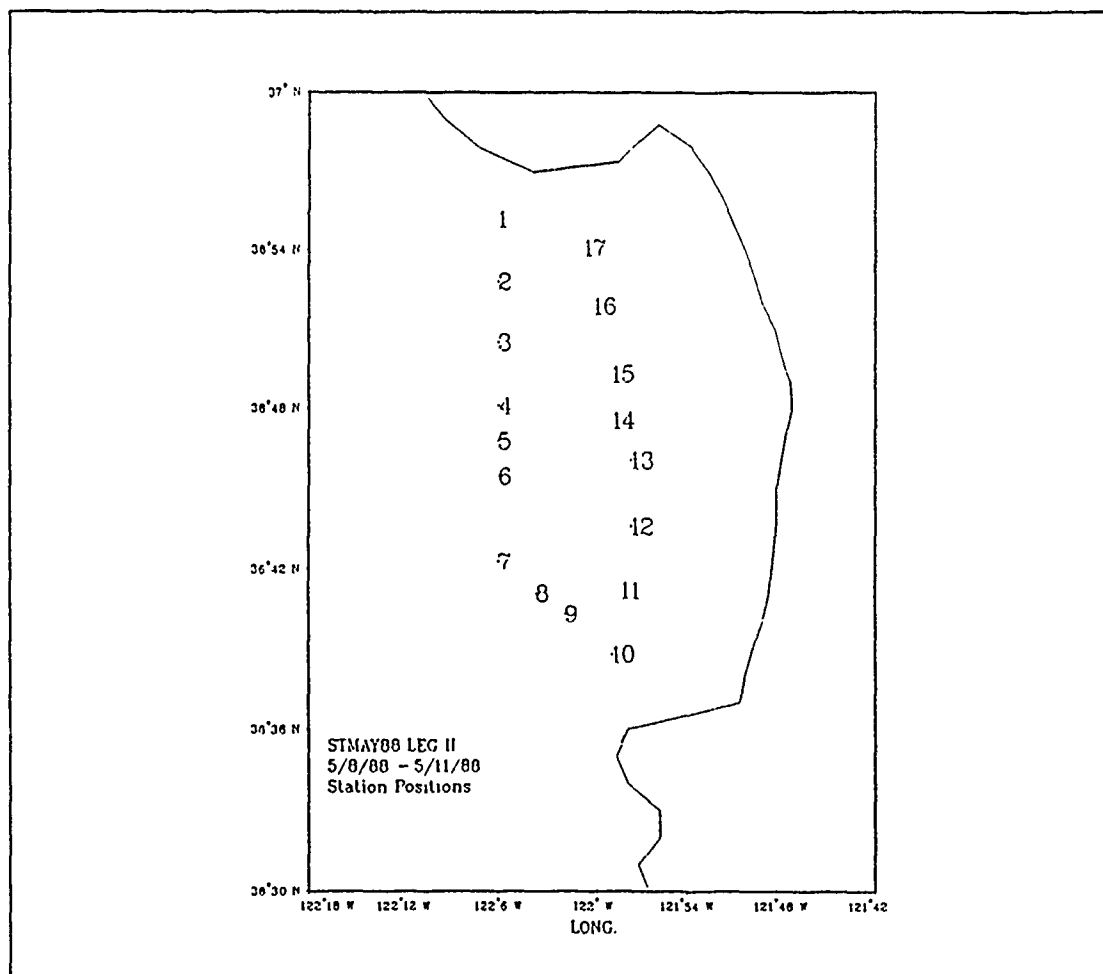


Figure 16. CTD stations occupied during May 1988 NPS student cruise: Stations 1-10 (designated "Line 1") were each sampled 5 times and stations 10-17 (designated "Line 2") were each sampled 4 times. The sampling interval was approximately 15.5 hours.

oratory (NOARL) - West, located in Monterey, CA. GOES - West visual and infra-red imagery were also obtained for the period of the cruise. Finally, synoptic weather charts were collected from the National Meteorological Center (NMC) for the months of April and May 1988 via facsimile broadcast.

A continuous (5 minute averaged) record of sea surface temperature, wind speed and direction, tidal height, and current speed and direction was obtained from the Monterey Bay Aquarium (MBA) data base for the period 21 April through 20 June 1988 (Figure 21 on page 37). The MBA weather station is situated on the roof of the Aquarium which is located on the shore of the southern bight at 36° 37.1' N, 121° 54.0'

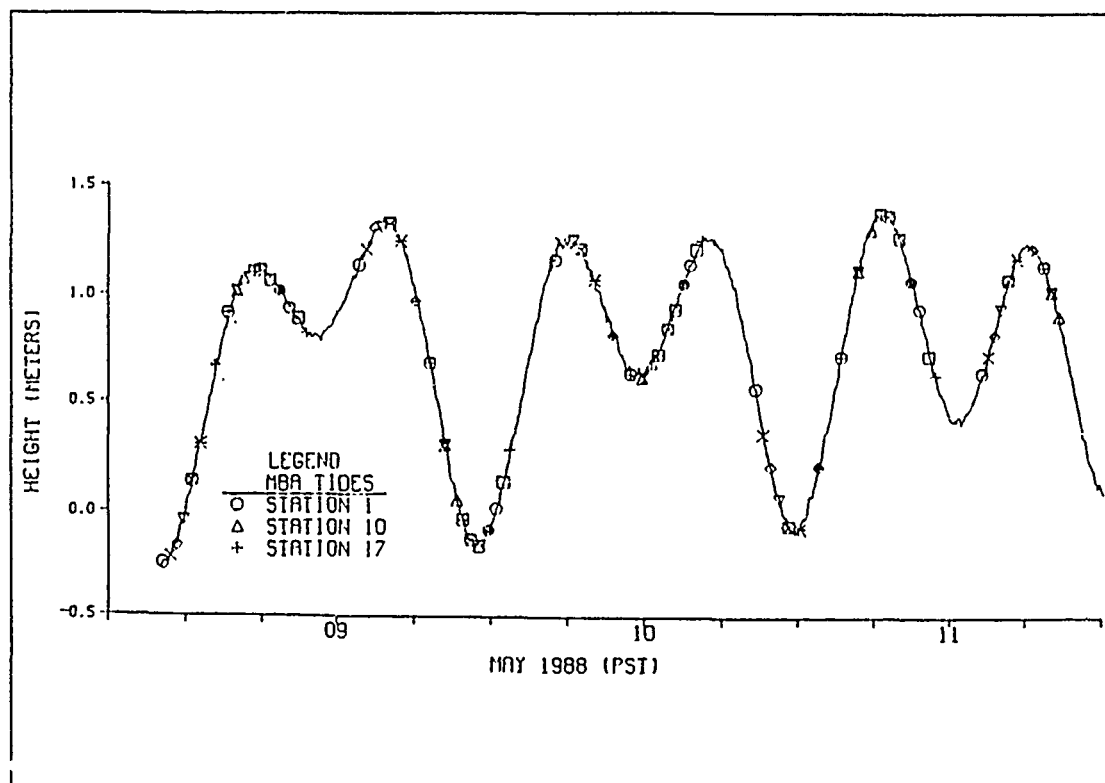


Figure 17. CTD sampling interval overlayed on observed surface tidal heights: Each station is represented by a separate symbol. Stations 1-10 represent Line 1, stations 10-17, Line 2. The tide data were obtained from the MBA data base.

W at an elevation of 21 m above sea level. The MBA current meter, an electromagnetic InterOcean Model S4, is situated approximately 305 m seaward of MBA at a depth of 6.1 m below Mean Lower Low Water (MLLW) at  $36^{\circ} 37.3' \text{ N}$ ,  $121^{\circ} 53.6' \text{ W}$ . Tide data were obtained from a tide gauge located on Monterey Wharf #2 ( $36^{\circ} 36.3' \text{ N}$ ,  $121^{\circ} 53.5' \text{ W}$ ). The gauge is operated and maintained by the National Oceanic and Atmospheric Administration (NOAA). Raw tidal heights were corrected to MLLW by subtracting a 2.5 m offset.

## B. PROCESSING

### 1. Neil Brown Instrument Systems (NBIS) Mark IIIB CTD Probe

Casts were made at each station utilizing a NBIS Mark IIIB CTD probe with manufacturer sensitivities listed in Table 2 on page 30. Water samples were taken at the bottom of each cast and sea surface temperature measurements were obtained from bucket measurements. Pressure offset (the pressure recorded by the CTD while sitting



on deck) values were recorded just prior to deploying, and upon recovery of, the instrument. Finally, in order to insure accurate salinity measurements, the conductivity probe was rinsed with fresh water and covered after each hydrocast.

**Table 2. NBIS MARK IIIB CTD MANUFACTURER SPECIFICATIONS**

Variable	Range	Accuracy	Resolution
Pressure	0 to 3200 dbar	$\pm 3.2$ dbar	0.05 dbar
Temperature	-3 to +32 ° C	$\pm 0.005$ ° C	.0005 ° C
Conductivity	1 to 65 mmho	$\pm 0.005$ mmho	0.001 mmho

Calibrations were conducted prior to the cruise by checking the CTD conductivity, temperature, and pressure readings against standards in the laboratory. Differences obtained in this manner were then averaged and fit to a linear regression scheme in order to obtain the coefficients necessary to adjust the measurements made by the CTD to the reference standards. Temperature coefficients had a slope of 0.999363 and an intercept of 0.003435 while the pressure slope was calculated to be 1.000000.

Post-analysis of data in the laboratory consisted of first measuring the salinity from the collected water samples to obtain the "true" salinity, then determining the difference between salinities derived from the CTD data and those obtained in the laboratory (Figure 18 on page 31). Points more than two standard deviations from the mean (outliers) were considered to be the result of random errors (human errors, ship motion in areas of large salinity gradients, etc.) and were removed. The mean and standard deviation were then recalculated and outliers greater than two standard deviations from the mean were once more removed. A linear fit to the data obtained by this method had a slope of 1.036714 and an intercept of -0.347450 which resulted in a salinity offset of 0.868 psu. Temperature and pressure values were once again compared to values obtained by laboratory instruments. Finally, a program which used both pre-cruise and post-cruise calibration coefficients, including recorded pressure offsets, was applied to the raw data acquired by the CTD to obtain the values used in this study. A more detailed description of these calibration procedures is provided by Tisch (1990).

## **2. Acoustic Doppler Current Profiler (ADCP)**

After calibration of the raw data and correcting for the ship's velocity, current velocities to a depth of approximately 400 m were calculated. During collection, the ADCP data

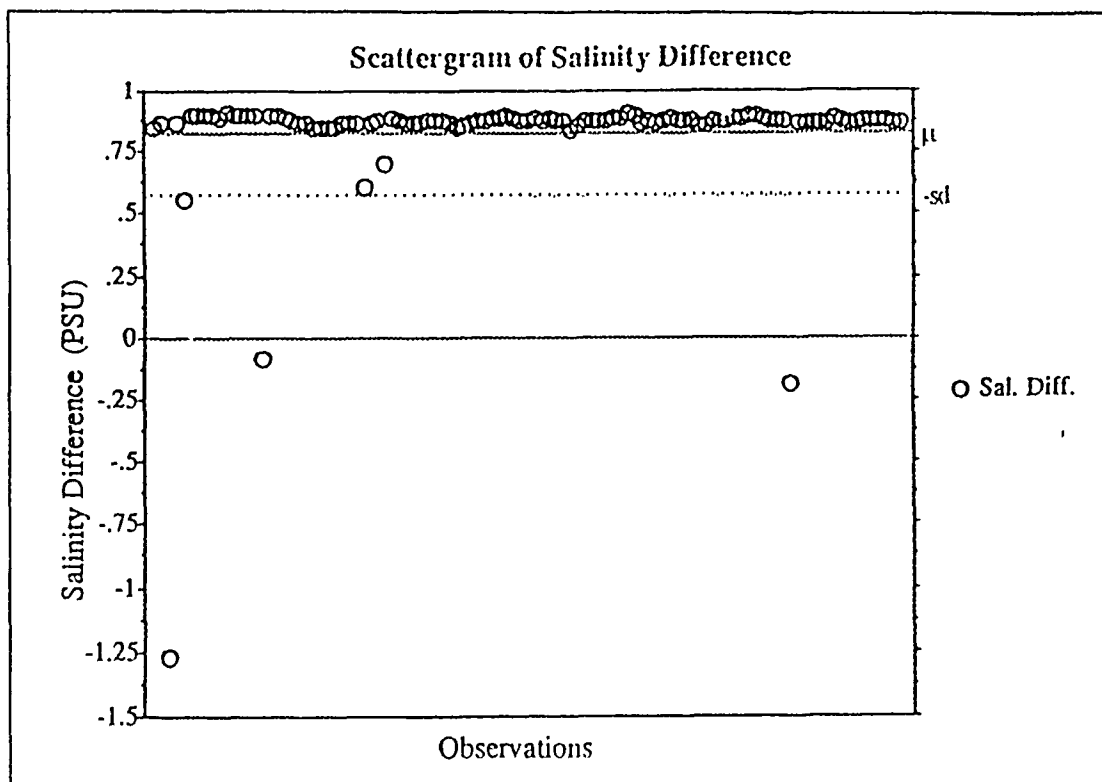


Figure 18. Scattergram of initial salinity difference for STMAY88: Plot represents differences between CTID and water sample salinity at the bottom of each cast. Positive values indicate the instrument is reading too low. Mean ( $\mu$ ) and standard deviation (sd) are indicated (Source: Tisch, 1990).

were averaged and stored every 3 minutes along with the ship's position. In this way, a unique position is associated with each ensemble average. To recover cross sectional velocity profiles, data is again averaged at specified increments along the entire line. Inaccuracies inherent in this method include errors induced through bad navigation data and through the averaging techniques. For instance, if the ship was stationary at one of the specified increments, but underway at the next increment, the previous station contains more data than the latter, so averaging is somewhat biased in this respect. For this reason the ADCP data acquired during this study was averaged at 4 km intervals, which approximately corresponds to the hydrographic station spacing, to minimize both the errors induced through navigation, and unequal ensemble averaging. A more detailed description of converting raw ADCP relative velocities into meaningful absolute

velocities is given by Kosro (1985). Accuracies in current velocities obtained using this method have been cited to be on the order of 4 to 5 cm s<sup>-1</sup> (Kosro, 1985).

Built into the ADCP system software are constraints which determine whether data is to be considered "good" or not, namely:

- The shallowest bin is no good due to side lobe interference reflected from the ship's hull and the ocean surface.
- There must be at least a 60% return in signal strength.
- Error velocity, defined as the difference in vertical velocities between orthogonal pairs of beams, must be within specifications in order for data within a certain bin to be labeled "good."
- If the Automatic Gain Control (AGC), or reflected energy, increases greater than 10%, the system classifies this depth as the bottom and negates data below this level. Typically, if no bottom is present, the AGC signal will simply decrease with depth (beam distance). In contrast, if a bottom is present within range of the ADCP beam, a jump, or increase in the AGC signal will result and data below this depth will be flagged as invalid.

Data from the deepest good bin, determined by the above constraints, to the ocean surface is considered "good." During this cruise, ADCP data were suppressed below approximately 75 to 100 m in the areas near the northern half of the Monterey Canyon due to the AGC constraint. During replay of the acquired ADCP data over this area, it was noted in three out of the five passes, that a strong anomalous "spike" occurred in the AGC plots at the depths mentioned. As expected, the AGC plot showed gradual decreasing values from the surface to approximately 75 m where a sharp increase was noted. Below this depth, values again gradually decreased. This spike was assumed to be the product of biological activity of unknown origin which persisted near the bottom of the thermocline in these areas throughout most of the cruise. At depths below the AGC "spike," data exhibited low propagation loss (greater than 60% return signal strength) lending some credibility to the fact that data acquired below this layer may, in fact, have been good, although to what extent it was biased or influenced by the "scattering" layer is unknown. At any rate, ADCP data in these areas were re-processed by Mr. Paul Jessen, an NPS Oceanographer, with the AGC constraint suppressed, to recover the velocities in the area along the northern wall of the Monterey Canyon.

### III. METHODS AND RESULTS

This chapter describes the results and observations obtained through the analysis of collected data. Methods used in obtaining stated results are provided in a separate subsection unless they are self-explanatory, such as in the section titled "synoptic meteorological situation." Evaluation of each data type is discussed separately with some limited comparison of results provided. An effort to tie all results together is given in Chapter IV. Results are presented in the following order: internal waves inferred through CTD data, mean geostrophic velocities, mean ADCP velocities, description of NOAA AVHRR sea surface temperature imagery, analysis of the synoptic meteorological situation both prior to and during the May 1988 student cruise, and finally, the methods and results of applying the mean flow field to a primitive equation numerical model of the Monterey Bay are presented. Some comparisons between the MBA data and results obtained from this study are made, when applicable.

#### A. INTERNAL WAVE FIELD

##### 1. Methods

To determine the extent of aliasing by internal wave processes and relate them to surface tidal oscillations, various depictions of the fluctuations of the 10°C isotherm were generated. The 10°C isotherm was chosen because of its apparent proximity to the center of the thermocline. Data were taken from CTD measurements. As a consequence of the sampling interval (approximately 15 h), only waves with periods greater than 30 hours (frequencies smaller than the Nyquist frequency) could be resolved. The total structure (period, wave number, and phase speed) of the internal wave field, therefore, could not be determined from these data. First, a graph of the 10°C isotherm pressure across the mouth of the bay (Line 1), along with the mean isotherm pressure was generated (Figure 19 on page 34). To obtain a relationship between surface tidal height and this internal wave field, plots of the surface tidal height versus isotherm pressure were then produced for each station (Figure 20 on page 35).

##### 2. Results

The plots of the 10°C isotherm pressure changes during each pass of Line 1 (Figure 19 on page 34) show the active internal wave structure encountered during data collection. The largest amplitudes (up to 30 m) were observed to be in the vicinity of the shelf breaks (stations 3 and 9 at 9 and 30 km on the graph), over the axis of the

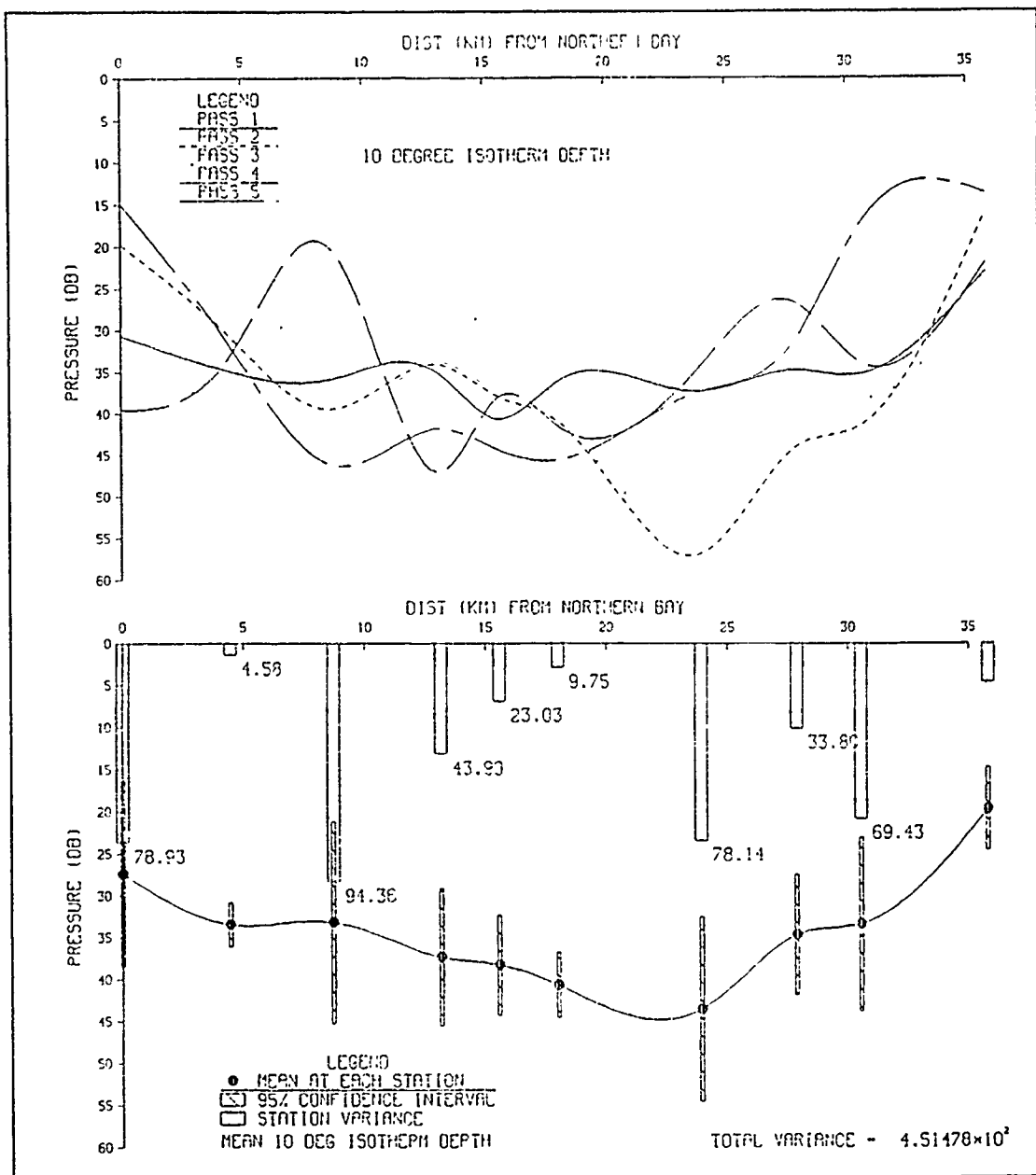


Figure 19. Isotherm variance along Line 1: Top figure shows the pressure of the 10°C isotherm across the mouth of the Monterey Bay during each pass (see legend). North is to the left, south is to the right. Bottom figure shows the mean 10°C isotherm depth and the calculated isotherm variance at each station along the line. Note the large amplitude fluctuations near the shelf break (variances of  $94.36 \text{ m}^2$  and  $69.43 \text{ m}^2$ ) and over the center of the Monterey Submarine Canyon (variance of  $78.14 \text{ m}^2$ ).

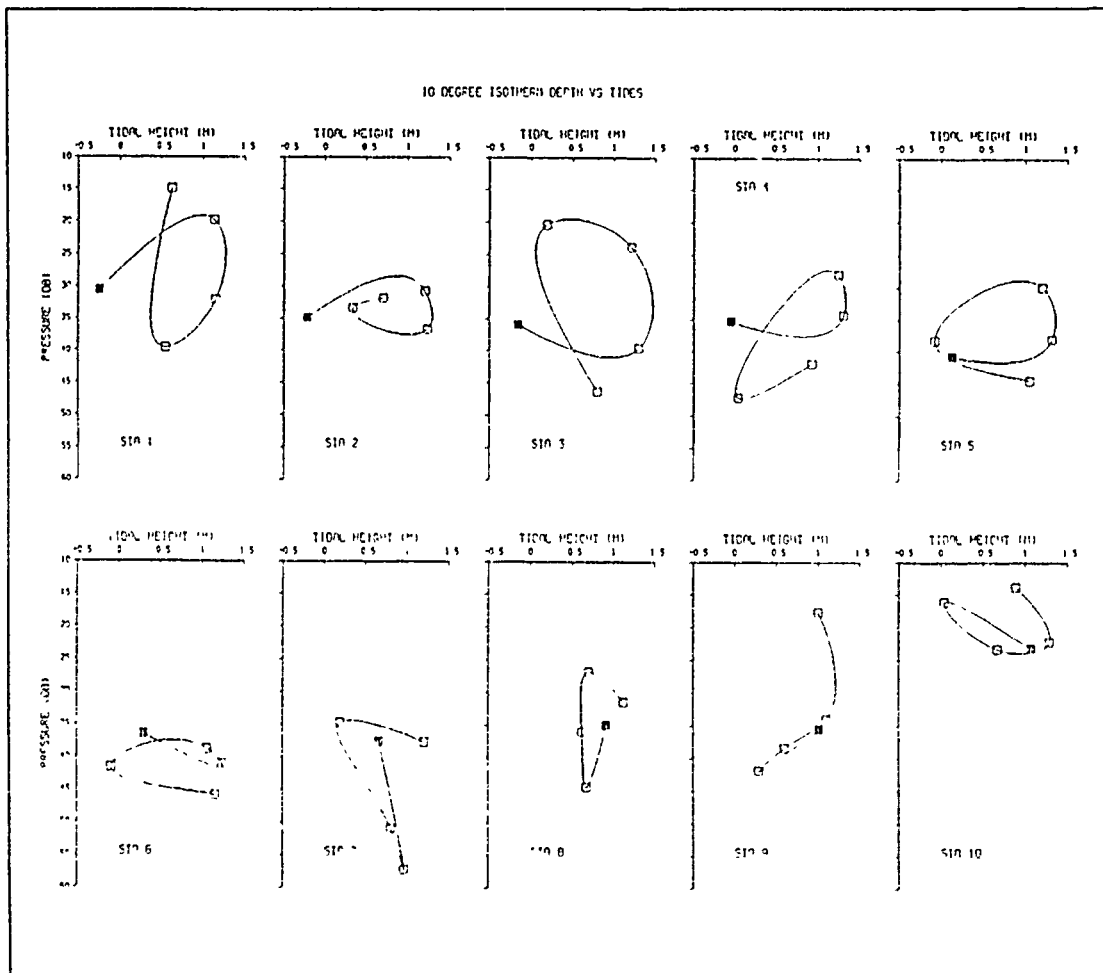


Figure 20. Isotherm depth versus observed surface tidal heights: Plots depict the change in pressure of the 10°C isotherm as a function of the observed surface tides. Tide data were obtained from MBA data base.

Monterey Submarine Canyon (near the 24 km mark on the graph), and near shore over the shelf at station 1. What appear to be nodal points can be seen near stations 2 and 6. The plotted mean 10°C isotherm pressure (Figure 19 on page 34) shows gradual deepening of the isotherm from the northern part of the bay (station 1) to the center of the canyon (station 7) then steep shoaling from station 7 to the southern shelf at station 10. Calculated variance shows high values in the areas of large amplitude fluctuations previously mentioned. In general, the observed internal wave amplitudes were smaller in Line 2 (stations 11-17) with most amplitudes falling within the 10 to 15 m range. This was somewhat surprising considering past studies (Shea and Broenkow, 1982, and Broenkow and McKain, 1972) which showed higher amplitude internal waves nearer the

head of the canyon than towards the mouth. This again may simply be the result of the relatively large station sampling interval, i.e. the internal waves in Line 1 may have had a different frequency or phase relation with the surface tidal heights than those encountered in Line 1, resulting in poorer resolution of these waves in Line 2 data.

The 10°C isotherm pressure versus tidal height at each station of Line 1 (Figure 20 on page 35) show no direct surface tidal correlation. Large differences in pressure can be seen even though the surface tidal height is at nearly the same level. For instance, at station 8, when the tide is approximately 0.5 m, the pressure of the 10°C isotherm ranges from 20 to 45 dbar (note 1 dbar  $\approx$  1 m in these ranges). Similar cases of varying isotherm pressure at constant tidal heights can be seen at other stations (station 1 had isotherm pressures which varied by as much as 25 dbar during two separate periods when the tide was at the same height). If internal tides were in phase with the external tides, these graphs should basically show a positive sloping line from the bottom left to the upper right (i.e. the isotherm would rise and fall with the external tidal height). Station 9, near the southern shelf break, is the only station which comes close to this description, where all points nearly lie on a straight line. A cross-spectral analysis between one week of continuous thermistor data near the canyon head and surface tidal heights, conducted by Shea and Broenkow (1982), revealed a 7 h phase lag. A similar analysis of approximately 3 months of thermistor data, from mid April to mid June 1988, collected from the MBA sensor at a depth of 6 m in the southern bight (Figure 21 on page 37), revealed an 8 h phase lag at the predominant semi-diurnal 12.8 h period. However, phase relationships between surface tidal heights and internal waves near the canyon head and over the shelf regions more than likely differ from those in the deeper regions of the bay, especially over the canyon.

In summary, the internal wave field encountered during the 08 to 11 May 1988 data collection period was highly energetic, especially along Line 1. Amplitudes varied across the bay, but appeared to reach a maximum over the shelf breaks which lends support to Shea and Broenkow's (1982) proposed model of processes occurring near the edge of the Monterey Canyon (see Figure 10 on page 17). Although the direction of propagation of these internal waves could not be determined from the available mass field data, the high variability across the mouth of the bay would seem to suggest at least some cross canyon component exists. Possibly the most useful information gained from the above analysis is the fact that the isotherm slopes created by the internal waves exceed the mean slopes due to geostrophic adjustment by two orders of magnitude. This implies that geostrophic velocities derived from one pass alone is virtually useless be-

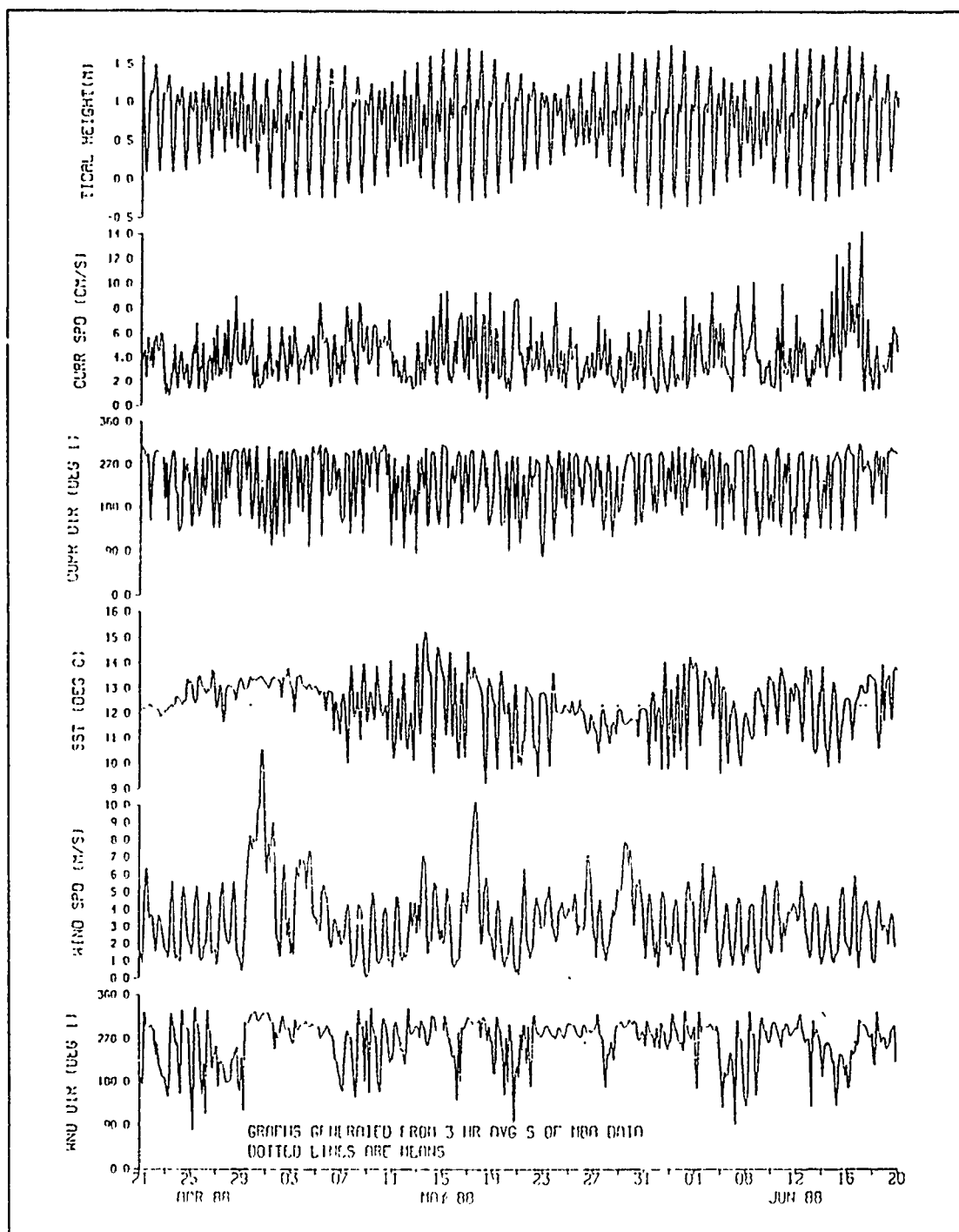


Figure 21. Acquired MBA ocean and atmospheric data 21 April - 20 June 1988: MBA data is averaged and stored every 5 minutes. Above curves were generated using a 3 hour running mean filter. Dashed lines represent total mean.



cause the internal wave "noise" will quite effectively mask the mean signal. Therefore, some sort of averaging scheme is a necessity. The next sections describe the geostrophic flow obtained from the mean mass field and the mean ADCP field.

## **B. MEAN TEMPERATURE, SALINITY, DENSITY, AND GEOSTROPHIC FLOW**

### **1. Method**

Analysis of the hydrographic data acquired during the May 1988 NPS student cruise was conducted in two steps. First, data from each pass were run through a computer program which utilizes horizontal density gradients between stations via the thermal wind equation:

$$\frac{\partial v}{\partial z} = -\frac{g}{f\rho_0} \frac{\partial \rho}{\partial x}, \quad (8)$$

to calculate geostrophic velocities throughout the water column. The second part consisted of averaging the mass field. This was accomplished by averaging the temperatures and salinities at each station (from 5 samples in Line 1 and 4 samples in Line 2). From this mean field, geostrophic velocities and cross-sections were then produced (using equation (8)) for both Lines (Figure 24 on page 42, Figure 26 on page 47, and Appendix A). Because of the sharp topography, the assumed level of no motion used in all geostrophic velocity calculations was the deepest common depth between stations.

As previously stated, the sampling interval was designed so that tidal oscillations could be averaged out of the water column. To measure the success of this particular aspect of the cruise, the mean tidal height for the period was calculated using MBA data, and the variance of tidal heights (from observed heights at each station during sequential passes) about this mean were then derived (Figure 22 on page 39). The calculated variance was relatively small at  $3.45 \times 10^{-3} \text{ m}^2$  for Line 1, and  $1.12 \times 10^{-3} \text{ m}^2$  for Line 2 (Figure 22 on page 39). Initially, averaging schemes using various pass combinations were tested in an attempt to minimize the variance of station tidal height about the MBA tidal mean. Although averaging all line passes did not produce the minimum variance about the MBA mean, it was decided to use all five because it was apparent that the internal tides were not in phase with the surface tidal heights (discussed in section on internal waves).

To further measure the "success" of this averaging process, the net mean mass transport across each line was calculated. In the mean, the net geostrophic mass transport into and out of the bay should be zero, assuming that the barotropic transport was

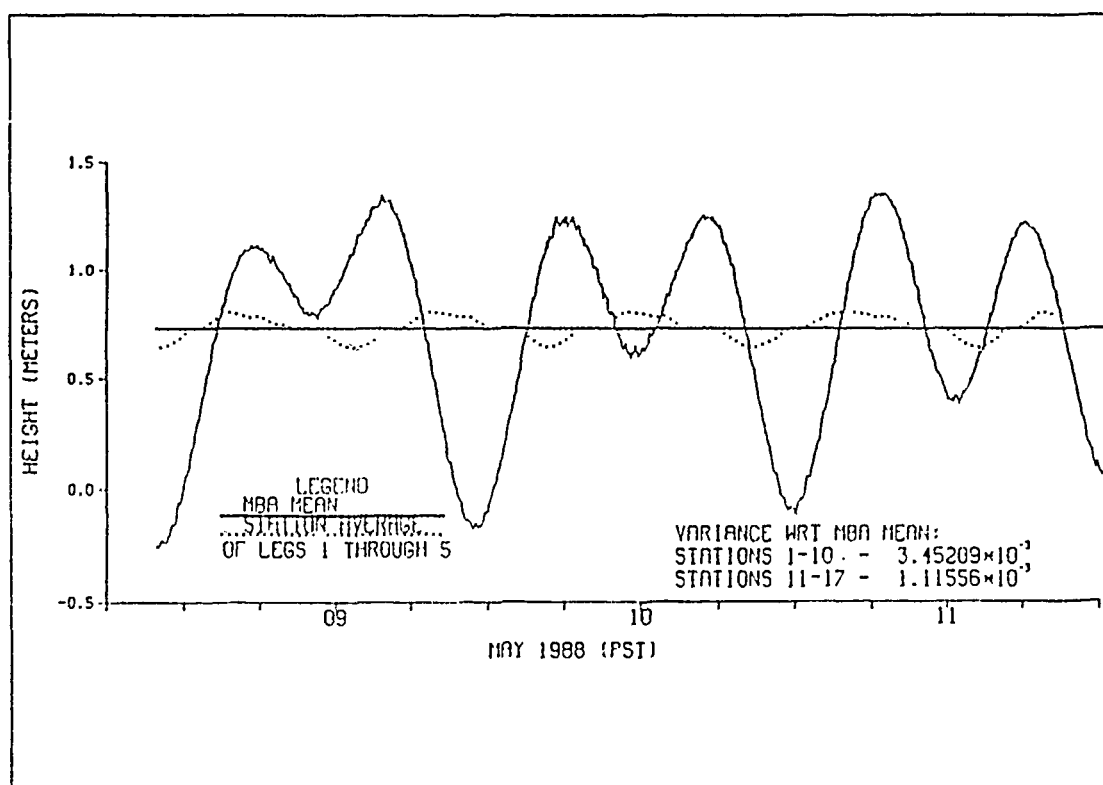


Figure 22. Effective tides: The plot shows surface tidal fluctuations from 5 minute averages of observed tidal height obtained from the MBA data base. Solid line shows mean MBA tidal height, dotted line shows effective surface tide derived through averaging of tidal heights observed at each hydrographic station (see also Figure 17 on page 29). Variance with respect to the MBA mean shown at the bottom right.

minimal. Calculated net volume transport was .152 Sv for Line 1 and .012 Sv for Line 2, both considered balanced within the resolution of the methods used within this study for reasons discussed shortly.

Finally, the standard error of the mean geostrophic velocity ( $\sigma_{\bar{x}}$ ) was calculated (Figure 24 on page 42 and Figure 26 on page 47) using the relationship:

$$\sigma_{\bar{x}} = \frac{\sigma}{(n)^{1/2}}, \quad (9)$$

where the standard deviation ( $\sigma$ ) is:

$$\sigma = \left( \frac{\sum (X - \bar{X})^2}{n} \right)^{1/2}. \quad (10)$$

The derived geostrophic velocities (X) between each station on each individual pass was used as the population (n).

In addition to geostrophic cross-sections, maps of the temperature fields at 0, 50, and 200 dbar, dynamic heights at 0 dbar relative to 50 dbar and 100 dbar and 200 dbar relative to 500 dbar, as well as cross sections of temperature, salinity, and density, were generated (Figure 27 on page 48, Figure 28 on page 49, Figure 23 on page 41, and Figure 25 on page 46). The dynamic height topographies were then used to infer the geostrophic flow patterns.

In summary, three parameters were calculated for each data set to determine the effectiveness of the averaging process in extracting the mean flow: station tidal variance about the MBA mean tidal height, section mean volume transport, and the standard error. Experimentation with the averaging of various pass combinations, to minimize the tidal variance of the data set about the MBA mean tidal height, did not reduce the net volume transport (i.e. increase the implied accuracy of the mean) through the section. This further illustrates the fact that the internal wave field was not in phase with the surface tidal heights. If they were in phase, the most accurate mean flow (smallest net volume transport) would naturally correlate with the averaging scheme which yielded the smallest variance about the mean MBA tidal height during the period. Since this was not the case, the decision to average all 5 passes in Line 1 and all 4 passes in Line 2 was arrived at, from a purely statistical viewpoint, to maximize the number of degrees of freedom. Statistically, this method worked well since calculated standard errors were smaller than the derived mean. With this in mind, the overall data acquisition method was successful at minimizing the variance of the tidal heights and creating a nearly balanced mean volume transport by virtue of pass averaging alone. The method was not entirely successful however, at systematically (deterministically) reducing the high frequency internal motions.

## 2. Results

### *a. Mean Property Cross Sections, Geostrophic Flow, and Mass Transport*

(1) *Line 1.* The Line 1 mean temperature and salinity cross sections (Figure 23 on page 41) indicate an area of warm, fresh water at the surface (greater than 12°C) extending across the mouth of the bay from station 5 to station 9. This warm, fresh "pool" of water appears well imbedded in the vertical structure and extends down to approximately 100 dbar, as the 8.5 and 9°C isotherms indicate. At deeper depths, over the Monterey Submarine Canyon, upwelling of cold water, most notably along the northern shelf break, appears to dominate the temperature field as shown by the 8 and

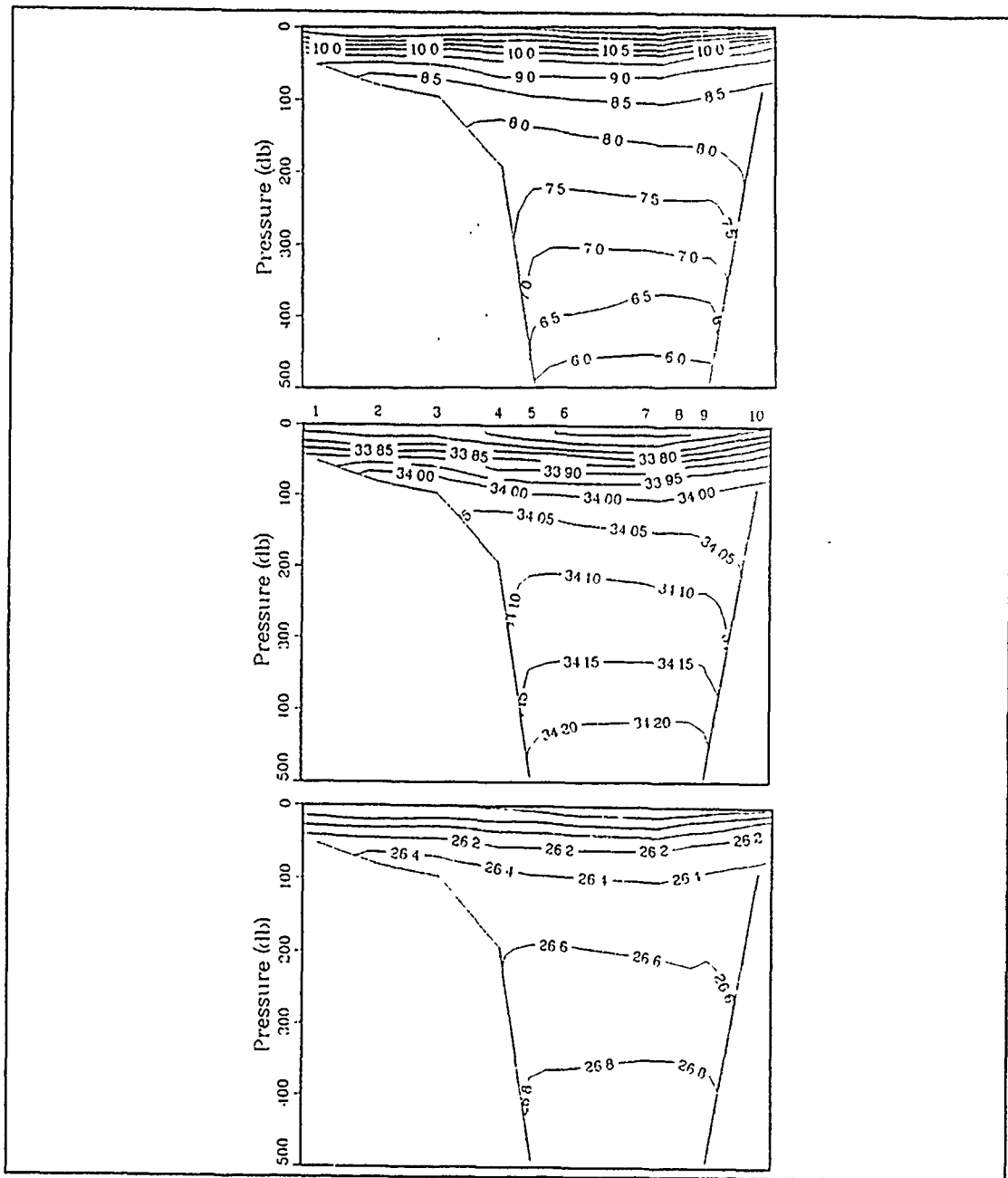


Figure 23. Line 1 mean temperature, salinity, and density cross sections: Figures depict mean temperature ( $^{\circ}\text{C}$ , top), salinity (psu, middle), and density ( $\text{kg m}^{-3}$ , bottom) sections for Line 1. Caution should be noted in interpreting deep isolines adjacent to the canyon walls. These steep slopes more than likely do not exist and are merely the product of the contouring program used to develop these graphs. Station positions are indicated across the top of the salinity section (see also Figure 16 on page 28 for locations).

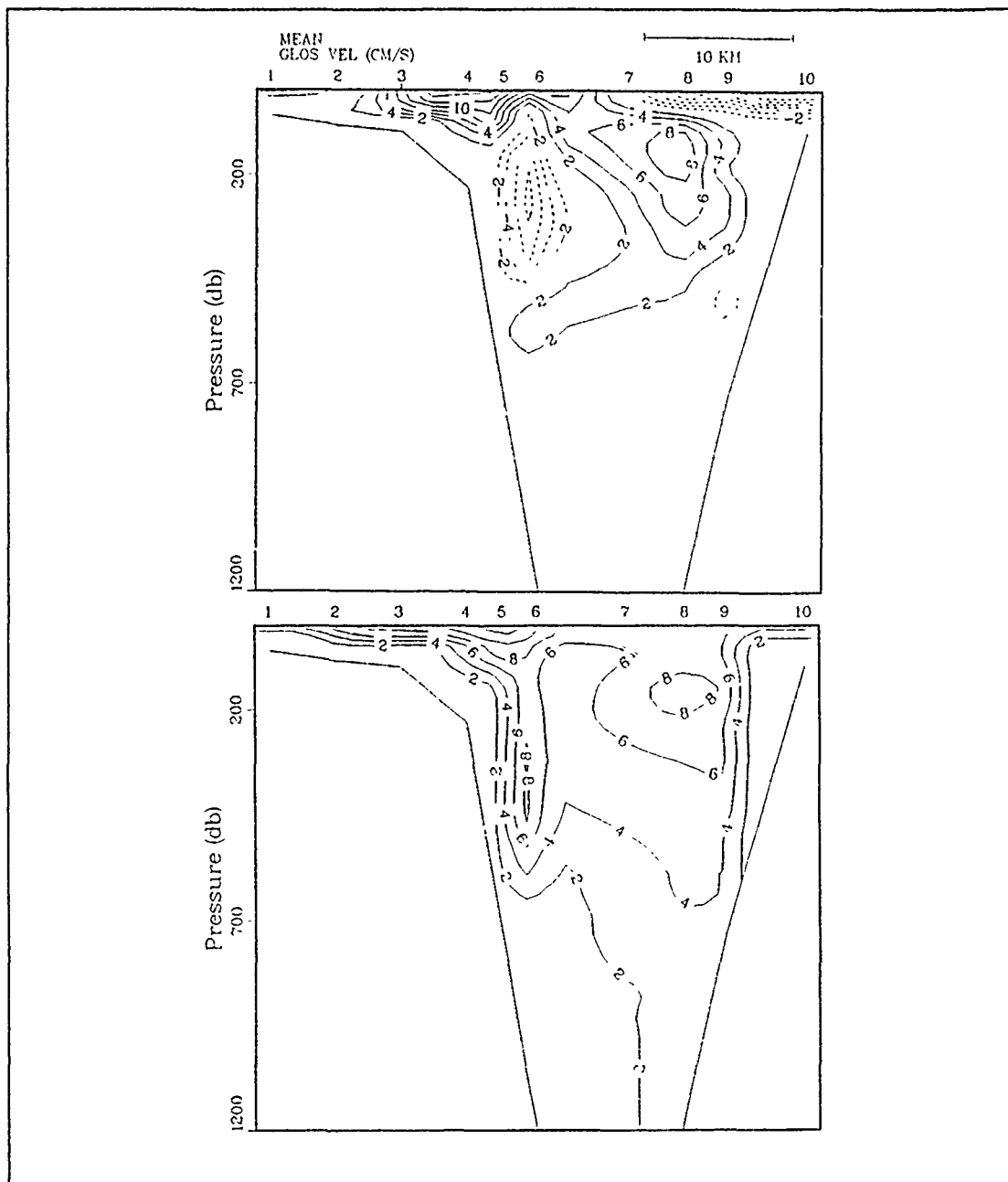


Figure 24. Line 1 mean geostrophic flow field and standard error: Top figure is the mean geostrophic flow, bottom is the standard error. Hydrographic stations are notated at the top of the section and are situated across the mouth of Monterey Bay (Line 1, see also Figure 16 on page 28 for station locations). Solid lines depict flow into the bay, dashed lines show flow out of the bay. Geostrophic velocities were calculated using the deepest common depth between stations as the level of no motion.

8.5°C isotherms. The salinity cross section shows the fresher water (33.65 psu) located between stations 6 and 9. Again, some indication of upwelling of denser, saltier water from the canyon onto the shelf region is indicated (again most notably over the northern shelf) by the 34.05 and 34.00 isohalines. Density anomaly cross sections (Figure 23) reflect the temperature and salinity fields by indicating relatively light water located in the top 100 dbar of the water column and centered nearly over the canyon axis with denser water extending up onto the northern shelf along the canyon wall from a depth of 200 m.

The calculated mean geostrophic flow (Figure 24 on page 42, and Appendix A) reveals two apparently separate flow patterns. At the surface (0 to approximately 75 dbar) flow is split into two regimes: broad inflow across the northern half of the Monterey Bay from stations 1 to 7; and, outflow across the southern half of the bay from stations 7 to 10. Inflow extends to a somewhat greater pressure (125 dbar) than the outflow region (50 dbar). Maximum surface inflow was calculated at 15.6 cm  $s^{-1}$  between stations 3 and 4 and a maximum outflow of -18.6 cm  $s^{-1}$ , situated between stations 9 and 10, was indicated. Corresponding standard errors of the mean at these locations were 9.9 and 4.8 cm  $s^{-1}$  respectively (Figure 24 on page 42). Analysis of the current speed and direction from the MBA current meter in the southern bight area (closest to station 10) over the period showed northwest/southeast flow reversals with the seaward flow predominating (Figure 21 on page 37). Also evident was the correlation between the strongest flow (highest velocities) and the seaward direction. Mean current speed and direction, derived from these data during the period of the May cruise, was 4.5 cm  $s^{-1}$  towards 245°T, or seaward. This outflow is smaller than the noted geostrophic flow between stations 9 and 10, not unusual considering the current meter's close proximity to shore. The second flow pattern is located over the Monterey Submarine Canyon between 100 and 600 dbar and consists of outflow along the northern wall of the canyon, with inflow indicated over the southern half of the canyon. The cores are found at 250 dbar (downcanyon flow of 10.6 cm  $s^{-1}$ ) between stations 5 and 6, and at 150 dbar (upcanyon flow of 10.1 cm  $s^{-1}$ ) under station 8. Standard errors calculated at these positions and depths yielded values of 8.3 and 9.1 cm  $s^{-1}$  respectively, showing that the deep flows were barely resolved with this averaging technique. The mean flow pattern shows strong vertical shears near stations 6 and 8, along with weaker horizontal shear zones over the center of the bay. Standard errors at each level (Figure 24 on page 42) indicate that the derived surface mean flow is much more re-

solved (especially the outflow in the southern half of the bay, past the Monterey Peninsula) than the mean flow at depth, which barely surpasses the standard error values.

The net mass transport calculated for the mean flow was .152 Sv. This result was not surprising and appears to be within the resolution of the geostrophic methods exploited for a number of reasons, namely:

- The geostrophic method does not take into consideration any non-linear effects, which can produce errors up to 10% in some areas of the ocean such as near eddies, high shear zones, etc. Because of the Monterey Bay's geometry, and apparently active internal wave system, non-linear processes more than likely are at work and are neglected in geostrophy. Rough estimates of the extent of non-linearity were obtained through calculations of the Rossby number ( $R_o$ ):

$$R_o = \frac{V}{fL}, \quad (11)$$

where  $f$ , the coriolis parameter is  $O(10^{-4})$ ; velocities ( $V$ ) are  $O(.1 \text{ m s}^{-1})$ ; and typical length scales ( $L$ ), estimated by the computed first internal Rossby radius of deformation (Appendix D), of  $O(5 \text{ to } 15 \text{ km})$ . Values range from approximately .1 to .2, implying that up to 20% of flow may be affected by non-linear processes in Monterey Bay.

- Recent studies (Tisch, 1990) indicate that geostrophic velocities calculated between stations with close spacing typically have higher errors than those calculated at larger grid spacing. When station spacing is less than approximately 4 to 5 km, which was the case in this study for nearly all the stations, small errors in positioning and measurement, along with the ship drift, tend to propagate larger errors in geostrophic velocity calculations than values derived from stations situated farther apart.
- Geostrophic velocities were calculated using the common deepest depth between stations. Thus, no deep flow (greater than 1000 dbar) is resolved in this study.
- Approximately 4 km of the bay, on both ends of Line 1, were not covered. This was particularly important in the southern part of the bay where strong outflow was indicated right up to station 10. If strong outflow continued right up to the Monterey Peninsula, a mass transport rate of roughly -.036 Sv ( $4000 \text{ m} \times 50 \text{ m} \times 0.18 \text{ m s}^{-1}$ ) was missed in Line 1.
- The barotropic flow was not resolved through geostrophy. Rough estimates of this component were obtained by first calculating the surface area within the bay and bounded by Line 1 ( $882 \text{ km}^2$ ), then computing the flow that would be required to raise the water level 1.5 m (approximate tidal range of the bay) and the ensuing transport rate. From these calculations, barotropic flow was determined to be on the order of .1 to .3  $\text{cm s}^{-1}$  which would account for a mass transport of  $\pm .06 \text{ Sv}$ .

Therefore, errors on the order of .1 Sv can be accounted for by reasoning of missed coverage across the bay, deep flow, and barotropic transport. Errors of  $O(.1) \text{ Sv}$  are also probably a realistic estimate of errors propagated through geostrophy (i.e. non-linearity, station spacing, assumed level of no motion, etc.). In view of this, and calculations of

the standard error, the derived mean flow field appears balanced within the limitations of available data and methods. Within the confines of this study, the term "mean flow" refers to the flow during the period from 08-11 May 1988 and may not represent a "typical" flow pattern in the Monterey Bay (if such a pattern even exists). An attempt will be made later to relate this "mean flow" to processes believed to have been occurring at the time these particular data were collected.

(2) *Line 2.* The mean Line 2 temperature and salinity cross sections (Figure 25 on page 46) show smaller perturbations in the thermocline than the Line 1 data. Somewhat warmer water can be seen at the surface over the northern and southern shelf regions but overall isotherms are relatively level. This is in contrast to the Line 1 isotherms which show a temperature maximum over the center of the canyon. This may be a consequence of increased heating of the shallower shelf waters which rapidly dominate the bathymetry as the canyon head is approached. This warmer water situated over the shelf regions of the inner portions of the bay can also be seen on the 08 May 1988 satellite imagery (Figure 32 on page 58), discussed later. The salinity field also displays relatively level isohaline contours within the thermocline except for somewhat fresher water indicated over the southern shelf region (Figure 25 on page 46). The cross section of mean density shows somewhat lighter (less dense) water situated over the northern and southern shelf regions as indicated by the 25.6 isopycnal.

The mean currents derived for Line 2 shows broad inflow over the center of the section between stations 15 and 12 with a maximum at the surface between stations 12 and 13 of  $7.4 \text{ cm s}^{-1}$  and a subsurface maximum at 50 dbar of  $6.2 \text{ cm s}^{-1}$  (Figure 26 on page 47). Standard errors were calculated at  $2.7$  and  $1.4 \text{ cm s}^{-1}$  respectively. The calculated mean outflow was again narrower, but stronger, than the inflow, and confined mainly to the southern portion of the bay, over the shelf region, between stations 11 and 10. Maximum outflow was calculated at  $15.9 \text{ cm s}^{-1}$  in this area with a standard error of  $6.2 \text{ cm s}^{-1}$ . As noted earlier, both mean velocities (hence, mass transport) and velocities calculated during each pass, were smaller than those calculated for Line 1, implying that much of the circulation derived in Line 1 is closed, and does not extend significantly into the heart of the bay itself. The net mass transport, derived from mean flow values, was .012 Sv (an order of magnitude smaller than that of Line 1). Again, similar arguments for not attaining mass balance closure in Line 1 can also be applied to Line 2.

(3) *Mean Temperature and Dynamic Height Maps.* The mean surface temperature map (Figure 27 on page 48), interpreted by hand, depicts two pools of



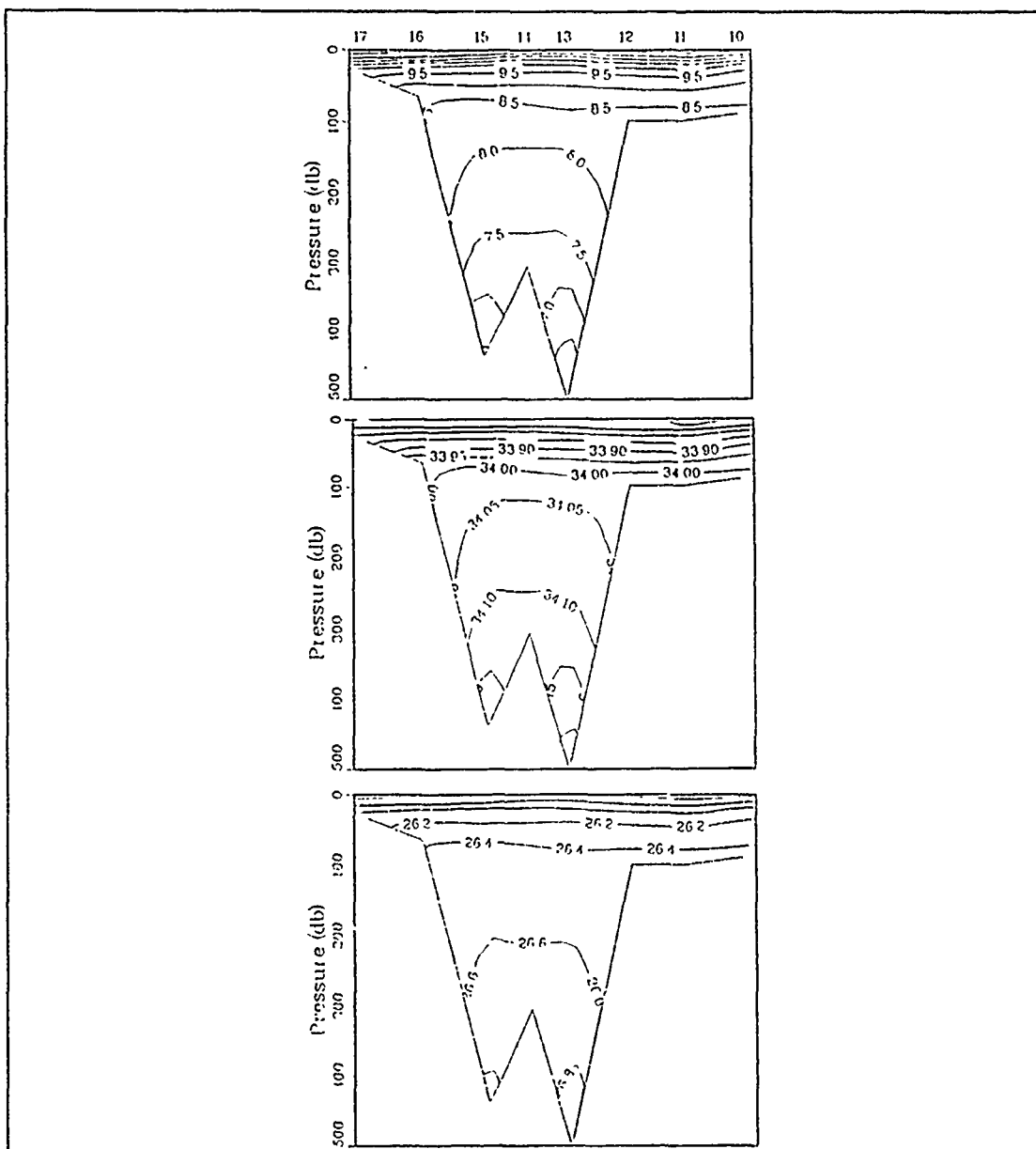


Figure 25. Line 2 mean temperature, salinity, and density cross sections: Figures depict mean temperature ( $^{\circ}\text{C}$ , top), salinity (psu, middle), and density ( $\text{kg m}^{-3}$ , bottom) sections extending roughly north-south across the center of the Monterey Bay (Line 2) and shows both the Soquel (left) and Monterey (right) Submarine Canyons. Caution should be noted in interpreting deep isolines adjacent to the canyon walls. These steep slopes more than likely do not exist and are merely the product of the contouring program used to develop these graphs. Station positions are indicated across the top of the temperature section (see also Figure 16 on page 28 for locations).

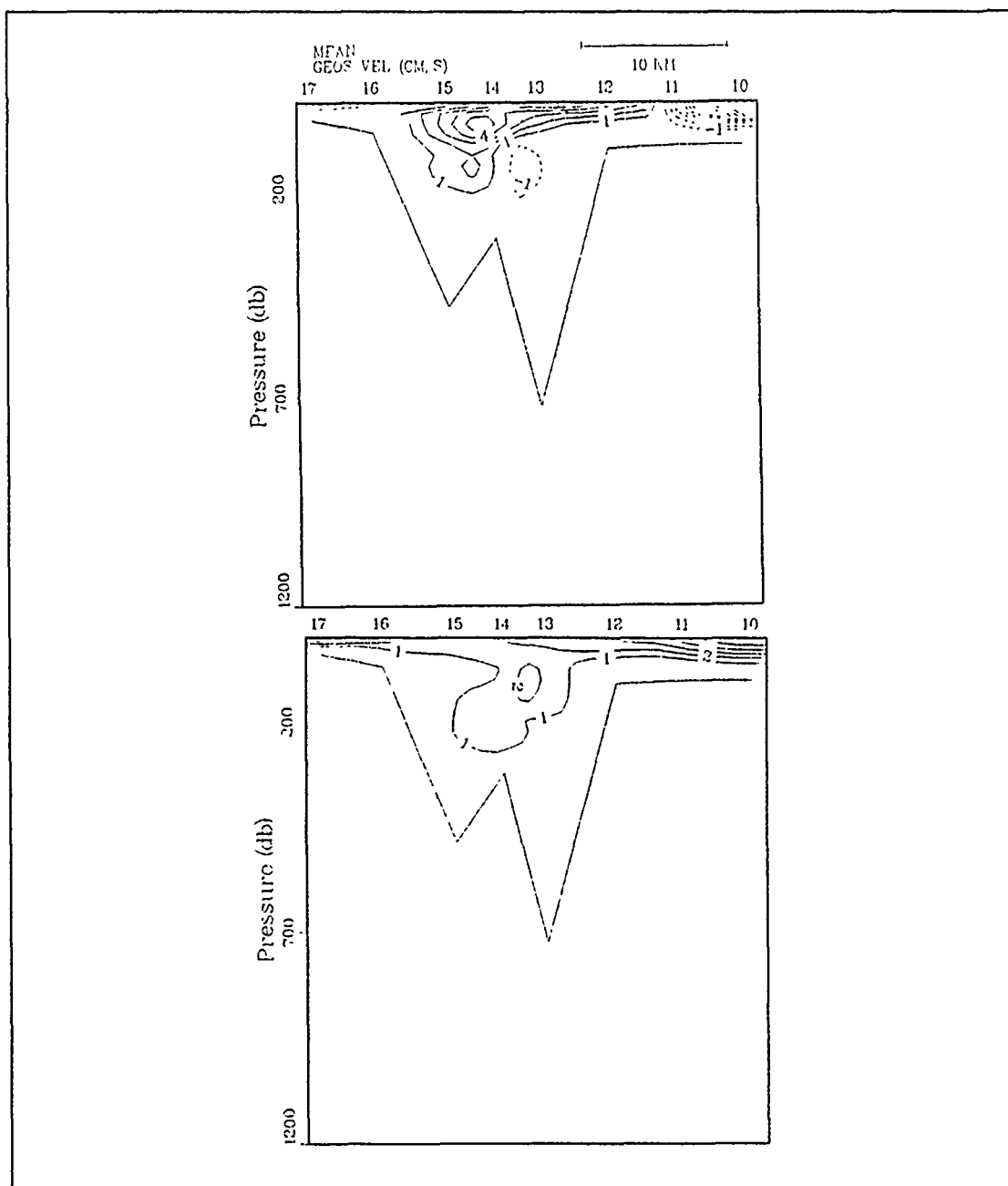


Figure 26. Line 2 mean geostrophic flow field and standard error: Top figure is mean geostrophic flow, bottom is standard error. Hydrographic stations are notated at the top of the section and run roughly north-south across the center of Monterey Bay (Line 2, see Figure 16 on page 28 for station location). Solid lines depict flow into the bay, dashed lines show flow out of the bay. Geostrophic velocities were calculated using the common deepest depth between stations as the level of no motion.

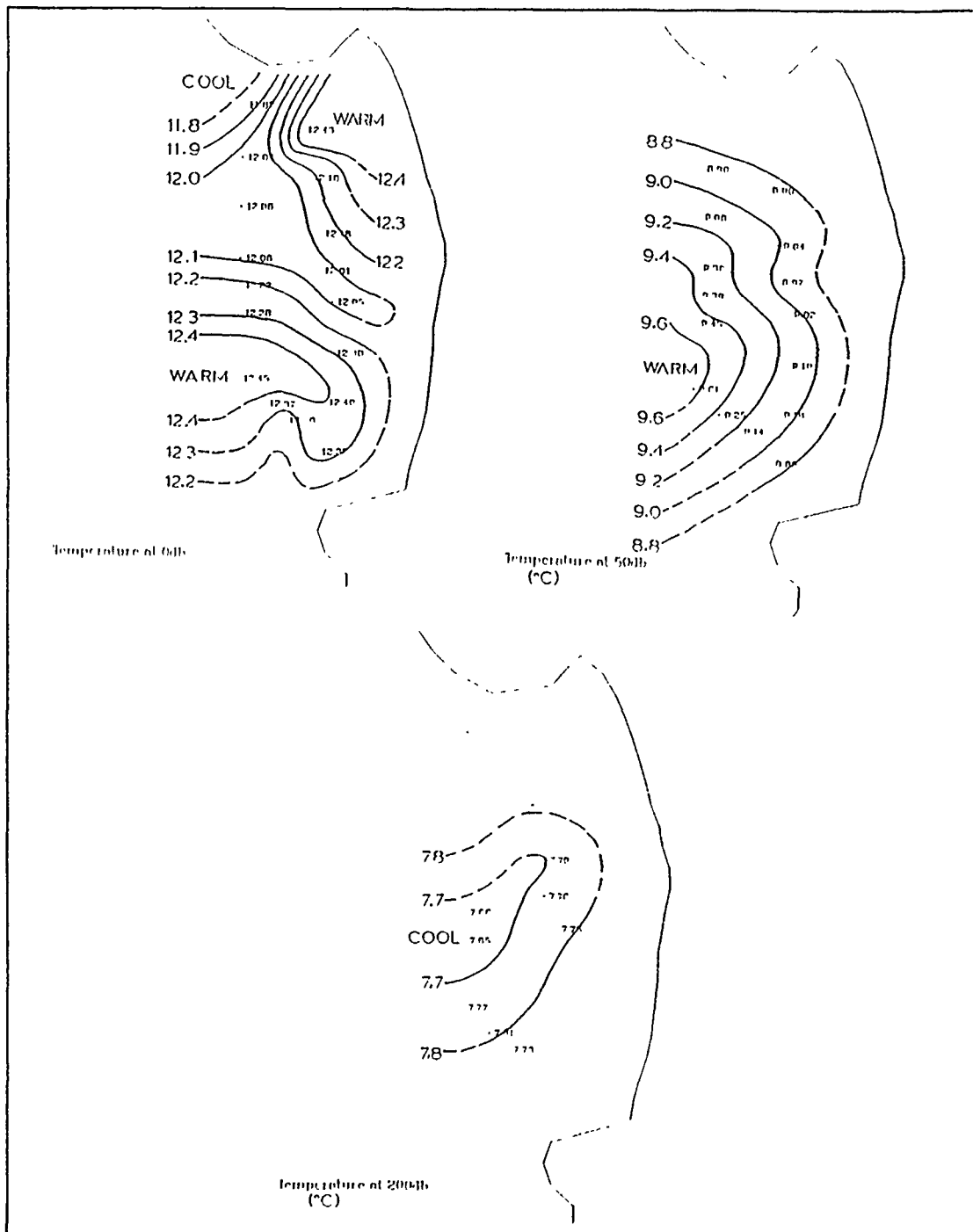


Figure 27. Mean temperature fields: Mean temperature fields (°C) on the 0 dbar (top-left), 50 dbar (top-right), and 200 dbar (bottom) pressure surfaces.

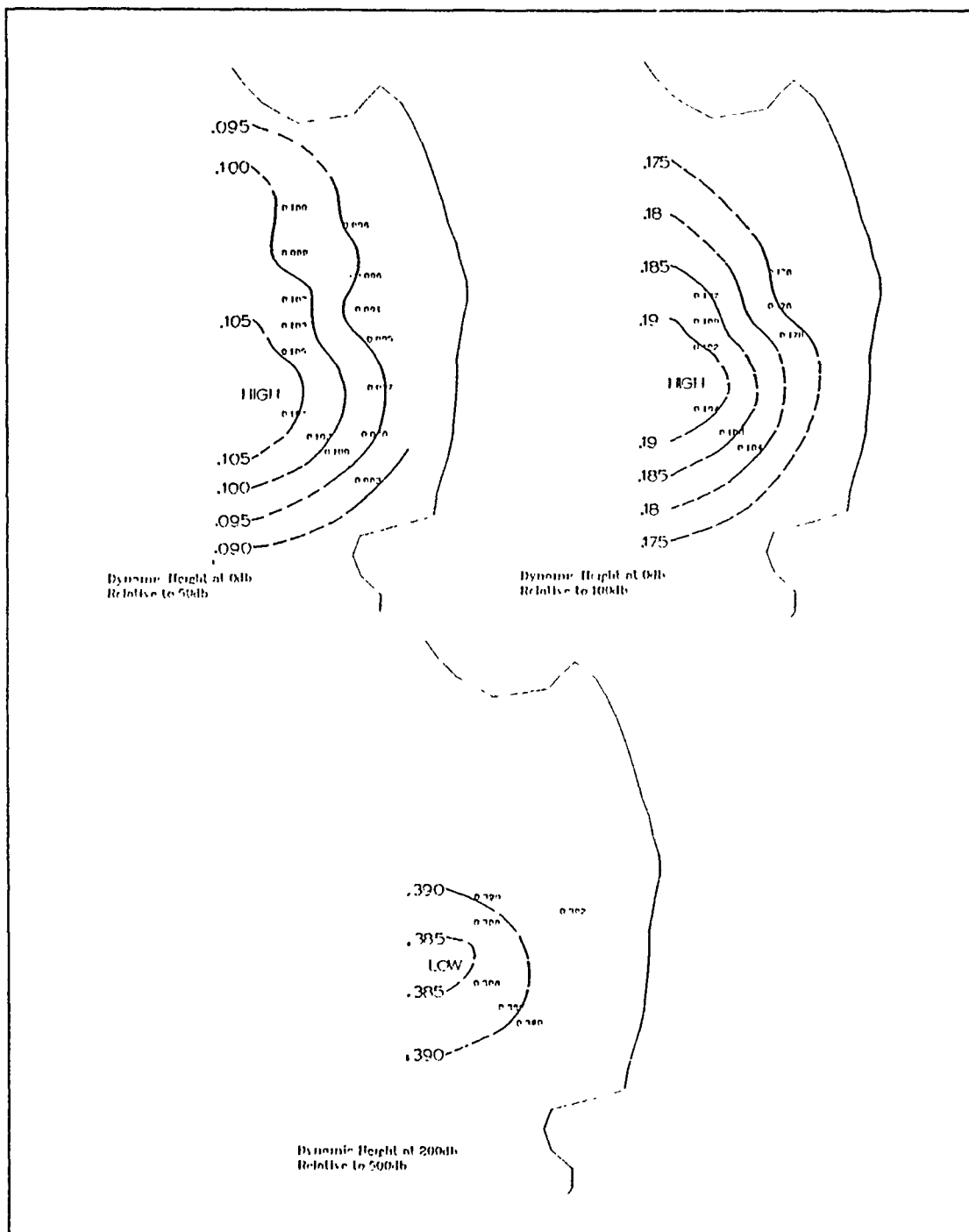


Figure 28. Mean dynamic height fields: Mean dynamic heights at 0 dbar relative to 50 dbar (top-left) and to 100 dbar (top-right) and at 200 dbar relative to 500 dbar (bottom).

warm water at the surface. The first is centered over the mouth of the canyon with a  $12.45^{\circ}\text{C}$  maximum at station 7, and the second appears to be contained in the northern bight area with a  $12.43^{\circ}\text{C}$  maximum at station 17. The pool of warm water centered at station 7 maintains its identity down to 50 dbar (the approximate base of the mixed layer), with station 7 retaining the maximum 50 dbar temperature at  $9.61^{\circ}\text{C}$ . Evidence of the warmer water present at the surface in the vicinity of the northern bight disappears at depth. This may be a consequence of the previously mentioned surface heating of shelf waters in the northern bight, which typically does not extend down through the thermocline. Other satellite SST data (Tracy, 1990) also show enhanced surface heating in the northern bight, possibly since the area is sheltered from the northwesterly winds by the Santa Cruz mountains. Temperatures at 200 dbar are slightly colder over the canyon, especially towards the northern wall, as evidenced by the minimum temperature ( $7.65^{\circ}\text{C}$ ) at station 6.

The mean dynamic topographies (Figure 28 on page 49) at the surface relative to 50 and 100 dbar, show higher relative heights near the mouth of the bay, roughly centered over the canyon axis with maximum values of .192 and .194 dy m at stations 6 and 7 respectively and implies anticyclonic geostrophic circulation within the mixed layer over the Monterey Bay. Deeper circulation is cyclonic with low dynamic heights over the canyon axis at stations 6 and 7 of .388 and .386 dy m respectively.

### C. MEAN FLOW FROM ADCP DATA

#### 1. Method

As an alternative method in determining a mean flow (and to compare with geostrophically derived mean velocities), ADCP data were analyzed for Line 1. This was accomplished by first breaking the ADCP data up into two portions, the first with the ship on a heading of  $180^{\circ}\text{ T}$  (i.e. between stations 1 and 7), and the second part, when the ship was on a heading of roughly  $145^{\circ}\text{ T}$  (between stations 7 and 10). This was necessary so the applied program could compute velocities that would correspond to the directions obtained from geostrophic calculations. Data were averaged every 4 km along each portion of Line 1 (stations 1-7 and 7-10). After the velocities for each pass were computed, they were again averaged, over all 5 passes. Horizontal distance averaging was done since the 3 minute profiles were not co-located from pass to pass (see Figure 29 on page 51). Finally, mean files from both portions (stations 1-7 and 7-10) were combined to produce one plot of ADCP mean velocities that would extend from station 1 to 10 so that direct comparisons could be made with the geostrophic velocities.

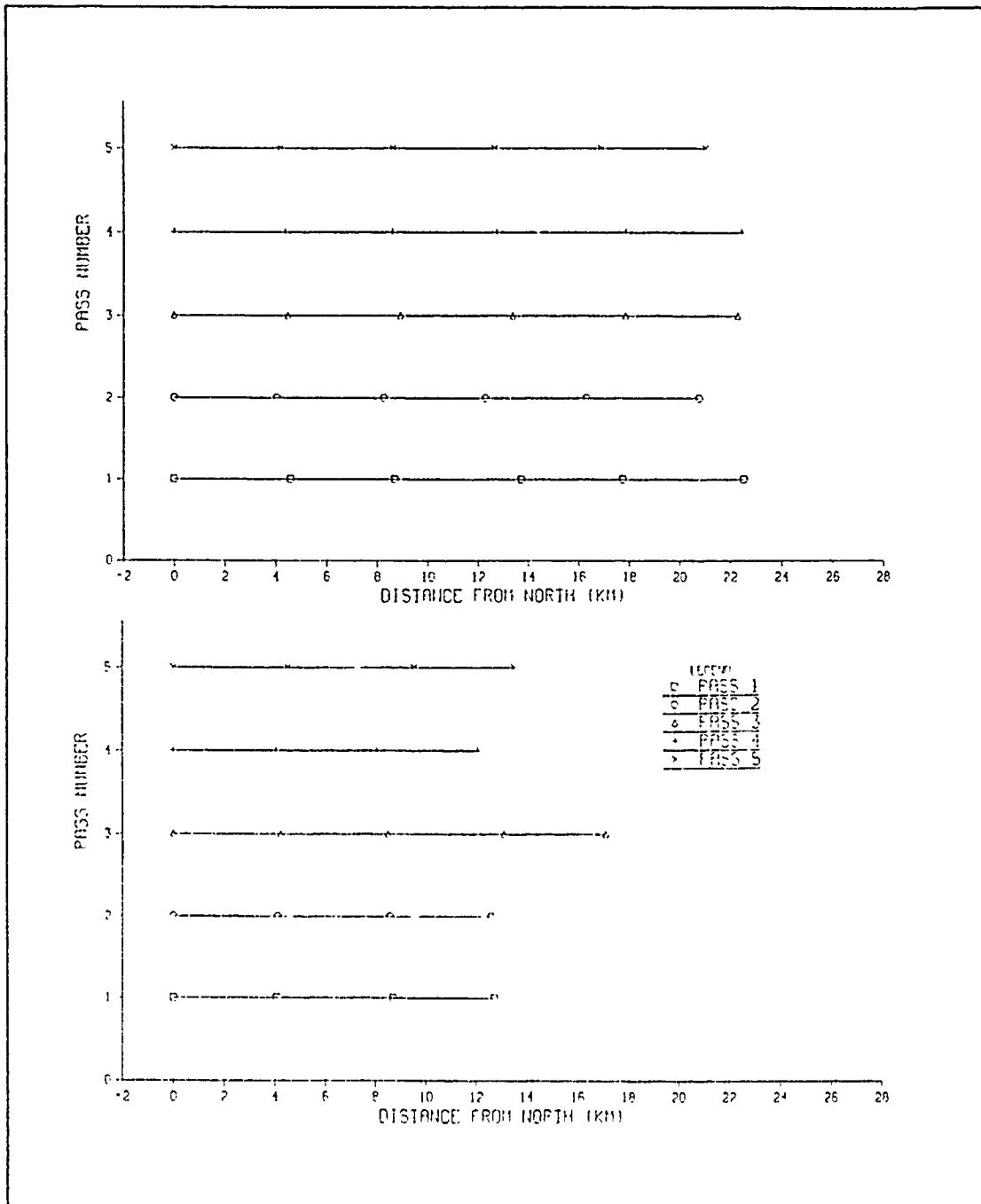


Figure 29. Line 1 ADCP averaging scheme: Top figure shows averaging interval for stations 1-7 and the bottom figure for stations 7-10. Horizontal averaging as well as vertical averaging of each pass was done to minimize errors induced through slight offsets of data profiles along each pass.

(see Figure 30 on page 53, and Appendix B for numerical outputs). Standard errors were calculated using the mean ADCP velocities and the velocities obtained during each separate pass in the same manner as was done with the geostrophic data.

## 2. Results

### *a. ADCP Velocities Obtained During Successive Passes of Line 1*

Contrary to velocities obtained through geostrophy from individual passes, ADCP velocities will not be influenced by mass fluctuations and detect the total velocities (both the geostrophic and ageostrophic components) present at the time. Although ADCP velocities collected during each pass undoubtedly are also influenced by internal wave motions, it is felt that results obtained during each pass warrant a brief description.

ADCP velocities obtained during successive passes of Line 1 ranged from light flow up to  $20 \text{ cm s}^{-1}$  in pass 3. Numerous current reversals between successive passes were noted and effectively demonstrate the active dynamical processes at work within the bay. Also, large shear zones, both in the vertical and horizontal, were in evidence in virtually all passes. In general, ADCP velocities were less than the geostrophic velocities calculated during each pass, especially at depth. This is not surprising since the calculated geostrophic response to the large swings in isopycnal slopes, created by the large amplitude internal waves, would tend to produce unrealistically large velocities, especially in the thermocline.

No definite relationship between the surface tidal heights and flow within the bay could be determined from the ADCP passes. During pass 3 of Line 1, the surface tide was in the ebbing phase between stations 4 and 9 (see Figure 17 on page 29), going from Higher High Water (HHW) at station 4 to Higher Low Water (HLW) at station 9. During this period the ADCP data depicted virtually all flow going upcanyon (into the bay) with a  $20 \text{ cm s}^{-1}$  maximum centered over the canyon axis at a pressure of approximately 100 dbar. On the next pass (pass 4), the tide was in a flooding stage between station 5 (at Lower Low Water (LLW)) and station 10 (at Higher High Water (HHW)). In this case a total reversal in flow was noted with no evidence of the  $20 \text{ cm s}^{-1}$  maximum previously noted. Virtually all flow was directed out of the bay with a  $-18 \text{ cm s}^{-1}$  maximum at the surface near stations 8 and 9. These two passes tend to support Gatje and Pizinger's (1965) current meter observations which correlated downcanyon flow with surface flood tides, and upcanyon flow with surface tidal heights in the ebbing stage. The apparent correlation between surface tidal heights and bay flooding/flushing periods implied by these two passes does not hold in the other passes however. For instance, pass 1, again in a flooding stage from LLW at station 1 to Lower High Water

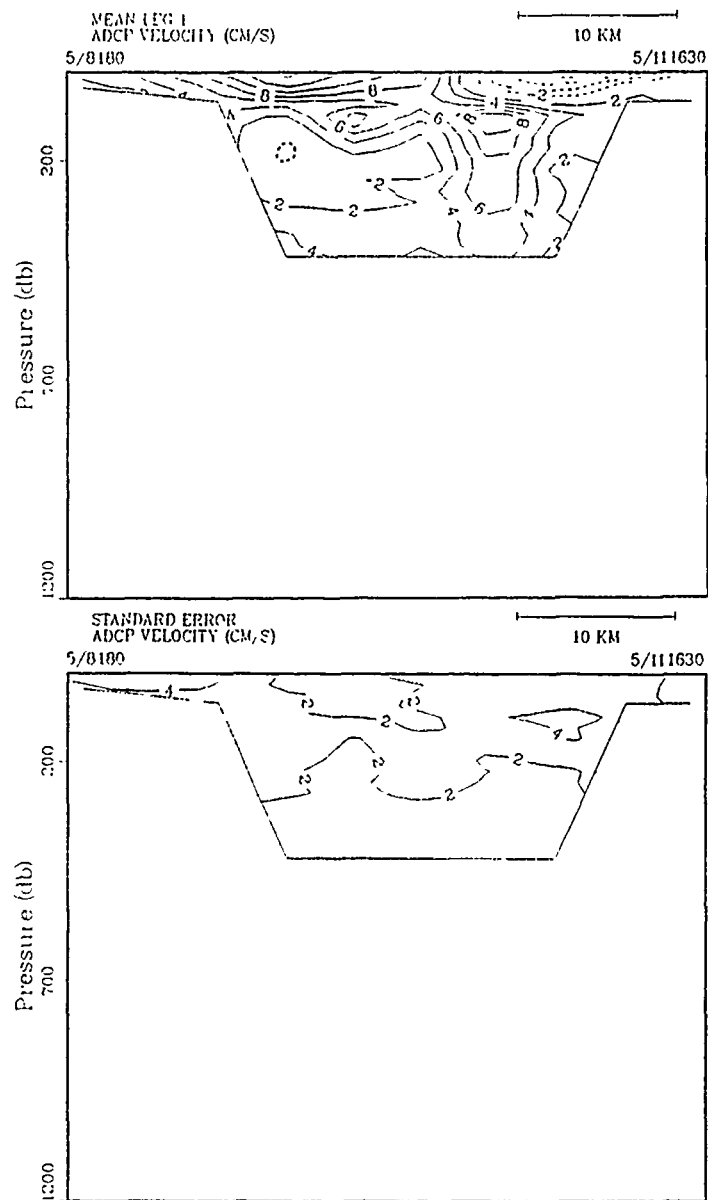


Figure 30. Line 1 mean ADCP velocities and standard error: Top figure shows mean ADCP velocities along Line 1. Negative values indicate flow out of the bay, positive values indicate flow into the bay. Bottom figure represents standard error values calculated for the ADCP velocities.



(LHW) at station 10, depicted outflow over the northern shelf and along the north canyon wall, but inflow over the center of the canyon and over the southern shelf. Also, during pass 2, which went from HHW at station 4 to nearly LLW at station 10 (ebbing tides), the ADCP velocity section depicted outflow at the surface but inflow at 100 dbar. These passes tend to support observations made by Shepard, et al. (1979), and by Broenkow and McKain (1972), that the baroclinic and barotropic tides are generally not in phase.

***b. Mean ADCP Velocities and Standard Errors***

The mean ADCP velocity structure shows broad surface inflow over the northern half of the bay from station 1 to station 7 with the core situated approximately 17 km south of station 1 having a maximum velocity of  $15 \text{ cm s}^{-1}$ . A narrower region of outflow is revealed along the southern half of the bay, south of station 7, with a maximum velocity of  $10.5 \text{ cm s}^{-1}$  centered approximately 34.5 km south of station 1 along the Line 1 track. Weak outflow ( $-2 \text{ cm s}^{-1}$ ) is indicated near the northern canyon wall at 182 dbar with stronger inflow ( $13.7 \text{ cm s}^{-1}$  at 150 dbar) indicated over the southern half of the canyon axis between stations 7 and 8. Standard errors ranged from  $1.7 \text{ cm s}^{-1}$  for the surface inflow center to  $4.1 \text{ cm s}^{-1}$  for the core of the deeper inflow between stations 7 and 8 (see Figure 30 on page 53). This represents a better signal to noise ratio for the ADCP data than for the velocities derived through geostrophy and implies that ADCP techniques may have an advantage over geostrophy when attempting to determine mean flow patterns within the Monterey Bay.

***c. Comparison of Mean ADCP and Geostrophic Velocities***

Table 3 on page 55 summarizes the maximum velocity values and their locations, obtained by using both mass averaged geostrophy and by averaging the ADCP velocities. Considering the major differences in the two techniques, the results of both methods compare favorably in the location and in the magnitude of the flow centers. Horizontal differences in the location of maximum velocities were at most 4 km's apart. This is expected since the ADCP continuously collects and averages velocity data, while geostrophic velocities can only be calculated for the water column centered between CTD stations. Maximum velocities at depths were also fairly close, differing by an average of 50 m. Velocity magnitudes were comparable for the surface flows, differing by an average of  $4 \text{ cm s}^{-1}$ . At depth, velocities at the inflow region agreed well on the southern side of the canyon, with differences of only  $3.6 \text{ cm s}^{-1}$  between the two methods. The strong geostrophic outflow region at depth along the northern slope of the canyon did not fare as well. The sense of flow was the same but the velocities differed

by almost  $8 \text{ cm s}^{-1}$ . A few possible explanations for this discrepancy in flow at this location follow:

- Anomalously high AGC values were observed during the processing of the ADCP data (see Chapter II) over this region. The "scattering layer", cited as the possible culprit for the unusual signal, could have adversely effected ADCP measurements below, rendering data collected in this area "suspect."
- Standard error calculations are smaller than mean values of both geostrophic and ADCP flow, with the exception of the ADCP mean obtained for this deep outflow region where the mean is  $-2.10 \text{ cm s}^{-1}$  and the standard error is  $3.18 \text{ cm s}^{-1}$ . This is another reason to label the ADCP data obtained in this area as "suspect".
- CTD station spacing was very tight (approximately 2 km vice 4 for the other stations) over the northern canyon shelf whereas ADCP velocities were averaged every 4 km over the whole of Line 1. This larger averaging interval could have resulted in smoothing the center of the outflow core and resulted in a much smaller velocity.

**Table 3. SUMMARY OF LINE 1 MEAN VELOCITIES:** Negative velocities indicate flow out of the bay, positive values denote flow into the bay.

Type	Location (km from sta 1)	Depth(dbar)	Velocity ( $\text{cm s}^{-1}$ )	Std Err ( $\text{cm s}^{-1}$ )
GEOSTROPHIC	13.16	0	15.62	9.95
ADCP	17.32	0	14.97	1.72
GEOSTROPHIC	33.17	0	-18.57	4.81
ADCP	34.48	0	-10.48	3.49
GEOSTROPHIC	16.78	250	-10.65	8.3
ADCP	17.32	182	-2.10	3.18
GEOSTROPHIC	25.89	150	10.15	9.11
ADCP	29.99	118	13.71	4.10

#### D. DESCRIPTION OF NOAA AVHRR SATELLITE IMAGERY

Cloud-free Satellite imagery was available for 04, 08, and 11 May 1988 (Figure 31 on page 57 and Figure 32 on page 58). The 04 May image reflects strong coastal upwelling near Pt. Ano Nuevo, 35 km to the north of the Monterey Bay. This cold, upwelled water ( $7$  to  $8^\circ\text{C}$ ) appears to extend into Monterey Bay from the north. Warm water from inside the bay appears to be advecting southward past Pt. Sur. The implied circulation is inflow at the north of the bay and outflow at the south.

The images taken on 08 and 11 May are nearly identical and only the 08 May image is shown. Skin temperatures over the bay showed a sharp rise in temperature of approximately  $5^{\circ}\text{C}$  over the four day period from 04 May. Whether this is a result of warm water advected into the bay, or simply a product of solar heating which ensued upon the cessation of winds and upwelling, cannot be determined. Coastal upwelling is still in evidence to the north and south of the bay on the 08 May image. Colder waters, either being upwelled along the coast or advected into the northern part of the bay, again appear on the 11 May imagery.

## **E. METEOROLOGICAL SYNOPSIS**

### **1. The Period Prior to Data Acquisition (25 April - 08 May 1988)**

On 25 April, the central California coast was dominated by a 1026 mb high pressure center situated over the center of the state. This pattern resulted in a relatively light pressure gradient overall, allowing the mesoscale land-sea breeze processes to dominate the flow pattern. A low pressure system was located approximately 900 n mi west of Washington state. By the 26<sup>th</sup> the high began to break down under the influence of this low pressure system and by the 27<sup>th</sup>, this low, with its associated cold front, passed over the Monterey Bay. While no significant weather or winds were produced by this system, it did clear the path for a second cold frontal system which was approximately 600 n mi west of Monterey Bay at this time. By 28 April, the pressure field in the vicinity of the Monterey Bay began feeling the influence of this system generating a light ( $3$  to  $5\text{ m s}^{-1}$ ) southwesterly pre-frontal wind region regime. This strong frontal system passed over the Monterey Bay early in the morning of 29 April causing the winds to rapidly veer to the northwest and increase in magnitude to  $18\text{ m s}^{-1}$ . As this front continued eastward across the state, strong high pressure ridging behind this front moved over the Monterey Bay and maintained a strong pressure which continued generating  $13$  to  $18\text{ m s}^{-1}$  winds over the area through the morning of 01 May. From the afternoon of 01 May through 07 May, the winds remained out of the northwest at moderate velocities ( $5$ - $8\text{ m s}^{-1}$ ) increasing slightly the morning of the 4<sup>th</sup> when a third front, weaker than the previous one, passed over the Monterey Bay. In summary, this period was very "unsettled" for May, with three separate frontal systems passing over the bay. Winds were predominantly out of the northwest to north, at times very strong, for a period of approximately nine days, from 29 April to 07 May.



Figure 31. NOAA AVHRR satellite imagery from 2336 Z 04 May 1988: Darker shades along the coast to the north and south of the Monterey Bay depict colder water. Lighter shades over the extreme eastern portion of the bay and within the northern and southern bights of the bay depict warmer water. The light streak extending southwest from the Monterey Peninsula represents warmer waters. The large areas of black over the ocean are cloud cover. Latitude and longitude lines are in one-half degree increments. Rectangle at left is SST scale meant for use with color copy and is not usable with this black and white reproduction.

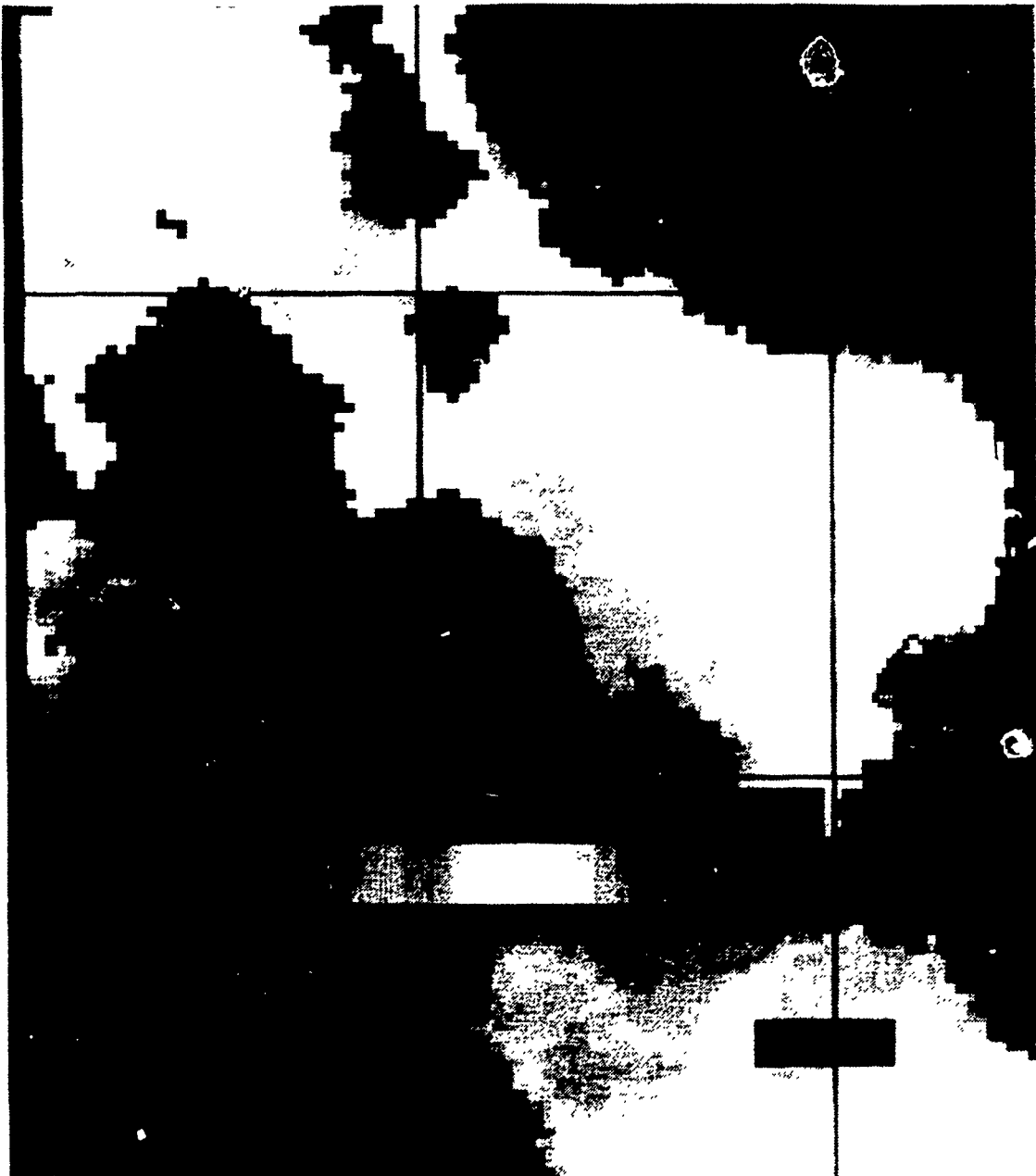


**Figure 32.** NOAA AVHRR satellite imagery from 2247 Z 08 May 1988: Darker shades within the Monterey Bay and to the west of the bay depict warmer water. Darker areas along the coast, south of the Monterey Peninsula, depict cooler upwelled water. Black areas over the ocean are clouds. Latitude and longitude lines are the same as Figure 31. Rectangle at bottom is SST scale meant for use with color copy and is not usable with this black and white reproduction.

## **2. Synoptic Situation During the Period 08 - 11 May 1988**

The synoptic meteorological situation during the period of data acquisition was high pressure, centered to the southwest of the bay, which was strong enough during this period to block the advance of any atmospheric low pressure systems or cold fronts. The pressure gradient was not strong enough to influence the mesoscale land-sea breezes which dominated this entire period (see Figure 21 on page 37). Calm conditions prevailed, with very low (less than 1 m) sea states during the entire survey cruise.

## **3. The Monterey Bay Aquarium Wind Field**

Review of the MBA wind data taken over a 3 month period, from the last week of April to the last week in June 1988, shows the predominant diurnal land-sea breeze fluctuations evident during periods of light winds. The wind events previously mentioned during the last part of April and continuing to approximately 07 May is evident in this time series (Figure 21 on page 37). During this period winds were predominantly out of the northwest and attained velocities of up to  $15 \text{ m s}^{-1}$ . The overall mean wind speed for the three month period was approximately  $3.5 \text{ m s}^{-1}$  from  $260^\circ T$ . Calculated mean wind speed and direction for the period of the May 1988 cruise was  $2.3 \text{ m s}^{-1}$  from  $260^\circ T$ . Also of note is the predominantly stronger winds during afternoon seabreeze events, with winds dying off rapidly during the evening hours.

## **F. SUMMARY OF MEAN CURRENT FLOW**

Surface flow implied through satellite imagery, geostrophic flow, ADCP flow, and dynamic height analyses were consistent. They show mean surface inflow over the northern half of the bay and stronger, more concentrated outflow over the southern half of the bay. At depth, geostrophic and ADCP data were consistent on the southern side of the canyon and show inflow on the order of  $10 \text{ cm s}^{-1}$ . Because of the possible problems noted in the acquisition of ADCP data along the northern wall of the canyon, the geostrophic mean is believed to be more reliable over this area. For this reason, and because the geostrophic and ADCP mean data were similar in the other areas of the bay, the geostrophic mean field was used to force the numerical ocean model of the Monterey Bay.

## G. NUMERICAL OCEAN MODELING OF THE MONTEREY BAY CIRCULATION

### 1. Model Description

#### a. Dynamics

The model used in this study is a two layer, semi-implicit, primitive equation model which uses a 63 by 37 element C-grid for finite differencing. The numerical scheme utilized in this model was initially derived by Hurlburt (1974) to study ocean mesoscale circulation features (Bruner, 1988) and later adapted for use in studying circulation processes within the Monterey Bay by Prof. David C. Smith IV of the Naval Postgraduate School, Monterey, CA. Linear test cases with analytic solutions have been run in tandem by Smith and Reid (1982) to validate the model (Bruner, 1988). The equations used in the model are the vertically integrated momentum equation:

$$\frac{\partial V_i}{\partial t} + (\nabla \cdot V_i + V_i \cdot \nabla) v_i + k \times f V_i = -h_i \nabla P_i - B_h \nabla^4 V_i + \frac{\delta_{i1}}{\rho_i} \tau^{aw} - \delta_{i2} r v_i, \quad (12)$$

and a continuity equation:

$$\frac{\partial h_i}{\partial t} + \nabla \cdot V_i = 0, \quad (13)$$

for layer ( $i=1$  upper and  $i=2$  lower) thickness  $h_i$ , transports  $V_i$  and velocities  $v_i$ . The relation:

$$P_1 = g(h_1 + h_2 + d) \quad (14)$$

was used to calculate pressure in the upper layer, and:

$$P_2 = P_1 - g' h_1 \quad (15)$$

was used for lower layer pressure calculations where the reduced gravity ( $g'$ ) is calculated using:

$$g' = g \frac{(\rho_2 - \rho_1)}{\rho_2}. \quad (16)$$

The Coriolis parameter ( $f$ ) is equal to  $2\Omega \sin \phi$  where  $\Omega$  is the angular velocity of the earth in  $\text{rad s}^{-1}$  and  $\phi$  is the latitude. The Kronecker Delta ( $\delta_{ij}$ ) is equal to one when  $i=j$  and zero when  $i \neq j$ . Subgrid scale dissipation is modeled using biharmonic ( $\nabla^4$ ) friction

with the diffusivity constant ( $B_H$ ) equal to  $-1 \times 10^7 \text{ m}^4 \text{ s}^{-1}$ . Wind stress between the air and water ( $\tau^{aw}$ ) is included as a forcing parameter along with bottom friction which employs a linear bottom drag coefficient ( $r$ ) equal to  $5 \times 10^{-4} \text{ m s}^{-1}$  (Winant and Beardsley, 1979) in the relation  $-rv_2$  (Shaw and Csanady, 1983). The reduced gravity ( $g'$ ) value used was  $2 \times 10^{-2} \text{ m s}^{-2}$ .

#### ***b. Boundary Conditions and Domain***

The north, east, and south boundaries are closed (no slip). The west boundary is open (following Camerlengo and O'Brien, 1980) except where forcing (inflow and outflow) is specified. Forcing along the western boundary can be applied separately to the upper (which encompasses the free surface to 50 m) and lower (50 m to the bottom) layers, allowing both barotropic and baroclinic modes.

The 63 by 37 grid is spaced at 500 m intervals resulting in a model domain encompassing a 32 by 18 km rectangle. The domain is orientated roughly north-northwest to south-southeast (see Figure 33 on page 62) to encompass as much area of the Monterey Bay as possible. Realistic topography (Figure 33 on page 62) was incorporated by applying an interpolated field of gridded bathymetry. Because of numerical considerations, the layer interface cannot intersect either the free surface or bottom topography. For this reason, bottom topography shallower than 100 m was not allowed so unrestricted vertical displacement of the interface could occur (Bruner, 1988).

### **2. Initialization Methods**

#### ***a. Methods of Model Forcing***

The first problem encountered was whether to use the mean flow obtained through geostrophy or through ADCP measurements. Since the sense and magnitude of the two means were similar and, because of the doubtful reliability of the ADCP data at depth near the northern wall of the canyon (discussed at length in the ADCP section), it was decided to use the mean obtained through geostrophy. Aside from that one region, they were not significantly different. Since the model is a two layer system, the mean geostrophic flow was averaged over the top 50 m to obtain  $v_1$  values, then averaged between 50 m and the bottom depth between each station (Figure 34 on page 63) to obtain values for  $v_2$ . This averaging was performed in order to conserve the mean mass transport of the mean geostrophic flow field. This procedure left the surface velocities relatively unscathed, but resulted in lowered velocities at depth since most of the mean deep flow lay above 250 m. The next obstacle was how to force the model with known data at inconsistent intervals and not in coincidence with the western boundary of the model (see Figure 33 on page 62). Since both Line 1 and the western boundary of the



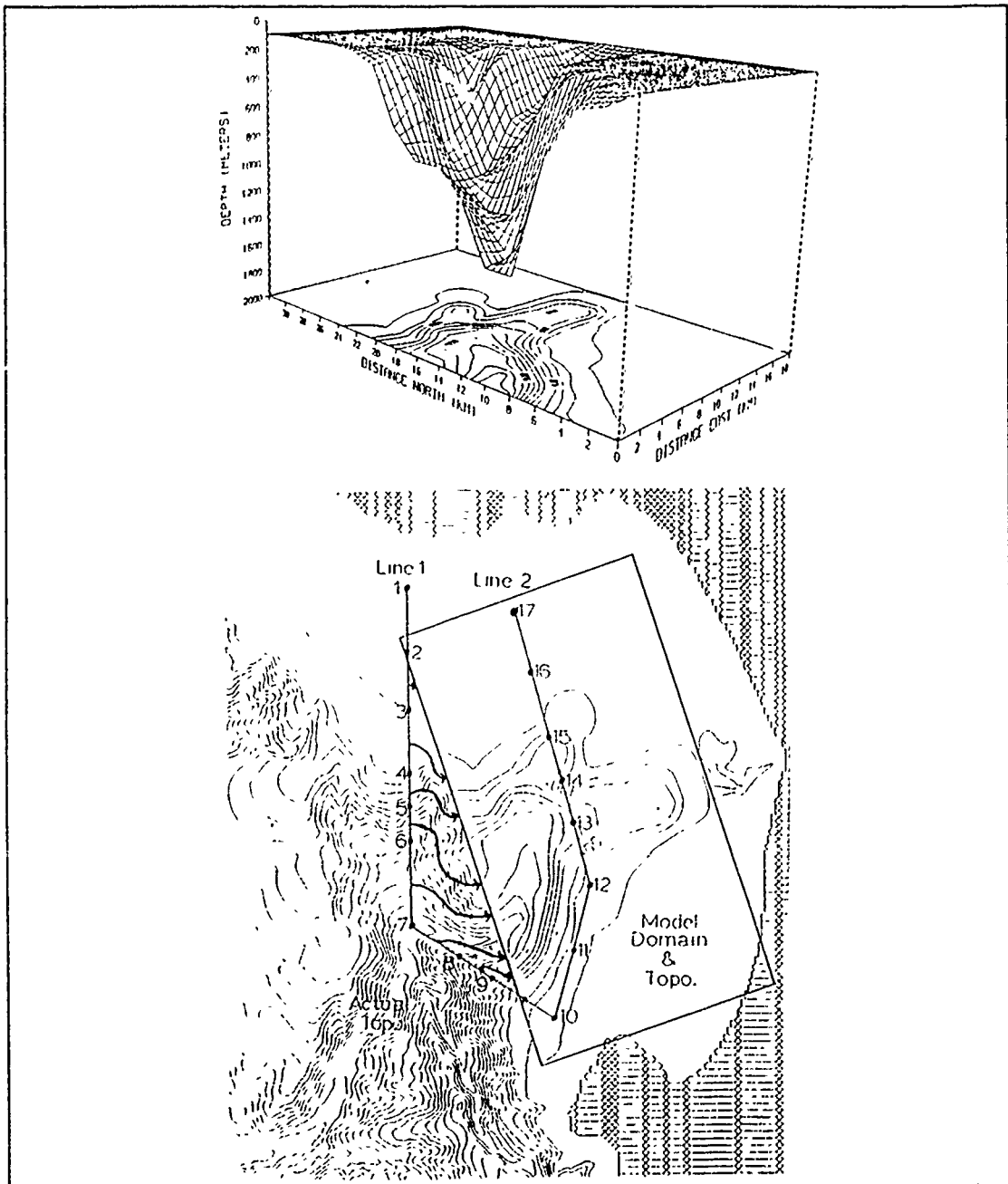


Figure 33. Numerical model bathymetry (top) and spatial domain (bottom): Top figure shows the bathymetry used in the Monterey Bay numerical model, bottom figure shows the domain (box) and its orientation within the bay. Line 1 (stations 1-10) and Line 2 (stations 10-17) are also depicted in relation to the model domain. Arrows roughly approximate the method used in projecting the mean geostrophic flow onto the model's western (open) boundary.

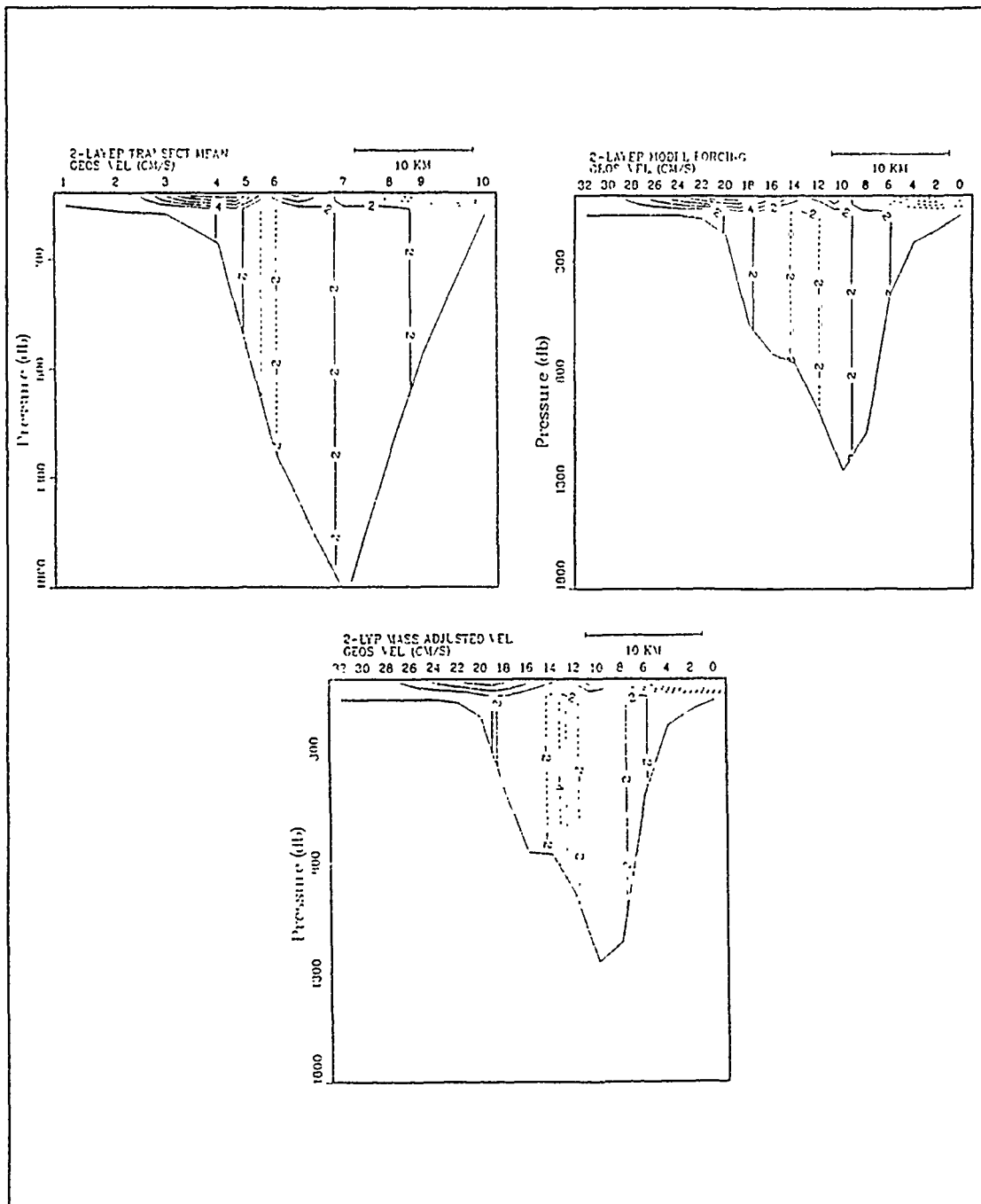


Figure 34. Cross sections of model inputs: Top (left) figure shows the result of vertically averaging the mean geostrophic flow along Line 1. Top (right) figure depicts the projection of these averaged flows onto the western boundary of the model. The bottom figure represents the mass balanced flow input into the model during subsequent experiments.

model are orientated roughly perpendicular to bottom slope, the simplest solution was to project the mean flow at known points onto the western boundary of the model grid (see Figure 33 on page 62) along isobaths. This of course is a realistic assumption if vorticity is conserved over the mouth of the bay and if the predominant flow was perpendicular to Line 1. Once the velocities were identified on the model boundary, the data were run through a linear interpolation scheme to define velocity values at each grid point along the boundary (see Figure 34 on page 63 and Appendix C). Runs were then made using this forcing scheme, both with and without the mean wind and bottom friction (Table 4 on page 65). These model runs ran approximately 8 days before the interface intersected the bottom. When this occurred the runs terminated because model assumptions were violated. This was not surprising since the original mean geostrophic flow was not exactly mass balanced (positive net transport, or flow into the bay), thus surplus water was continually being pumped into the bay at each time step with no outlet available. In an attempt to stabilize the model, the input mass field ( $m^2 s^{-1}$ ) originally derived from the geostrophic mean flow was adjusted so that net transport in both layers added up to zero. This was accomplished by applying linear correction coefficients to both layers (Appendix C). This adjustment of mass balance is considered justifiable and realistic for the following reasons:

- The "true" mean flow would be mass balanced.
- The amount of adjustment applied to the boundary forcing is probably less than the geostrophic resolution.
- As a consequence of the model's two layered system, averaging of the mean flow was only conducted down to 50 m for the upper layer. Inspection of the mean geostrophic flow field (Figure 24 on page 42) shows that, while it definitely appears to be an uncoupled, two layer system, the top layer most likely extends deeper than 50 m. Therefore, much of the flow in the lower layer was artificially introduced during the partitioning process.

Runs with the balanced flow field appeared more stable numerically, and ran out to an average of 19 days.

To see what the model response would be to wind forcing alone, a run was made simulating the actual winds over the bay during a strong frontal passage (similar to what was described in the Meteorological Synoptic Situation section). Input winds were first "ramped" (i.e. gradually increased each time step to avoid numerical instability) from 0 to  $2 m s^{-1}$  from the south to southeast. Then, from day 3 to day 7, the winds were ramped from southerly to southwesterly, and the winds were ramped up to  $8.5 m s^{-1}$  to simulate pre-frontal winds. From day 7 to day 8, winds were kept strong, but di-

rection was shifted each time step from southwest to northwest to represent frontal passage. Winds were gradually decreased from  $8.0 \text{ m s}^{-1}$  to  $1.0 \text{ m s}^{-1}$ , while direction was backed to westerly, over the next two days to day 10. Past day 10 the winds were turned off so the "spun down" state could be observed. Both layers were initially at rest and the entire western boundary was left open (allowing inflow and outflow anywhere).

All model runs were made with bottom topography included (for topographic effects see Bruner, 1988). Open boundary conditions were specified wherever mean forcing was determined to be zero along the boundary to allow inflow or outflow at that point. As previously mentioned, the entire boundary was open for the wind forcing experiments. The mean MBA wind speed and direction was used in those mean forcing runs which applied a constant wind stress throughout. A summary of the five runs conducted is provided in Table 4 (outputs appear in Figure 35 on page 66 to Figure 39 on page 70).

**Table 4. SUMMARY OF MONTEREY BAY NUMERICAL MODEL SIMULATIONS**

Run No.	Boundary Forcing	Bottom Friction	Wind Stress
1	Geostrophic Mean	No	No
2	Geostrophic Mean	Yes	$260^\circ T$ at $2.3 \text{ m s}^{-1}$
3	Mass Balanced Geostrophic Mean	No	No
4	Mass Balanced Geostrophic Mean	Yes	$260^\circ T$ at $2.3 \text{ m s}^{-1}$
5	None	No	Variable (see text)

### 3. Results of Experiments

Results of run number one (Figure 35 on page 66) shows anticyclonic rotation over the southern half of the bay with a closed cyclonic eddy situated in the northern bight region in the surface layer. At depth, velocities are weakly cyclonic (less than  $2.5 \text{ cm s}^{-1}$ ) over the mouth of the canyon with weak anticyclonic curvature in the northern and southern bights. The addition of mean winds and bottom friction (run two) did not seem to have a marked effect on the overall flow (Figure 36 on page 67). Flow patterns were similar in both cases, with the exception that, as expected, velocities were decreased in run two by the effect of bottom friction. To gain a quantitative comparison with the mean flow calculated across Line 2, geostrophic velocities were averaged down to 50 m

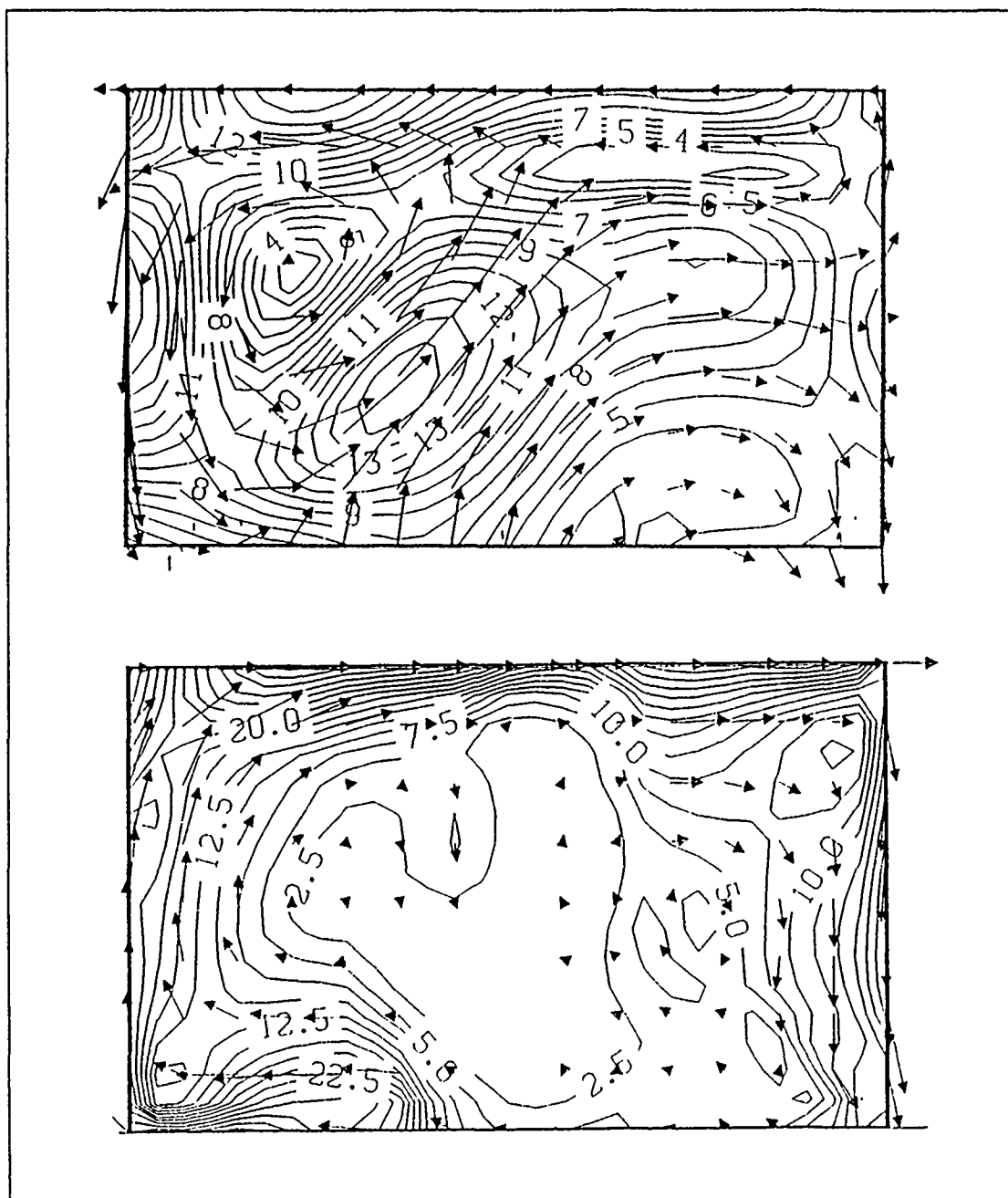


Figure 35. Monterey Bay model output from run No. 1: North is to the left in each figure (i.e. figures are orientated as if you are looking into the bay). Arrows are velocity vectors, solid lines are isotachs ( $\text{cm s}^{-1}$ ). Top figure depicts upper level flow and bottom figure shows deep flow, both at day 7 of the run. Mean geostrophic flow was used to force the model along the western (bottom of plots) boundary. The effects of wind and bottom friction are neglected.

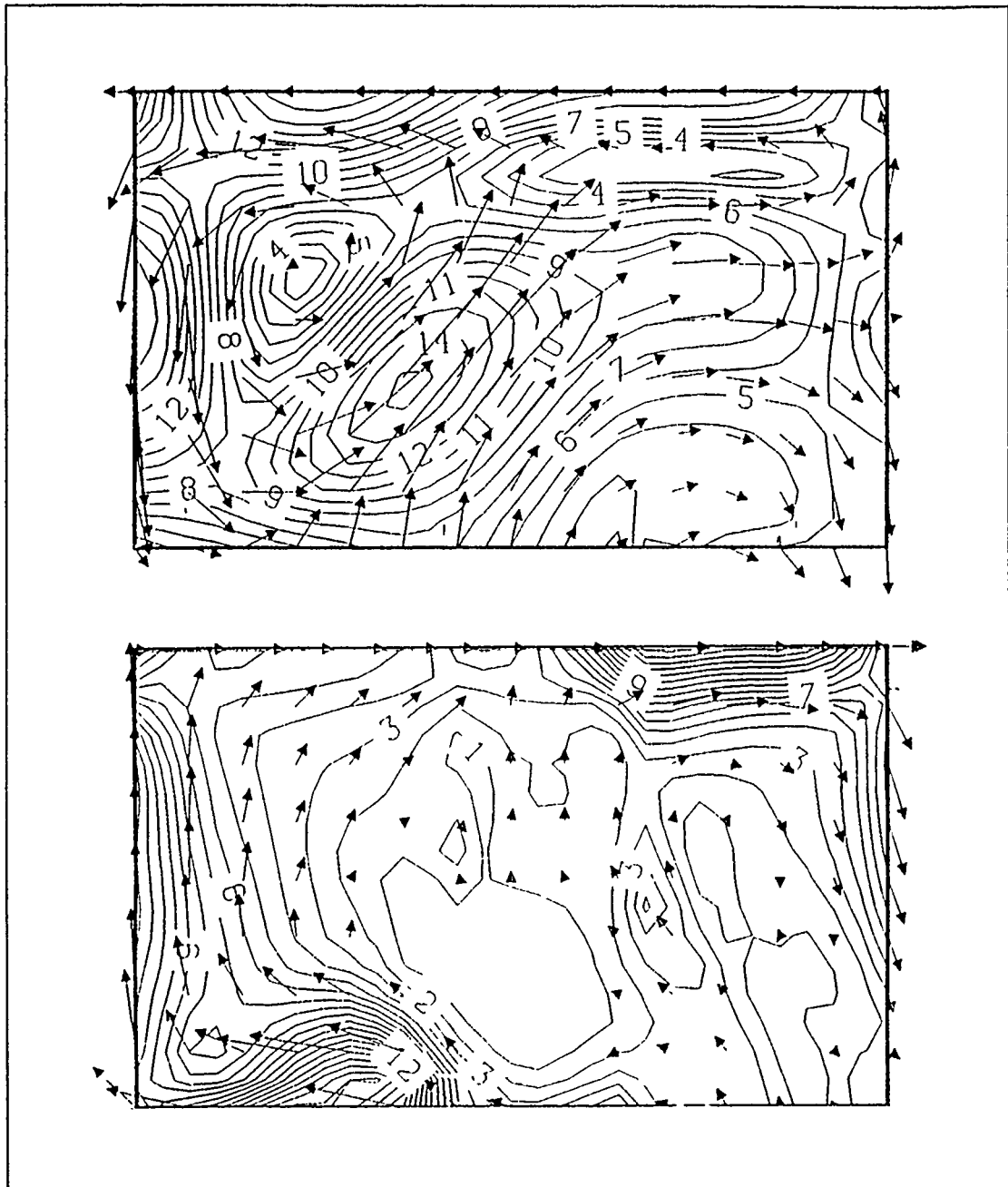


Figure 36. Monterey Bay model output from run No. 2: North is to the left in each figure (i.e. figures are orientated as if you are looking into the bay). Arrows are velocity vectors, solid lines are isotachs ( $\text{cm s}^{-1}$ ). Top figure depicts upper level flow and bottom figure shows deep flow, both at day 7.25 of the run. Mean geostrophic flow was used to force the model along the western (bottom of plots) boundary. The effects of wind and bottom friction are included.

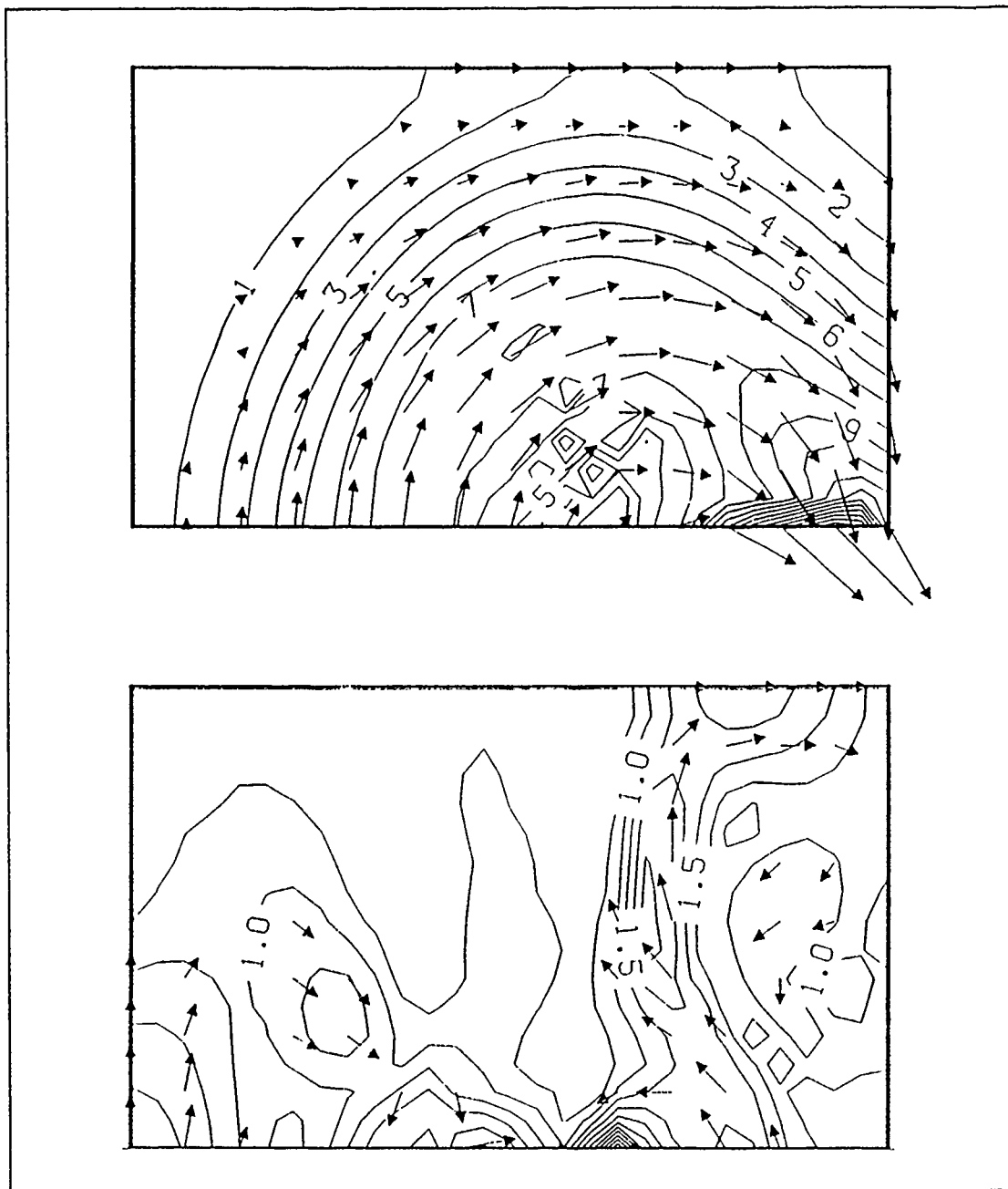


Figure 37. Monterey Bay model output from run No. 3: North is to the left in each figure (i.e. figures are orientated as if you are looking into the bay). Arrows are velocity vectors, solid lines are isotachs ( $\text{cm s}^{-1}$ ). Top figure depicts upper level flow and bottom figure shows deep flow, both at day 15.8 of the run. Mass balanced mean geostrophic flow was used to force the model along the western (bottom of plots) boundary. The effects of wind and bottom friction are neglected.

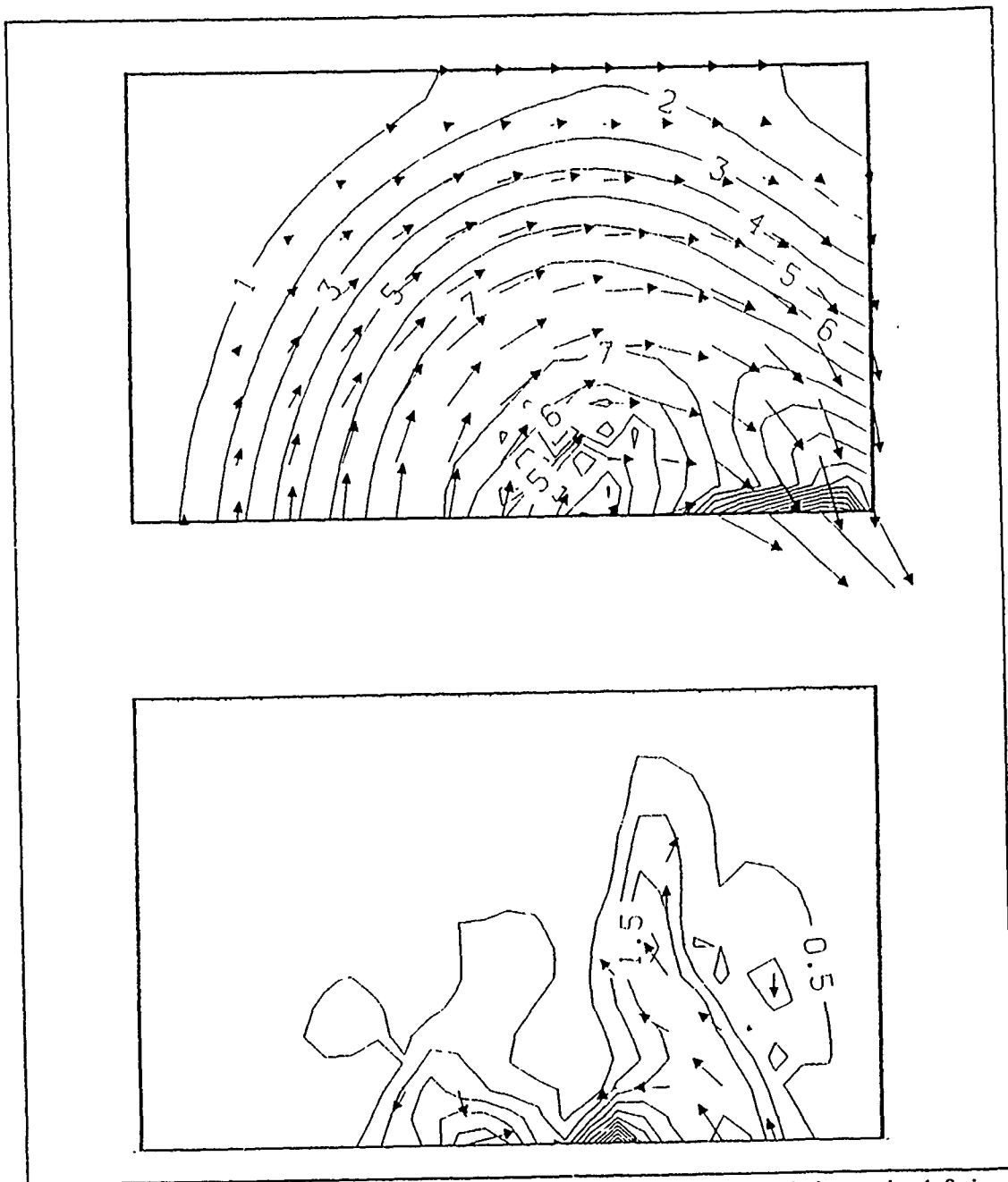


Figure 38. Monterey Bay model output from run No. 4: North is to the left in each figure (i.e. figures are orientated as if you are looking into the bay). Arrows are velocity vectors, solid lines are isotachs ( $\text{cm s}^{-1}$ ). Top figure depicts upper level flow and bottom figure shows deep flow, both at day 15.8 of the run. Mass balanced mean geostrophic flow was used to force the model along the western (bottom of plots) boundary. The effects of wind and bottom friction are included.



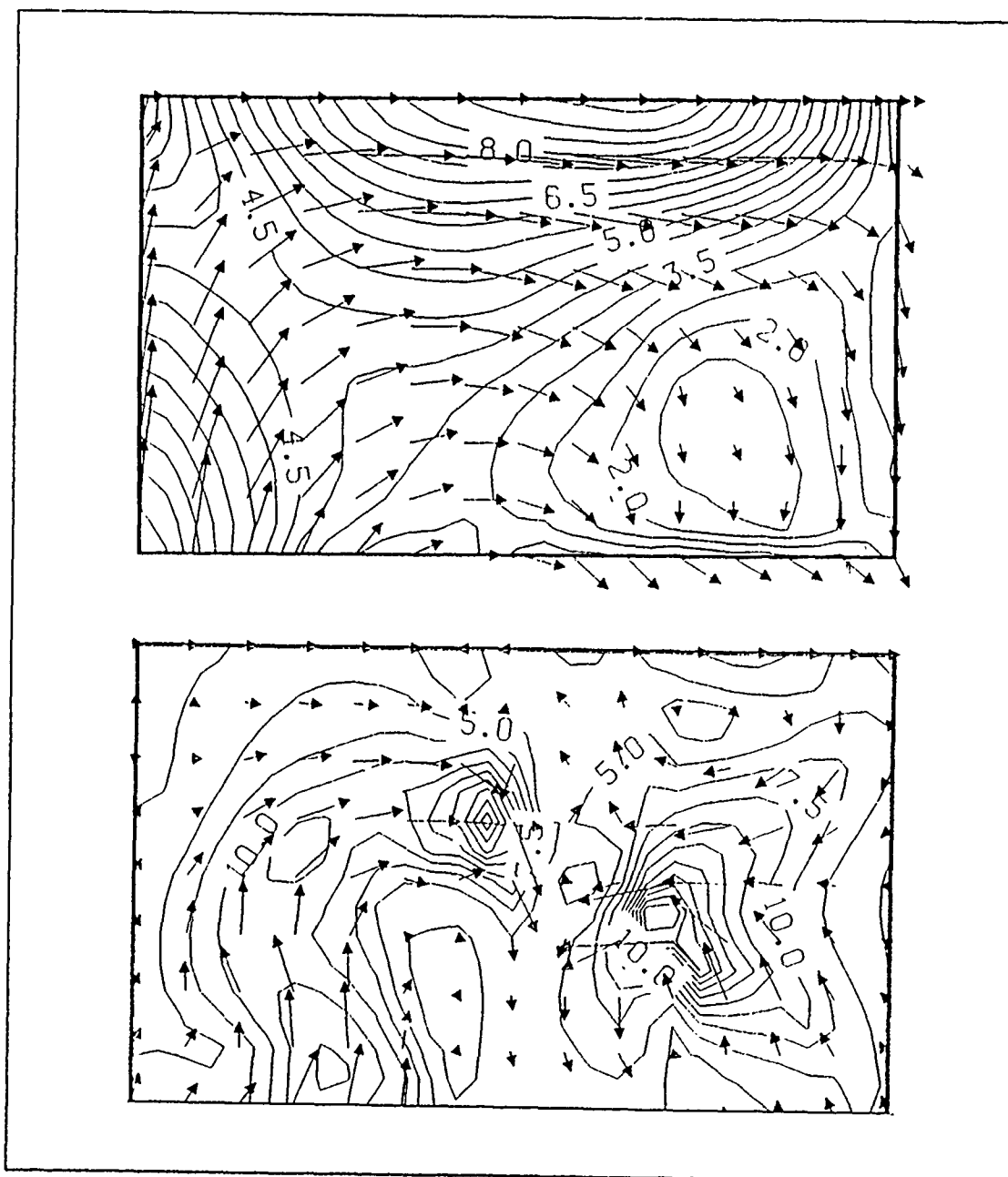


Figure 39. Monterey Bay model output from run No. 5: North is to the left in each figure (i.e. figures are orientated as if you are looking into the bay). Arrows are velocity vectors, solid lines are isotachs ( $\text{cm s}^{-1}$ ). Top figure depicts upper level flow and bottom figure shows deep flow, both at day 13.6 of the run. Wind forcing alone was used to force flow in the model. Both layers were initially at rest. The entire western boundary (bottom of plots) was open to allow flow to develop at will. The effect of bottom friction was neglected.

and from 50 m to the bottom and compared with model outputs at these grid points (Table 5 on page 71, see also Figure 33 on page 62 for station positions). The mean Line 2 data were not used to force the model in any way. The mean geostrophic flow between stations 17 and 16 does show light outflow in the extreme northern part of the bay, although not to the extent the model shows. Outflow is not indicated in the mean Line 1 geostrophic velocities implying that some sort of weak, closed circulation may, in fact, exist in the northern bight area. Model output across Line 2 also shows strong inflow in the lower layer over the northern part of the bay and outflow in the southern part. Line 2 mean velocities show no such flow in these areas. In fact, the mean Line 2 geostrophic flow shows very little flow in the lower layer at all, with  $1.94 \text{ cm s}^{-1}$  inflow between stations 15 and 14, and  $-0.99 \text{ cm s}^{-1}$  outflow between stations 14 and 13. In general, the overall flow patterns predicted by the bay model are much stronger, in both upper and lower layers, than those found in the observed mean flow field. Circulation in the northern bight which was generated in runs 1 and 2 can be explained in terms of compression and expansion of vortex tubes. As water is pumped into the northern part of the bay (too much water) in the upper layer, it travels into the northern bight region where it forces the interface down producing vortex stretching in the upper layer and compaction of tubes in the lower layer resulting in cyclonic circulation in layer one, and anticyclonic circulation in layer two.

**Table 5. COMPARISON OF MODEL OUTPUT AND LINE 2 GEOSTROPHIC MEAN:** Negative velocities indicate flow out of the bay, positive values denote flow into the bay. Velocities are in  $\text{cm s}^{-1}$ .

Station	Observed Mean		Run 2		Run 4		Run 5	
	$v_1$	$v_2$	$v_1$	$v_2$	$v_1$	$v_2$	$v_1$	$v_2$
17-16	-0.7	0	-5	9	1	0	4	10
16-15	-0.3	0	2	3	3	0	3	7
15-14	4	2	10	0	4	0	1	-.5
14-13	4	-1	6	0	5	-.5	-.6	-.5
13-12	4	0	5	1	3	1	-.5	-2
12-11	2	0	4	1	1	-.5	-1	12
11-10	-9	0	-1	0	-3	-.5	-1	2

The effect of balancing the mass transport along the western boundary produced major changes in the flow pattern (Figure 37 on page 68). The circulation in

the northern bight produced by run one and run two is no longer evident in runs three and four (Figure 37 on page 68 and Figure 38 on page 69). The surface layer consists of a broad anticyclone encompassing practically the entire bay, and centered over the canyon axis. In run three, flow in the lower layer generally follows topography with weak cyclonic circulation over the canyon mouth, somewhat stronger anticyclonic rotation over the northern shelf, and anticyclonic circulation contained in the southern bight region. Flow appears to diverge from the cyclone in the canyon's mouth, travel deeper into the bay along the canyon axis (east), then enters the southern bight via the canyon head where it ties into the previously mentioned lower layer anticyclone located in this area. The addition of bottom friction effectively keeps the flow trapped in the canyon (Figure 38 on page 69). Magnitude and direction of flow in both layers from run four compares favorably with the observed mean geostrophic flow (Table 5 on page 71) with the exception of not predicting weak outflow in layer one over the extreme northern part of the bay. The model also appears to under predict the outflow in the southern part of the bay in layer one ( $-3$  vice  $-9 \text{ cm s}^{-1}$  which was observed). A Silicon Graphics "movie" of this run, made at 1000 s intervals, showed that the model was highly stable using this balanced forcing. The predicted high dynamic height center remained quasi-stationary over the canyon mouth throughout the 19 day animation, agreeing well with the inferred flow from the actual mean dynamic height analyses (Figure 28 on page 49). Again, the model realistically predicts the observed Line 2 mean flow, especially in the lower layer, which supports the hypothesis that much of the cyclonic circulation within the canyon at depth does not penetrate into the canyon to any appreciable extent, but rather recirculates near the mouth of the canyon.

The final model simulation (Figure 39 on page 70), which used variable wind stress as the sole forcing parameter, showed that strong atmospheric frontal passages, such as the type previously described, can set up circulation patterns which are similar in nature, at least in the upper layer, to those observed in the mean geostrophic flow (Figure 39 on page 70). The upper layer outflow along the southern portion of the open boundary is forced to the southwest, similar to what was depicted in the 04 May satellite imagery. Reproducing flow similar to that observed in the lower layer mean geostrophic flow using this method was not as successful. The model output shows anticyclonic turning in the northern shelf area and cyclonic turning in the lower layer over the southern shelf break. These flows then converge near the canyon head and flow out to sea along the axis. One major shortcoming of using this forcing method is the fact that there is no model topography above sea level to produce lee effects such as in the

northern and southern bight regions which, in reality, are fairly protected from northwesterly winds (Breaker and Broenkow, 1989). Animation of this simulation showed height anomalies to vary widely in location and intensity. This run never quite reached a stable state, even after day 10, when wind stress was turned off implying wind alone is not the only factor.

## IV. DISCUSSION

### A. COASTAL PROCESSES

Strong northwesterly winds, produced by post-frontal high pressure ridging across California, prevailed over the central California coast from the last week of April through the first week of May 1988. The oceanic response to this wind stress was coastal upwelling, produced by Ekman transport, and the appearance of a strong equatorward geostrophic jet along the central coast. NOAA satellite imagery from 04 May 1988 clearly shows this upwelling and the presence of equatorward flow, entering the Monterey Bay from the north, and advecting warm Bay waters south past Pt. Sur, 37 km to the south of the Monterey Bay. This pattern is similar to observations made by Breaker and Broenkow (1989), who noted that, during upwelling events, cold, upwelled water was advected across the bay, producing a strong thermal front near Pt. Pinos. A geostrophic velocity cross section, produced from hydrographic data collected along a line perpendicular to Pt. Sur on 04 May 1988 depicts a strong  $25 \text{ cm s}^{-1}$  equatorward flow extending from the coast to 50 km seaward and limited to pressures of less than 100 dbar, typical of coastal upwelling geostrophic jets (Figure 40 on page 75). These descriptions of the winds, upwelling, and coastal geostrophic flow are all consistent with the findings and observations of Halliwell and Allen (1987), Huyer (1983), and Hickey (1979). Of final note, the CLC was not evident on the 04 May geostrophic cross section at Pt. Sur, consistent with Chelton's (1984) observations that this poleward, deep current was weak and equatorward during April and May at Monterey and Pt. Sur.

The 08-11 May 1988 Monterey Bay hydrographic survey commenced at the cessation of strong northwesterly winds. Winds were light and seas were calm throughout the period. As a result of this period of calm winds, satellite imagery taken on 08 and 11 May 1988 showed waters within the bay to have warmed significantly, either by advection of warmer oceanic waters into the bay (Breaker and Broenkow, 1989), or simply through solar radiative processes. While no quantitative evidence exists to support the continued presence of the equatorward coastal current during this period, weak upwelling was still visible to the north and south of the Monterey Bay.

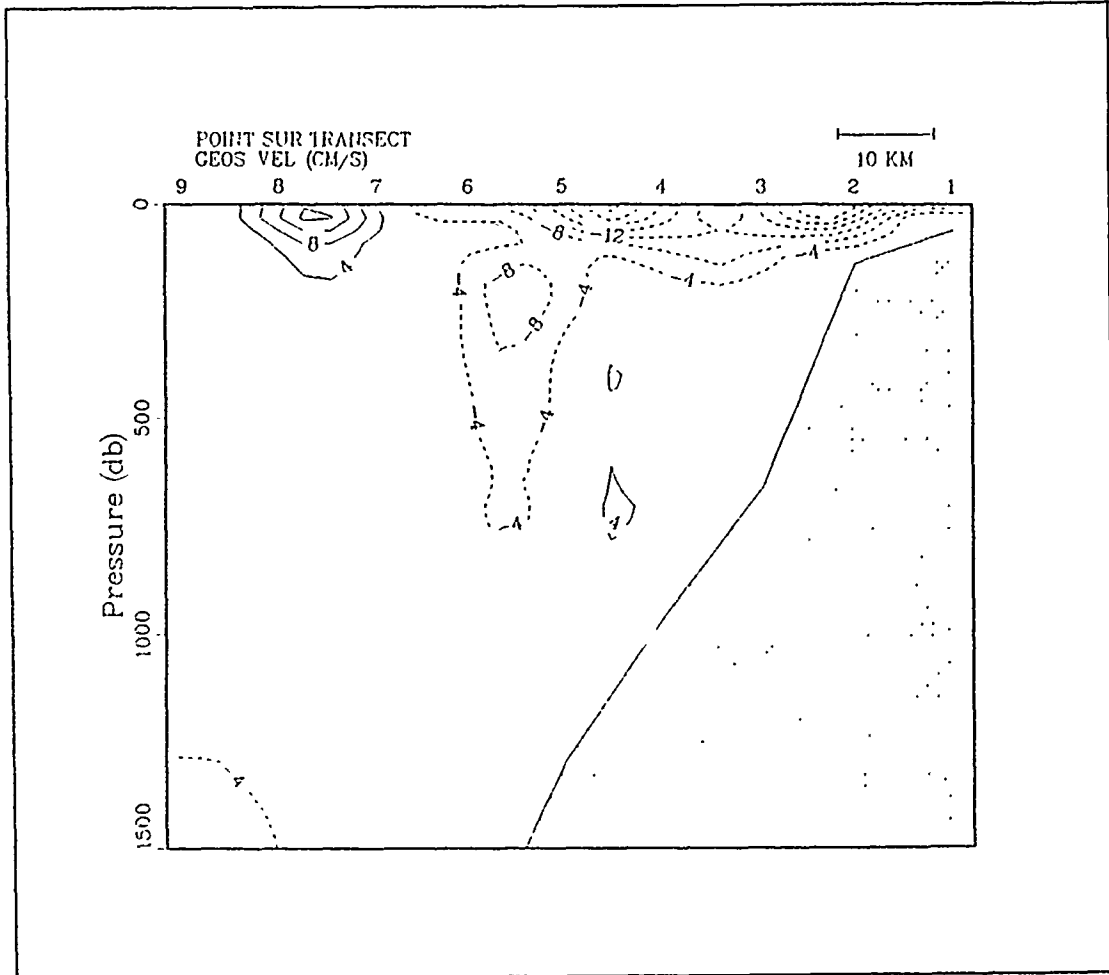


Figure 40. Pt. Sur geostrophic velocity cross-section: Geostrophic Velocities were derived from CTD casts collected on 04 and 05 May 1988. The section runs roughly east-west, perpendicular to the coast, from Pt. Sur seaward. Pt. Sur is located roughly 20 n mi (37 km) south of the Monterey Peninsula. Positive values denote poleward flow, negative values denote equatorward flow.

## B. INTERNAL WAVES

The mean flow signal, especially over the shelf break and the Monterey Submarine Canyon, was highly aliased by the internal wave field throughout the data acquisition period (Figure 19 on page 34). The process of averaging the mass field and ADCP velocities appears to have effectively removed the majority of this "noise." Examination of the ADCP passes along Line 1 showed that surface tidal heights and the flow within the canyon were not in phase. The internal wave amplitudes of 30 m, observed in Line 1, are smaller than the 50-120 m amplitudes observed by Shea and Broenkow (1982) near

the canyon head. This difference can be explained by their hypothesis that internal wave energy is focused near the head as they shoal, thus producing the somewhat higher amplitudes they observed. This is also consistent with Broenkow and McKain's (1972) observations that internal tidal waves generally decreased seaward. Why observed internal wave amplitudes observed in Line 2 data, which is inshore of Line 1, were smaller than those observed in Line 1 is unknown.

### C. CIRCULATION

The mean flow during the data acquisition period is an uncoupled two layer system, consisting of a warm core anticyclone at the surface over a cold core, cyclone which is "trapped" within the confines of the Monterey Submarine Canyon under the thermocline. Inflow at the surface is broad, extending from the northern part of the bay south to the center of the canyon, while outflow is relatively stronger but narrower and is confined to the area between the Monterey Peninsula and the center of the canyon (station 7). Mean flow at depths of 100 to 200 m consists of two cores with outflow along the northern wall of the canyon and inflow along the southern half of the canyon axis. Both ADCP and geostrophic means (Figure 30 on page 53 and Figure 24 on page 42), along with dynamic topographies (Figure 28 on page 49), support this description. The only major discrepancy noted between the ADCP and the geostrophic means was in the outflow region along the north canyon wall.

Evaluation of the mean flow pattern in Line 2 also shows surface inflow over the center of the bay with outflow along the southern portion. Surface velocities are generally weaker in Line 2 and no evidence of cyclonic circulation at depth is evident, just a weak inflow near the center of the canyon. This leads to the conclusion that the surface flow is turning over Line 2, thus accounting for the small east-west velocity components, and that the cyclonic flow noted in the canyon itself is limited to the deeper portions of the canyon, near the mouth.

As seen in the cross-sections of mean temperature and density, as well as in the mean 10°C isotherm plots, the isotherms and isopycnals had a much more pronounced slope from the canyon axis to the Monterey Peninsula explaining the higher geostrophic and ADCP velocities found there. Map contours of mean temperature and dynamic heights support these flow patterns at the surface and at depth. The tighter dynamic height gradient over the southern portion of the bay is also indicative of stronger geostrophic flow in this area. Satellite imagery, especially the 04 May 1988 pass, supports anticyclonic surface flow. The surface flow pattern agrees with the findings of

Bigelow and Leslie (1930), Skogsberg (1936), Lammers (1971), and with Pirie and Stellar's (1974) inferred southward flow from March through July. The noted reversal in flow confirms Skogsberg's (1936) suspicions that flows within the bay at different depths may be in opposition to one another. Lasley (1977), Smethie (1973), Broenkow and Smethie (1978), Reise (1973), Moomy (1973), and Breaker and Broenkow (1989) determined flow to be predominantly cyclonic within the bay but most acknowledged that periods of flow reversals do occur within the bay. During the period of this study, one of these "reversals" was obviously taking place.

As previously mentioned the CUC was not in evidence, at least at Pt. Sur, during the period so momentum transfer from this current does not seem a viable flow generation mechanism (Breaker and Broenkow, 1989) during the May 1988 cruise. The best explanation for the observed flow patterns stems from the results of Klinck's (1989) three-layer geostrophic adjustment model of flow over a canyon. Despite the obvious differences between modeled shelf and canyon geometry, and the actual bathymetry of the Monterey Canyon and vicinity, there are similarities between his results and the flow patterns observed in the Monterey Bay. His model results showed that, for a narrow canyon (shown to be the case here in Chapter III), anticyclonic surface flow over cyclonic, canyon trapped flow would be produced by the geostrophic adjustment process that takes place when a surface current encounters a submarine canyon. Similarities between the 50 km wide current used in forcing his model, and the 50 km wide, equatorward surface current depicted in the Pt. Sur geostrophic velocity cross-section (Figure 40 on page 75) is also noted. Klinck's results also indicated that once a canyon width narrows to less than half of the internal Rossby radius, it has little perturbing effect on the cross canyon flow. The calculated internal Rossby radius at station 13 was 11.4 km and the canyon width in this area is approximately 6 to 7 km. This may, in part, explain the absence of any significant deep flow at depth in Line 2, where the Monterey Submarine Canyon begins to narrow rapidly.

Whether or not flow reversals within the Monterey Bay are correlated to strong upwelling events cannot be determined from the results of this study alone. The findings of Broenkow and Smethie (1978) implied predominantly northward flow within the bay even during the spring and summer upwelling period. This may suggest that the observed mean flow pattern may only develop during periods of strong equatorward, coastal flows. The minimum velocity required to drive such flows, the amount of time this coastal current requires to "spin-up" the observed flow, or the length of time this flow



pattern remains after cessation of this current, remain unknown quantities and are left as topics of future research.

#### **D. MEAN FLOW MODELING**

The general flow pattern described above was also reflected in numerical model simulations, particularly when forced by a balanced flow (runs 3 and 4). The differences between the unbalanced (Figure 36 on page 67) and balanced (Figure 38 on page 69) runs can be seen by analyzing model outputs of height anomalies (Figure 41 on page 80). Run 2 height anomalies showed surface heights of approximately 7 cm over the mouth of the canyon with a relative minimum of 5.6 cm over the northern bight resulting in anticyclonic and cyclonic circulations respectively in the upper layer. The interface from run 2 showed a depression of 28 m over the northern bight but 38 m over the canyon mouth creating relative highs and lows respectively. Analysis of Run 4 height anomalies only showed one high in the upper layer and one low in the lower layer, both vertically stacked and situated roughly over the mouth of the Monterey Submarine Canyon. These balanced runs seem more realistic than those produced by the unbalanced mean forcing (runs 1 and 2) and depict broad anticyclonic flow in the upper layer which effectively fills the bay. These runs also appear to agree better with observed mean flows derived from Line 2, and also with geostrophic flows implied from dynamic topographies (Figure 28 on page 49). The strong southwesterly outflow near Pt. Pinos, noted in the observed mean flow and in satellite imagery, appears to have been handled well by the model. When the effects of bottom friction were added, the majority of the deep flow was confined to the canyon topography, also supported by the observed weak flow at depth in the Line 2 mean. The effects of friction are similar to those noted by Garcia (1971) who observed that in deep areas of the bay, friction played a small role but in shallower areas, friction significantly altered the flow. Some evidence exists in the mean Line 2 data to support outflow (or return flow) along the northern coast of the bay where the inflow diverges however not to the extent of that predicted by the model from the unbalanced mean forcing (runs 1 and 2).

The major limitations of these model results include:

- The assumptions used in projecting the mean flow field onto the model's open boundary. The mean flow inferred by Line 1 data (west of the open boundary) may not, in reality, have extended all the way into the model's western boundary, as was assumed when forcing was applied. However, in view of satellite imagery and dynamic height analyses, it is felt that model flow was fairly representative of the actual flow encountered over the period of data acquisition.

- The upper layer actually extends to the bottom over the shelf regions of the Monterey Bay however, due to model assumptions, these areas must be treated as two layers to avoid surfacing or grounding of the layer interface.
- The observed flows indicate that a three-layer model is actually required, i.e. the top layer to model flow over the shelf area, a second layer to model flow at intermediate depths of 100 to 500 or 600 m, and a bottom layer to model flow in the quiescent regions of the Monterey Submarine Canyon below about 600 m.

Results of these runs are in general agreement with Bruner's (1988) observations that, when lower layer velocities are weak and vertical shear is large, the model effectively "decouples" the two layers, resulting in independent flow patterns. Bruner noted that, for narrow inflow to the north, and broadened outflow to the south, anticyclonic circulation ensued over the entire bay. In contrast, anticyclonic flow also resulted in the runs produced in this study for broad inflow over the northern bay, and narrow outflow over the southern bay.

Finally, model runs which were forced solely by variable wind stress, while obtaining similar mean flow patterns in the upper level, did not correspond to observed mean flow at depth. The wind forcing did, however, show decoupling of the two layers. Obviously, other factors besides wind stress were at work here but these experiments do imply that wind forcing may play some part in shaping mean flow patterns, at least at the surface, during strong wind events lasting on the order of a week. Another interesting aspect of this model result is the fact that approximately 4 days after the wind forcing was turned off (Figure 39 on page 70), flow remained relatively strong in both layers implying the "signal" of these wind events may be seen in the mean flow for a reasonable amount of time after the winds have abated. Modeled current flow appeared to respond rapidly to changes in both wind direction and magnitude, agreeing with Hickey's (1979) observations that oceanic responses to changes in wind stress are rapid ( $O(\text{days})$ ). However, as noted in Chapter III, model runs using only wind stress forcing did not achieve any appreciable level of stability and displayed highly variable height anomaly patterns.

From modeling results it can be seen that the combined effects of winds, bottom friction, and, of course, boundary forcing all play key roles in producing mean circulation patterns within the Monterey Bay. Strong winds appear to have a significant effect on surface flow, while light mesoscale land and sea breezes typically encountered under weak high atmospheric pressure gradients have little effect on surface flow. Bottom friction played a key role in suppressing lower level flow out of the Monterey Submarine Canyon. It was also shown that the model was highly sensitive to mass balanced flow, yielding strikingly different flow patterns from balanced and unbalanced flows.

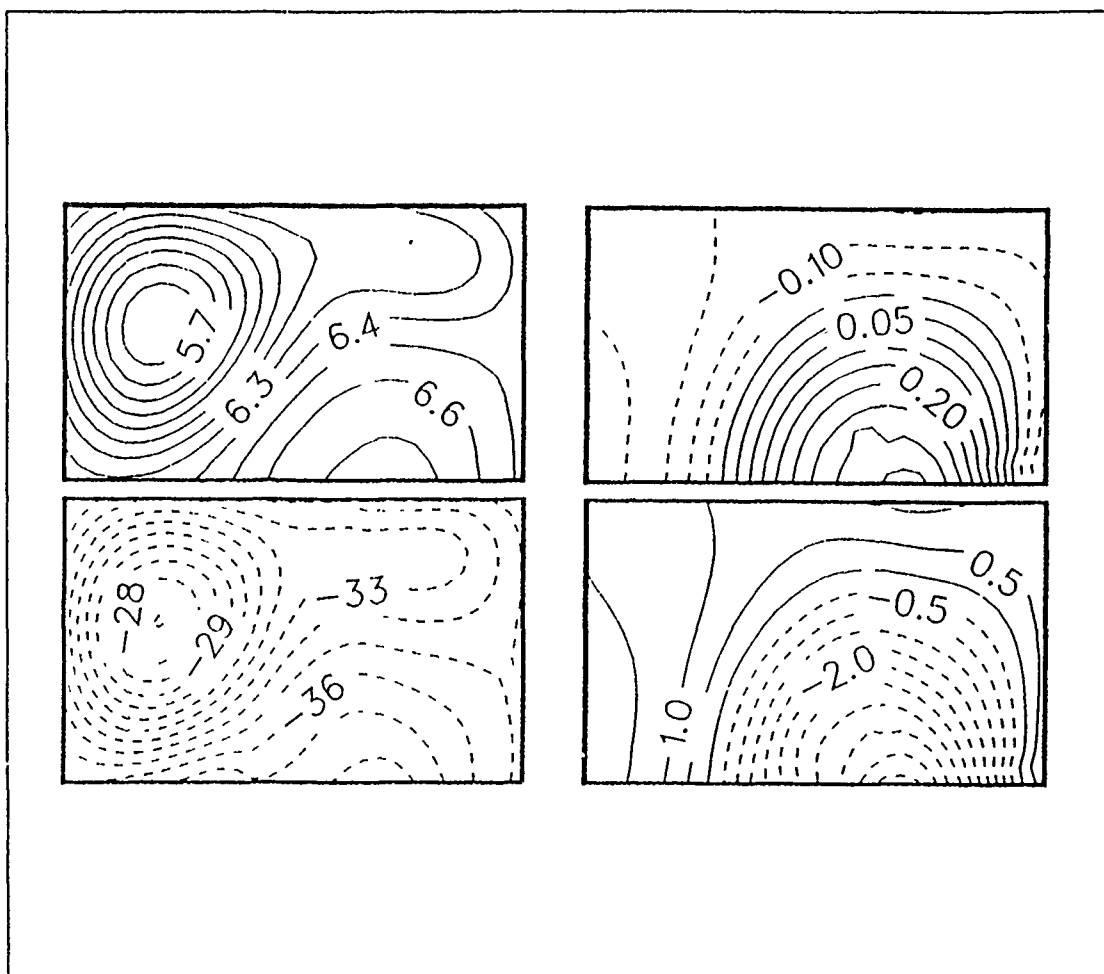


Figure 41. Run 2 (left) and run 4 (right) height anomalies.: Left figures depict Run 2 height anomalies (m) for the upper layer (top) and bottom layer (bottom). Right figures show Run 4 height anomalies for upper layer (top) and bottom layer (bottom).

Finally, while the model used in this study could not be forced by an alongshore current, this component was probably at work during the period of this study. Actual flow was undoubtedly influenced by an alongshore geostrophic jet and, as previously stated, similarities to results obtained by Klinck (1989) are noted. This near coastal jet was probably the major generation mechanism of the observed mean flow patterns.

## V. CONCLUSIONS AND RECOMMENDATIONS

### A. CONCLUSIONS

Both prior to and during the period studied in this report, upwelling was occurring along the entire central California coast. Both satellite imagery and the 04 May 1988 geostrophic velocity cross section at Pt. Sur supports this conclusion. Within the Monterey Bay itself, the observed internal wave field was quite active and effectively masked the mean signal throughout the period. Previous studies suggest these internal waves are quite common within the bay and not an anomalous situation during this study. Averaging the mass field and measured ADCP flows effectively filtered out this "noise." Because of this high noise level, any type of hydrographic data acquired over a short time period from the bay is of little use. Only long term averaged data can be used to infer any type of semi-permanent flow pattern within the bay. Also, because of the large amplitudes of these internal waves, geostrophic velocities derived from single section mass field observations will typically yield unrealistically high values, especially within the thermocline.

During periods of strong surface inflow in the northern part of the bay, the flow within the Monterey Bay becomes a two-layered uncoupled system consisting of anticyclonic flow at the surface and weak, canyon trapped, cyclonic flow below the thermocline, limited mainly to the deep waters over the canyon mouth. The main mechanism responsible for this flow pattern during May 1988 was the alongshore, geostrophic, equatorward flow turning into the northern half of the bay. As this equatorward flow encountered the Monterey Submarine Canyon, the geostrophic adjustment process caused upwelling within the canyon which resulted in vortex tube compaction (anticyclonic flow) in the upper layers and stretching of vortex tubes at depth (cyclonic flow) below the thermocline (Klinck, 1989). Numerical simulations of the mean flow pattern suggest that the effects of bottom friction may act to confine lower layer flows to the canyon itself. Other numerical simulations suggested that wind stress may induce anticyclonic surface flow when pre-frontal and post-frontal winds were used to force the model although these experiments were inconclusive due to lack of evolution to a steady state.

If surface flow within the Monterey Bay is predominantly cyclonic as previous authors suggest (Breaker and Broenkow, 1989), upwelling periods may coincide with p i-

ods of flow reversals that have been observed in previous studies (Breaker and Broenkow, 1989). The amount of time this flow reversal lasts after the cessation of upwelling and the alongshore geostrophic jet is unknown. The suggested scenario leading up to the mean flow pattern encountered in this study involves:

- A 7 to 10 day period of strong northwesterly winds produced by high pressure ridging across California behind a series of atmospheric cold fronts.
- Wind stress induced Ekman transport resulting in strong upwelling along the central California coast.
- Development of a strong geostrophic, equatorward, coastal jet along the central coast.
- A geostrophic adjustment process, such as that described by Klinck (1989), as this coastal jet encounters the Monterey Submarine Canyon, resulting in the flow patterns described above.

Since winds are upwelling favorable during most of the summer season, anticyclonic circulation within the Monterey Bay may be more common than previously believed.

## **B. RECOMMENDATIONS FOR FUTURE STUDIES**

### **1. Currents**

The internal wave field within the Monterey Bay needs to be resolved. Once a solid grasp of the frequency and wavenumber spectrum is known, different sampling schemes can more effectively cancel out their influence on the mean field. In this way mean flow can be resolved with a minimum number of samples, thereby saving expensive ship time. To accomplish this, an array of fast sampling thermistor chains should be deployed at strategic locations throughout the bay such as on the shelf breaks. An alternative approach to averaging out the internal wave aliasing is simply through statistical averaging. A higher sampling population should result in smaller standard errors and a better resolution of the mean flow, although cost constraints could be more of a consideration in this case.

Because of non-linear processes at work within the Monterey Bay, current meters and ADCP velocities are probably of somewhat more value than geostrophy in determining flow within the bay. The better resolution of the mean flow by ADCP techniques was apparent in the smaller calculated standard errors of this data set. Again, the longer the time series, the better. Bottom moored ADCP data, especially along the shelf break, would yield valuable information concerning the cross-canyon velocities and upwelling, if any, that is taking place from canyon depths. Seasonal

spectral analyses of the MBA time series data should continue to reveal much about the shelf processes that are occurring within the Monterey Bay.

Finally, as with any scientific hypothesis, results should be reproducible. Therefore, a similar study, conducted during or shortly after a comparable upwelling event, should be undertaken to see if flow patterns similar to those found in this study exist. In this way, flow "reversals" within the Monterey Bay could perhaps be correlated with strong upwelling events. Likewise, a study conducted during a strong poleward flow event would also be enlightening. Current meter moorings placed on the shelf regions to the north and the south of the Monterey Bay during the period of these studies could verify correlations, if any, between these alongshore flows and circulation within the bay.

## **2. Numerical Studies**

While many insights into the behavior of flow within the Monterey Bay were gained from the numerical model used in this study, a few added features would greatly enhance its meaningfulness, namely:

- Future studies which use actual flow to force this model should be from data along a line coincident with the model's open boundary. This would negate the necessary assumptions made in this study in projecting the flow field onto the model grid.
- As mentioned earlier, it would appear that a three-level model would be more appropriate in modeling the Monterey Bay currents. This would diminish the effects of vertical averaging and keep flows closer to their "true" velocities.
- The addition of a realistic coastline and surface topography would enhance the effectiveness of wind forced flow experiments within the bay.
- Since local heating may play a role in circulation processes within the bay (Bigelow and Leslie, 1930), the addition of thermodynamic equations to model air-sea heat exchanges would most likely yield interesting results.
- Expanding the model domain used in this study westward, to encompass the deeper seaward portions of the Monterey Bay Submarine Canyon, and northward and southward, to model the shelf regions in these areas, would provide more realistic results. The additional capability of forcing the model with northward or southward alongshore currents, similar to Klinck's (1989), would also be of great value.

## APPENDIX A. MEAN GEOSTROPHIC VELOCITIES

The following pages contain the mean Geostrophic velocities for the section across the mouth of the Bay (stations 1 to 10). Velocities were derived by calculating the mean mass field (mean temperatures and salinities) from data collected during the 08-11 May 1988 NPS Student Cruise, and then using the thermal wind relation to calculate the velocities.

```

1          ***** GEOSTROPHIC VELOCITY AND TRANSPORT FOR DATA OF THE CRUISE MAY 1988 *****
              (UNITS IN DYNAMIC METERS)

0          ***** GEOSTROPHIC VELOCITY BETWEEN STATIONS 1 AND 2 *****
0 Z(DB)  AV DYN( 1)  AV DYN( 2)  SUM DYN( 1)  SUM DYN( 2)  VELOCITY(CM/S)  TRANSPORT(M3/S)  SUM OF TRANS.
          0. 0.0551  0.0570  0.05507  0.05598  4.91  0.27298E+04  0.27298E+04
          25 0.0190  0.0474  0.00000  0.00000  0.00  0.00000E+00  0.00000E+00
0
0          TOTAL TRANSPORT = 0.27298E+04
0          VELOCITY CALCULATED ASSUMING A LEVEL OF NO MOTION OF 25. DB
          DISTANCE BETWEEN STATIONS = 4.451 KM

0          ***** GEOSTROPHIC VELOCITY BETWEEN STATIONS 2 AND 3 *****
0 Z(DB)  AV DYN( 2)  AV DYN( 3)  SUM DYN( 2)  SUM DYN( 3)  VELOCITY(CM/S)  TRANSPORT(M3/S)  SUM OF TRANS.
          0 0.0570  0.0562  0.14523  0.14522  -0.02  0.96488E+03  0.45425E+04
          25 0.0474  0.0472  0.08825  0.08893  1.85  0.22768E+04  0.35777E+04
          50 0.0408  0.0417  0.04080  0.04171  2.44  0.13008E+04  0.13008E+04
          75 0.0013  0.0262  0.00000  0.00000  0.00  0.00000E+00  0.00000E+00
0
0          TOTAL TRANSPORT = 0.45425E+04
0          VELOCITY CALCULATED ASSUMING A LEVEL OF NO MOTION OF 75. DB
          DISTANCE BETWEEN STATIONS = 4.262 KM

0          ***** GEOSTROPHIC VELOCITY BETWEEN STATIONS 3 AND 4 *****
0 Z(DB)  AV DYN( 3)  AV DYN( 4)  SUM DYN( 3)  SUM DYN( 4)  VELOCITY(CM/S)  TRANSPORT(M3/S)  SUM OF TRANS.
          0. 0.0562  0.0572  0.14522  0.15129  15.62  0.16010E+05  0.31724E+05
          25. 0.0472  0.0494  0.08893  0.09405  13.17  0.11519E+05  0.15714E+05
          50 0.0417  0.0446  0.04171  0.04465  7.54  0.41949E+04  0.41949E+04
          75. 0.0262  0.0407  0.00000  0.04000  0.00  0.00000E+00  0.00000E+00
0
0          TOTAL TRANSPORT = 0.31724E+05
0          VELOCITY CALCULATED ASSUMING A LEVEL OF NO MOTION OF 75. DB
          DISTANCE BETWEEN STATIONS = 4.450 KM

0          ***** GEOSTROPHIC VELOCITY BETWEEN STATIONS 4 AND 5 *****
0 Z(DB)  AV DYN( 4)  AV DYN( 5)  SUM DYN( 4)  SUM DYN( 5)  VELOCITY(CM/S)  TRANSPORT(M3/S)  SUM OF TRANS.
          0. 0.0572  0.0578  0.30500  0.30802  14.37  0.78477E+04  0.29556E+05
          25. 0.0494  0.0496  0.24776  0.25021  11.69  0.67019E+04  0.21709E+05
          50. 0.0446  0.0446  0.19825  0.20058  10.57  0.63729E+04  0.15007E+05
          75 0.0407  0.0417  0.15271  0.15594  10.59  0.49532E+04  0.86337E+04
          100. 0.0286  0.0293  0.11299  0.11422  5.85  0.25938E+04  0.36805E+04
          125. 0.0374  0.0379  0.07436  0.07494  2.76  0.95891E+03  0.10867E+04
          150. 0.0270  0.0371  0.03697  0.03706  0.42  0.12793E+03  0.12793E+03
          175. 0.0188  0.0364  0.00000  0.00000  0.00  0.00000E+00  0.00000E+00
0
0          TOTAL TRANSPORT = 0.29556E+05
0          VELOCITY CALCULATED ASSUMING A LEVEL OF NO MOTION OF 175. DB
          DISTANCE BETWEEN STATIONS = 2.409 KM

```

0 \*\*\*\*\* GEOSTRAPHIC VELOCITY BETWEEN STATIONS 5 AND 6 \*\*\*\*\*

0 Z (DB)	AV DYN( 5)	AV DYN( 6)	SUM DYN( 5)	SUM DYN( 6)	VELOCITY(CM/S)	TRANSPORT(M3/S)	SUM OF TRANS.
0.	0.0578	0.0589	0.91508	0.91644	6.51	0.23187E+04	-0.70078E+05
25.	0.0496	0.0507	0.85726	0.85752	1.19	-0.80090E+03	-0.72397E+05
50.	0.0446	0.0450	0.80763	0.80782	-3.85	-0.27964E+04	-0.71596E+05
75.	0.0417	0.0419	0.76299	0.76164	-5.44	-0.34851E+04	-0.68800E+05
100.	0.0393	0.0396	0.72127	0.71998	-6.14	-0.41078E+04	-0.65315E+05
125.	0.0379	0.0382	0.68199	0.68042	-7.50	-0.50737E+04	-0.61207E+05
150.	0.0371	0.0372	0.64411	0.64215	-9.34	-0.58890E+04	-0.56133E+05
175.	0.0364	0.0365	0.60705	0.60490	-10.21	-0.62065E+04	-0.50244E+05
200.	0.0358	0.0358	0.57061	0.56842	-10.40	-0.62695E+04	-0.44037E+05
225.	0.0352	0.0352	0.53481	0.53262	-10.42	-0.63457E+04	-0.37768E+05
250.	0.0346	0.0346	0.49966	0.49742	-10.65	-0.63716E+04	-0.31422E+05
275.	0.0341	0.0339	0.46506	0.46285	-10.51	-0.60690E+04	-0.25051E+05
300.	0.0334	0.0333	0.43094	0.42891	-9.65	-0.56260E+04	-0.18982E+05
325.	0.0328	0.0328	0.39749	0.39549	-9.03	-0.52901E+04	-0.13256E+05
350.	0.0323	0.0322	0.36458	0.36279	-8.53	-0.50936E+04	-0.80656E+04
375.	0.0316	0.0317	0.33231	0.33055	-8.38	-0.50875E+04	-0.29719E+04
400.	0.0311	0.0307	0.30068	0.29889	-8.51	-0.45281E+04	0.21155E+04
425.	0.0304	0.0308	0.26956	0.26819	-6.52	-0.31092E+04	0.66437E+04
450.	0.0297	0.0291	0.23915	0.23835	-3.80	-0.14271E+04	0.97528E+04
475.	0.0289	0.0285	0.20941	0.20921	-0.94	0.60063E+02	0.11180E+05
500.	0.0281	0.0278	0.18049	0.18073	1.14	0.10924E+04	0.11120E+05
525.	0.0272	0.0269	0.15244	0.15296	2.49	0.18961E+04	0.10028E+05
550.	0.0264	0.0263	0.12527	0.12607	3.81	0.25203E+04	0.81315E+04
575.	0.0255	0.0257	0.09885	0.09991	4.56	0.24561E+04	0.56112E+04
600.	0.0249	0.0252	0.07234	0.07409	3.59	0.17197E+04	0.31551E+04
625.	0.0245	0.0247	0.04845	0.04889	2.12	0.10362E+04	0.14354E+04
650.	0.0239	0.0242	0.02594	0.02422	1.23	0.39912E+03	0.39912E+03
675.	0.0008	0.0236	0.00000	0.00000	0.00	0.00000E+00	0.00000E+00

0 TOTAL TRANSPORT = -0.70078E+05

0 VELOCITY CALCULATED ASSUMING A LEVEL OF NO MOTION OF 675. DB

0 DISTANCE BETWEEN STATIONS = 2.409 KM

0 \*\*\*\*\* GEOSTRAPHIC VELOCITY BETWEEN STATIONS 6 AND 7 \*\*\*\*\*

0 Z (DB)	AV DYN( 6)	AV DYN( 7)	SUM DYN( 6)	SUM DYN( 7)	VELOCITY(CM/S)	TRANSPORT(M3/S)	SUM OF TRANS.
0	0.0589	0.0600	1.21529	1.22080	10.47	0.13949E+05	0.74720E+05
25	0.0507	0.0517	1.15946	1.16077	8.34	0.10927E+05	0.60771E+05
50.	0.0450	0.0453	1.10576	1.10907	6.40	0.90085E+04	0.49844E+05
75	0.0419	0.0422	1.06079	1.06279	5.75	0.80936E+04	0.40836E+05
100.	0.0396	0.0402	1.01892	1.02159	5.16	0.67187E+04	0.32742E+05
125.	0.0383	0.0390	0.97936	0.98137	3.90	0.46864E+04	0.26023E+05
150.	0.0372	0.0379	0.94109	0.94234	2.62	0.27117E+04	0.21337E+05
175.	0.0365	0.0371	0.90385	0.90449	1.24	0.97184E+03	0.18625E+05
200.	0.0359	0.0363	0.86727	0.86741	0.08	-0.57250E+03	0.17654E+05
225.	0.0352	0.0356	0.83152	0.83112	-0.25	-0.17914E+04	0.18226E+05
250.	0.0346	0.0350	0.79627	0.79556	-1.57	-0.28917E+04	0.20017E+05
275.	0.0339	0.0341	0.76179	0.76059	-2.32	-0.37321E+04	0.22909E+05
300.	0.0333	0.0334	0.72786	0.72646	-2.70	-0.40879E+04	0.26641E+05
325.	0.0328	0.0325	0.69452	0.69309	-2.81	-0.38007E+04	0.30729E+05
350.	0.0322	0.0316	0.66173	0.66053	-2.31	-0.25668E+04	0.34530E+05
375.	0.0317	0.0310	0.62949	0.62890	-1.15	-0.68313E+03	0.37097E+05
400.	0.0307	0.0301	0.59783	0.59795	0.23	0.11230E+04	0.37780E+05
425.	0.0298	0.0295	0.56714	0.56780	1.29	0.23338E+04	0.36657E+05
450.	0.0291	0.0290	0.53729	0.53926	1.86	0.29944E+04	0.34233E+05
475.	0.0285	0.0282	0.50816	0.50928	2.18	0.36235E+04	0.31329E+05
500.	0.0278	0.0277	0.47968	0.48108	2.71	0.41080E+04	0.27705E+05
525.	0.0269	0.0271	0.45191	0.45327	2.83	0.38415E+04	0.23597E+05
550.	0.0262	0.0265	0.42591	0.42623	2.25	0.31012E+04	0.19756E+05
575.	0.0257	0.0260	0.39875	0.39979	1.84	0.23567E+04	0.16654E+05
600.	0.0252	0.0254	0.37304	0.37373	1.24	0.17694E+04	0.14298E+05
625.	0.0247	0.0248	0.34784	0.34838	1.04	0.13887E+04	0.12529E+05
650.	0.0242	0.0241	0.32316	0.32359	0.83	0.14179E+04	0.11140E+05
675.	0.0236	0.0235	0.29994	0.29950	1.08	0.16831E+04	0.97224E+04
700.	0.0231	0.0231	0.27538	0.27599	1.19	0.17602E+04	0.80393E+04
725.	0.0227	0.0227	0.25227	0.25288	1.19	0.16791E+04	0.62791E+04



750.	0.0223	0.0224	0.22958	0.23014	1.06	0.14688E+04	0.46000E+04
775.	0.0219	0.0221	0.20728	0.20776	0.93	0.11074E+04	0.31112E+04
800.	0.0217	0.0219	0.18535	0.18564	0.57	0.65195E+03	0.20038E+04
825.	0.0215	0.0215	0.16362	0.16379	0.31	0.39484E+03	0.13519E+04
850.	0.0211	0.0212	0.14212	0.14224	0.22	0.16362E+03	0.95702E+03
875.	0.0209	0.0209	0.12099	0.12099	0.00	0.24526E+02	0.79341E+03
900.	0.0206	0.0205	0.10011	0.10013	0.03	0.98910E+02	0.76888E+03
925.	0.0203	0.0202	0.07954	0.07959	0.19	0.20237E+03	0.66997E+03
950.	0.0200	0.0200	0.05928	0.05937	0.17	0.22347E+03	0.46760E+03
975.	0.0198	0.0198	0.03927	0.03933	0.13	0.17071E+03	0.24413E+03
1000.	0.0195	0.0195	0.01949	0.01954	0.10	0.73419E+02	0.73419E+02
1025.	0.0068	0.0193	0.00000	0.00000	0.00	0.00000E+00	0.00000E+00

0 TOTAL TRANSPORT = 0.74720E+05

0 VELOCITY CALCULATED ASSUMING A LEVEL OF NO MOTION OF 1025. DB

DISTANCE BETWEEN STATIONS : 5.932 KM

0 \*\*\*\*\* GEOSTRPHIC VELOCITY BETWEEN STATIONS 7 AND 8 \*\*\*\*\*

0 Z(DB)	AV DYN( 7)	AV DYN( 8)	SUM DYN( 7)	SUM DYN( 8)	VELOCITY(CM/S)	TRANSPORT(M3/S)	SUM OF TRANS.
0.	0.0600	0.0584	1.09981	1.09598	-11.13	-0.87339E+04	0.10137E+06
25.	0.0517	0.0490	1.03978	1.03753	-6.54	-0.26449E+04	0.11011E+06
50.	0.0453	0.0437	0.98808	0.98849	1.19	0.35282E+04	0.11275E+06
75.	0.0422	0.0412	0.94277	0.94482	5.95	0.73700E+04	0.10922E+06
100.	0.0402	0.0400	0.90061	0.90366	8.89	0.91431E+04	0.10190E+06
125.	0.0390	0.0389	0.86039	0.86071	9.64	0.97788E+04	0.92761E+05
150.	0.0379	0.0380	0.82135	0.82485	10.15	0.98879E+04	0.82982E+05
175.	0.0371	0.0373	0.78250	0.78689	9.86	0.92898E+04	0.73094E+05
200.	0.0363	0.0367	0.74642	0.74956	9.14	0.84024E+04	0.63705E+05
225.	0.0356	0.0358	0.71014	0.71295	7.86	0.74849E+04	0.55302E+05
250.	0.0350	0.0349	0.67457	0.67708	7.28	0.72532E+04	0.47817E+05
275.	0.0341	0.0343	0.63960	0.64215	7.39	0.70117E+04	0.40564E+05
300.	0.0334	0.0337	0.60547	0.60781	6.79	0.63234E+04	0.33553E+05
325.	0.0325	0.0327	0.57209	0.57416	6.00	0.56917E+04	0.27229E+05
350.	0.0316	0.0319	0.53954	0.54144	5.52	0.51228E+04	0.21537E+05
375.	0.0310	0.0311	0.50791	0.50958	4.85	0.45097E+04	0.16415E+05
400.	0.0301	0.0304	0.47696	0.47843	4.28	0.39082E+04	0.11905E+05
425.	0.0295	0.0297	0.44681	0.44806	3.63	0.33025E+04	0.79967E+04
450.	0.0290	0.0291	0.41727	0.41822	3.05	0.28108E+04	0.46942E+04
475.	0.0282	0.0285	0.38829	0.38920	2.64	0.21792E+04	0.18834E+04
500.	0.0277	0.0279	0.36009	0.36070	1.77	0.14765E+04	-0.29585E+03
525.	0.0271	0.0274	0.33238	0.33280	1.22	0.90058E+03	-0.17724E+04
550.	0.0265	0.0269	0.30524	0.30545	0.61	0.47044E+03	-0.26729E+04
575.	0.0260	0.0260	0.27871	0.27882	0.35	0.35766E+03	-0.31434E+04
600.	0.0254	0.0253	0.25274	0.25287	0.38	0.38705E+03	-0.35010E+04
625.	0.0248	0.0248	0.22739	0.22753	0.41	0.33469E+03	-0.38881E+04
650.	0.0241	0.0243	0.20260	0.20270	0.27	-0.86030E+02	-0.42228E+04
675.	0.0235	0.0237	0.17851	0.17836	-0.45	-0.74780E+03	-0.41367E+04
700.	0.0231	0.0231	0.15501	0.15464	-1.07	-0.10707E+04	-0.33890E+04
725.	0.0227	0.0226	0.13189	0.13151	-1.10	-0.92448E+03	-0.23183E+04
750.	0.0224	0.0223	0.10915	0.10889	-0.77	-0.65159E+03	-0.13938E+04
775.	0.0221	0.0220	0.08677	0.08658	-0.55	-0.38830E+03	-0.74221E+03
800.	0.0219	0.0218	0.06465	0.06457	-0.24	-0.19064E+03	-0.35391E+03
825.	0.0215	0.0215	0.04280	0.04275	-0.15	-0.11804E+03	-0.16327E+03
850.	0.0212	0.0212	0.02125	0.02122	-0.09	-0.45235E+02	-0.45235E+02
875.	0.0209	0.0208	0.00000	0.00000	0.00	0.00000E+00	0.00000E+00

0 TOTAL TRANSPORT = 0.10137E+06

0 VELOCITY CALCULATED ASSUMING A LEVEL OF NO MOTION OF 875. DB

DISTANCE BETWEEN STATIONS : 3.953 KM

0 \*\*\*\*\* GEOSTRPHIC VELOCITY BETWEEN STATIONS 8 AND 9 \*\*\*\*\*

0 Z(DB)	AV DYN( 8)	AV DYN( 9)	SUM DYN( 8)	SUM DYN( 9)	VELOCITY(CM/S)	TRANSPORT(M3/S)	SUM OF TRANS.
0.	0.0584	0.0569	0.81715	0.81424	-12.04	-0.59551E+04	0.93366E+04
25.	0.0490	0.0482	0.75970	0.75743	-5.45	-0.24465E+04	0.15192E+05
50.	0.0437	0.0431	0.70966	0.70923	-1.86	-0.39201E+03	0.17638E+05
75.	0.0412	0.0409	0.66599	0.66515	0.68	0.10248E+04	0.18030E+05

100.	0.0400	0.0398	0.62483	0.62538	2.38	0.18674E+04	0.17005E+05
125.	0.0389	0.0390	0.58488	0.58562	3.20	0.19837E+04	0.15138E+05
150.	0.0380	0.0382	0.54402	0.54465	2.72	0.14638E+04	0.13154E+05
175.	0.0373	0.0372	0.50806	0.50845	1.65	0.12794E+04	0.11691E+05
200.	0.0367	0.0363	0.47074	0.47124	2.17	0.20578E+04	0.10411E+05
225.	0.0358	0.0356	0.43402	0.43495	3.97	0.28941E+04	0.83534E+04
250.	0.0349	0.0350	0.39825	0.39934	4.67	0.30613E+04	0.54593E+04
275.	0.0343	0.0343	0.36332	0.36436	4.47	0.29956E+04	0.23979E+04
300.	0.0337	0.0338	0.32898	0.33002	4.47	0.27893E+04	-0.59762E+03
325.	0.0327	0.0329	0.29533	0.29623	3.86	0.23172E+04	-0.32869E+04
350.	0.0319	0.0321	0.26261	0.26333	3.04	0.17398E+04	-0.57041E+04
375.	0.0311	0.0314	0.23075	0.23125	2.13	0.11069E+04	-0.74439E+04
400.	0.0304	0.0307	0.19960	0.19968	1.17	0.32530E+03	-0.85508E+04
425.	0.0297	0.0302	0.16824	0.16919	-0.20	-0.73630E+03	-0.88761E+04
450.	0.0291	0.0294	0.13949	0.13962	-2.00	-0.17234E+04	-0.81398E+04
475.	0.0285	0.0286	0.11037	0.10964	-3.15	-0.21831E+04	-0.64144E+04
500.	0.0279	0.0278	0.08187	0.08108	-2.37	-0.21536E+04	-0.42334E+04
525.	0.0274	0.0270	0.05397	0.05326	-3.06	-0.15526E+04	-0.20798E+04
550.	0.0266	0.0262	0.02662	0.02625	-1.57	-0.52724E+03	-0.52724E+03
575.	0.0260	0.0254	0.00020	0.00000	0.00	0.00000E+00	0.00000E+00

0 TOTAL TRANSPORT = 0.93366E+04

0 VELOCITY CALCULATED ASSUMING A LEVEL OF NO MOTION OF 575. DB

DISTANCE BETWEEN STATIONS = 2.678 KM

0 \*\*\*\*\* GEOTRAPHIC VELOCITY BETWEEN STATIONS 9 AND 10 \*\*\*\*\*

0 Z(EP)	AV DYN( 9)	AV DYN( 10)	SUM DYN( 9)	SUM DYN( 10)	VELOCITY(CM/S)	TRANSPORT(M3/S)	SUM OF TRANS.
0.	0.0569	0.0525	0.14819	0.13969	-18.57	-0.19499E+05	-0.31398E+05
25.	0.0482	0.0447	0.09128	0.08619	-11.11	-0.95985E+04	-0.11900E+05
50.	0.0431	0.0415	0.04307	0.04147	-3.50	-0.23011E+04	-0.23011E+04
75.	0.0408	0.0141	0.00000	0.00000	0.00	0.00000E+00	0.00000E+00

0 TOTAL TRANSPORT = -0.31398E+05

0 VELOCITY CALCULATED ASSUMING A LEVEL OF NO MOTION OF 75. DB

The following pages contain the mean Geostrophic velocities for the inland section, towards the head of the Monterey Submarine Canyon (stations 10 through 17). Velocities were derived by calculating the mean mass field (mean temperatures and salinities) from data collected during the 08-11 May 1988 NPS Student Cruise, and then using the thermal wind relation to calculate the velocities.

DISTANCE BETWEEN STATIONS : 5.256 KM

1 \*\*\*\*\* GEOSTROPHIC VELOCITY AND TRANSPORT FOR DATA OF THE CRUISE MAY 1988 \*\*\*\*\*  
(UNITS IN DYNAMIC METERS)

0 \*\*\*\*\* GEOSTROPHIC VELOCITY BETWEEN STATIONS 17 AND 16 \*\*\*\*\*  
0 Z(DB) AV DYN( 17) AV DYN( 16) SUM DYN( 17) SUM DYN( 16) VELOCITY(CM/S) TRANSPORT(M<sup>2</sup>/S) SUM OF TRANS.  
0. 0 0551 0.0554 0.05611 0.05525 -2.04 -0.10851E+04 -0.10851E+04  
25. 0 0058 0.0457 0.00000 0.00000 0.00 0.00000E+00 0.00000E+00  
0 TOTAL TRANSPORT = -0.10851E+04  
0 VELOCITY CALCULATED ASSUMING A LEVEL OF NO MOTION OF 25. DB  
DISTANCE BETWEEN STATIONS : 4.246 KM

0 \*\*\*\*\* GEOSTROPHIC VELOCITY BETWEEN STATIONS 16 AND 15 \*\*\*\*\*  
0 Z(DB) AV DYN( 16) AV DYN( 15) SUM DYN( 16) SUM DYN( 15) VELOCITY(CM/S) TRANSPORT(M<sup>2</sup>/S) SUM OF TRANS.  
0. 0 0554 0.0544 0.10101 0.10024 -1.55 -0.49842E+03 -0.33298E+02  
25. 0 0457 0.0460 0.04566 0.04598 0.75 0.46513E+03 0.46513E+03  
50. 0 0166 0.0415 0.00000 0.00000 0.00 0.00000E+00 0.00000E+00  
0 TOTAL TRANSPORT = -0.33298E+02  
0 VELOCITY CALCULATED ASSUMING A LEVEL OF NO MOTION OF 50. DB  
DISTANCE BETWEEN STATIONS : 4.963 KM

0 \*\*\*\*\* GEOSTROPHIC VELOCITY BETWEEN STATIONS 15 AND 14 \*\*\*\*\*  
0 Z(DB) AV DYN( 15) AV DYN( 14) SUM DYN( 15) SUM DYN( 14) VELOCITY(CM/S) TRANSPORT(M<sup>2</sup>/S) SUM OF TRANS.  
0 0 0544 0.0531 0.42900 0.42922 0.77 0.24220E+04 0.23695E+05  
25. 0 0460 0.0457 0.38465 0.38613 5.22 0.46050E+04 0.21272E+05  
50. 0 0415 0.0418 0.32867 0.34041 6.16 0.45626E+04 0.16666E+05  
75. 0 0291 0.0297 0.29717 0.29862 5.12 0.32365E+04 0.12102E+05  
100. 0 0384 0.0386 0.25809 0.25891 2.89 0.20456E+04 0.88659E+04  
125. 0 0379 0.0378 0.21971 0.22023 2.17 0.19496E+04 0.68203E+04  
150. 0 0373 0.0373 0.18183 0.18258 2.64 0.20047E+04 0.48709E+04  
175. 0 0367 0.0370 0.14457 0.14523 2.31 0.15496E+04 0.28662E+04  
200. 0 0364 0.0366 0.10784 0.10827 1.52 0.92618E+03 0.13167E+04  
225. 0 0259 0.0261 0.07147 0.07169 0.77 0.25102E+03 0.39049E+03  
250. 0 0355 0.0356 0.03554 0.03556 0.10 0.39465E+02 0.39465E+02  
275. 0 0250 0.0349 0.00000 0.00000 0.00 0.00000E+00 0.00000E+00  
0 TOTAL TRANSPORT = 0.23695E+05  
0 VELOCITY CALCULATED ASSUMING A LEVEL OF NO MOTION OF 275. DB  
DISTANCE BETWEEN STATIONS : 3.237 KM

0 \*\*\*\*\* GEOTRPHIC VELOCITY BETWEEN STATIONS 14 AND 13 \*\*\*\*\*

0 Z(DB)	AV DYN( 14)	AV DYN( 13)	SUM DYN( 14)	SUM DYN( 13)	VELOCITY(CM/S)	TRANSPORT(M3/S)	SUM OF TRANS.
0.	0.0531	0.0538	0.43922	0.44082	6.17	0.35307E+04	0.43559E+03
25.	0.0457	0.0458	0.38613	0.38699	3.75	0.23715E+04	-0.30952E+04
50.	0.0418	0.0423	0.34041	0.34120	3.04	0.15890E+04	-0.54667E+04
75.	0.0397	0.0403	0.29862	0.29894	1.24	0.15029E+02	-0.70556E+04
100.	0.0386	0.0387	0.25891	0.25859	-1.20	-0.11315E+04	-0.70707E+04
125.	0.0378	0.0378	0.22733	0.21985	-1.85	-0.14679E+04	-0.59392E+04
150.	0.0373	0.0373	0.18258	0.18203	-2.11	-0.15383E+04	-0.44713E+04
175.	0.0370	0.0368	0.14523	0.14470	-2.04	-0.13439E+04	-0.29330E+04
200.	0.0366	0.0364	0.10827	0.10786	-1.58	-0.95443E+03	-0.15891E+04
225.	0.0361	0.0360	0.07169	0.07144	-0.99	-0.50078E+03	-0.63466E+03
250.	0.0356	0.0355	0.03556	0.03547	-0.26	-0.13388E+03	-0.13388E+03
275.	0.0349	0.0348	0.00000	0.00000	0.00	0.00000E+00	0.00000E+00

TOTAL TRANSPORT = 0.43559E+03

0 VELOCITY CALCULATED ASSUMING A LEVEL OF NO MOTION OF 275. DB  
 0 DISTANCE BETWEEN STATIONS : 2.967 KM

0 \*\*\*\*\* GEOTRPHIC VELOCITY BETWEEN STATIONS 13 AND 12 \*\*\*\*\*

0 Z(DB)	AV DYN( 13)	AV DYN( 12)	SUM DYN( 13)	SUM DYN( 12)	VELOCITY(CM/S)	TRANSPORT(M3/S)	SUM OF TRANS.
0.	0.0538	0.0556	0.14187	0.14489	7.26	0.60781E+04	0.90320E+04
25.	0.0459	0.0466	0.08805	0.08928	3.00	0.23567E+04	0.29539E+04
50.	0.0423	0.0427	0.04225	0.04267	1.02	0.59720E+03	0.59720E+03
75.	0.0403	0.0391	0.00000	0.00000	0.00	0.00000E+00	0.00000E+00

TOTAL TRANSPORT = 0.90320E+04

0 VELOCITY CALCULATED ASSUMING A LEVEL OF NO MOTION OF 75. DB  
 0 DISTANCE BETWEEN STATIONS : 4.693 KM

0 \*\*\*\*\* GEOTRPHIC VELOCITY BETWEEN STATIONS 12 AND 11 \*\*\*\*\*

0 Z(DB)	AV DYN( 12)	AV DYN( 11)	SUM DYN( 12)	SUM DYN( 11)	VELOCITY(CM/S)	TRANSPORT(M3/S)	SUM OF TRANS.
0.	0.0556	0.0562	0.14489	0.14612	3.07	0.26982E+04	0.36582E+04
25.	0.0466	0.0472	0.08928	0.08993	1.62	0.96522E+03	0.95995E+03
50.	0.0427	0.0427	0.04267	0.04268	0.03	0.14738E+02	0.14738E+02
75.	0.0391	0.0393	0.00000	0.00000	0.00	0.00000E+00	0.00000E+00

TOTAL TRANSPORT = 0.36582E+04

0 VELOCITY CALCULATED ASSUMING A LEVEL OF NO MOTION OF 75. DB  
 0 DISTANCE BETWEEN STATIONS : 4.603 KM

0 \*\*\*\*\* GEOTRPHIC VELOCITY BETWEEN STATIONS 11 AND 10 \*\*\*\*\*

0 Z(DB)	AV DYN( 11)	AV DYN( 10)	SUM DYN( 11)	SUM DYN( 10)	VELOCITY(CM/S)	TRANSPORT(M3/S)	SUM OF TRANS.
0.	0.0562	0.0535	0.14612	0.13969	-15.89	-0.14590E+05	-0.23429E+05
25.	0.0472	0.0447	0.08993	0.08619	-9.23	-0.70997E+04	-0.88386E+04
50.	0.0427	0.0415	0.04268	0.04147	-2.99	-0.17389E+04	-0.17389E+04
75.	0.0393	0.0141	0.00000	0.00000	0.00	0.00000E+00	0.00000E+00

TOTAL TRANSPORT = -0.23429E+05

0 VELOCITY CALCULATED ASSUMING A LEVEL OF NO MOTION OF 75. DB  
 0 DISTANCE BETWEEN STATIONS : 4.646 KM

## APPENDIX B. MEAN ACOUSTIC DOPPLER CURRENT PROFILER (ADCP) VELOCITIES

### ADCP STATISTICS

(Note: Negative velocities are into the Bay,  
positive velocities are out of the Bay.)

GROUP: 1

MEAN DISTANCE FROM NORTH (KM): 4.313

DEPTH(M)	MEAN VELOCITY(CM/S)	STANDARD DEVIATION(CM/S)	STANDARD ERROR(CM/S)
22	-2.26	10.54	4.71
38	-0.95	7.94	3.55

GROUP: 2

MEAN DISTANCE FROM NORTH (KM): 8.620

DEPTH(M)	MEAN VELOCITY(CM/S)	STANDARD DEVIATION(CM/S)	STANDARD ERROR(CM/S)
22	-4.48	10.99	4.92
38	-3.02	10.84	4.85
54	-1.29	7.84	3.50

GROUP: 3

MEAN DISTANCE FROM NORTH (KM): 12.950

DEPTH(M)	MEAN VELOCITY(CM/S)	STANDARD DEVIATION(CM/S)	STANDARD ERROR(CM/S)
22	-9.46	10.67	4.77
38	-6.40	9.40	4.20
54	-5.94	9.57	4.28
70	-4.71	5.60	2.50

GROUP: 4

MEAN DISTANCE FROM NORTH (KM): 17.324

DEPTH(M)	MEAN VELOCITY(CM/S)	STANDARD DEVIATION(CM/S)	STANDARD ERROR(CM/S)
22	-14.97	3.86	1.72
38	-13.22	3.22	1.44
54	-10.58	5.02	2.24

70	-8.57	5.41	2.42
86	-4.28	4.97	2.22
102	-2.44	3.94	1.76
118	-0.86	5.45	2.44
134	1.03	6.66	2.98
150	1.64	7.57	3.39
166	1.94	6.89	3.08
182	2.10	7.11	3.18
198	1.78	6.70	3.00
214	1.31	6.07	2.71
230	0.63	5.23	2.34
246	-0.81	4.70	2.10
262	0.07	4.78	2.14
278	0.70	5.29	2.36
294	-0.10	4.67	2.09
310	-1.92	3.50	1.56
326	-2.97	2.82	1.26
342	-2.96	2.01	0.90
358	-3.24	1.45	0.65
374	-4.27	1.40	0.63
390	-4.52	1.99	0.89
406	-4.62	2.36	1.06
422	-4.64	3.42	1.53

GROUP: 5  
MEAN DISTANCE FROM NORTH (KM): 21.809

DEPTH(M)	MEAN VELOCITY(CM/S)	STANDARD DEVIATION(CM/S)	STANDARD ERROR(CM/S)
22	-11.47	3.81	1.70
38	-9.81	3.09	1.38
54	-8.36	4.50	2.01
70	-6.42	2.36	1.05
86	-4.99	2.87	1.28
102	-8.37	3.62	1.62
118	-8.86	5.29	2.36
134	-8.47	6.76	3.02
150	-6.66	5.64	2.52
166	-4.24	3.23	1.45
182	-3.19	3.59	1.60
198	-1.99	3.66	1.64
214	-1.17	2.85	1.27
230	-1.48	2.54	1.14
246	-1.71	3.15	1.41
262	-2.06	3.79	1.69
278	-0.63	3.45	1.54
294	-0.59	3.69	1.65
310	-1.59	3.19	1.42
326	-2.03	2.42	1.08
342	-2.11	2.16	0.97
358	-2.60	2.44	1.09
374	-2.30	1.93	0.86
390	-2.03	2.56	1.14
406	-2.24	4.21	1.88

422                -3.65                3.89                1.74

GROUP: 6  
MEAN DISTANCE FROM NORTH (KM): 25.809

DEPTH(M)	MEAN VELOCITY(CM/S)	STANDARD DEVIATION(CM/S)	STANDARD ERROR(CM/S)
22	-8.78	5.77	2.58
38	-8.19	4.36	1.95
54	-6.91	4.76	2.13
70	-6.35	4.97	2.22
86	-6.62	5.45	2.44
102	-6.49	4.20	1.88
118	-3.62	2.67	1.19
134	-2.34	3.54	1.59
150	-1.25	4.87	2.18
166	-1.31	6.53	2.92
182	-0.84	7.10	3.17
198	-0.48	6.26	2.80
214	-0.74	6.84	3.06
230	0.10	7.37	3.30
246	-0.70	6.68	2.99
262	-3.02	7.26	3.25
278	-3.34	6.10	2.73
294	-2.71	4.39	1.96
310	-1.91	3.84	1.72
326	-2.56	3.31	1.48
342	-2.69	2.47	1.10
358	-2.76	3.62	1.62
374	-2.56	4.07	1.82
390	-2.61	4.28	1.91
406	-2.10	4.06	1.82
422	-1.14	3.19	1.42

GROUP: 7  
MEAN DISTANCE FROM NORTH (KM): 29.986

DEPTH(M)	MEAN VELOCITY(CM/S)	STANDARD DEVIATION(CM/S)	STANDARD ERROR(CM/S)
22	5.46	3.46	1.55
38	5.07	6.89	3.08
54	1.79	5.97	2.67
70	-1.94	4.89	2.19
86	-5.37	5.89	2.63
102	-10.12	7.91	3.54
118	-13.71	9.17	4.10
134	-12.88	6.73	3.01
150	-11.07	6.02	2.69
166	-10.56	5.84	2.61
182	-10.25	4.53	2.03
198	-8.94	4.05	1.81
214	-8.69	3.50	1.57

230	-8.96	4.15	1.86
246	-8.77	4.43	1.98
262	-8.17	3.29	1.47
278	-8.14	2.88	1.29
294	-8.59	2.34	1.05
310	-7.85	1.62	0.72
326	-6.83	2.34	1.04
342	-6.00	3.68	1.64
358	-5.20	4.11	1.84
374	-5.51	3.39	1.52
390	-6.21	2.70	1.21
406	-5.83	2.51	1.12
422	-5.21	2.87	1.28

GROUP: 8

MEAN DISTANCE FROM NORTH (KM): 34.476

DEPTH(M)	MEAN VELOCITY(CM/S)	STANDARD DEVIATION(CM/S)	STANDARD ERROR(CM/S)
22	10.48	7.81	3.49
38	6.17	6.14	2.75
54	3.32	6.80	3.04
70	3.92	7.81	3.49
86	-1.56	8.79	3.93
102	-4.17	10.50	4.70
118	-4.34	10.49	4.69
134	-2.65	9.28	4.15
150	-1.89	9.24	4.13
166	-2.09	9.52	4.26
182	-2.35	8.21	3.67
198	-2.36	6.45	2.89
214	-1.00	4.76	2.13
230	0.03	3.53	1.58
246	-0.98	3.66	1.64
262	-1.08	3.77	1.69
278	-1.41	3.41	1.53
294	-1.14	2.61	1.17
310	-1.28	1.97	0.88
326	-1.10	1.37	0.61
342	-1.44	2.25	1.00
358	-1.78	2.84	1.27
374	-2.08	2.83	1.27
390	-1.89	3.13	1.40
406	-1.04	3.49	1.56
422	-0.56	3.36	1.50

GROUP: 9

MEAN DISTANCE FROM NORTH (KM): 38.597

DEPTH(M)	MEAN VELOCITY(CM/S)	STANDARD DEVIATION(CM/S)	STANDARD ERROR(CM/S)
22	7.02	7.88	3.52



38	-0.32	6.39	2.86
54	-0.98	5.19	2.32
70	-3.28	7.51	3.36

## APPENDIX C. MONTEREY BAY MODEL BOUNDARY CONDITIONS

MEAN (UNCORRECTED) VELOCITIES ALONG MOUTH SECTION				
POINT	DIST(KM) FROM SOUTH	V1	V2	DEPTH(M)
1	0.33573E+02	0.16357E+01	0.00000E+00	72
2	0.29217E+02	0.14175E+01	0.00000E+00	91
3	0.24861E+02	0.12107E+02	0.00000E+00	165
4	0.21431E+02	0.12209E+02	0.39263E+01	483
5	0.19022E+02	0.12831E+01	-0.46778E+01	971
6	0.14852E+02	0.84049E+01	0.78001E+00	1528
7	0.99097E+01	-0.54945E+01	0.34386E+01	1501
8	0.65941E+01	-0.64503E+01	0.12990E+01	940
9	0.26277E+01	-0.11061E+02	0.00000E+00	413

MEAN V VELOCITIES PROJECTED (INTERPOLATED) ON MODEL GRID				
GRID POINT	DIST(KM) FROM SOUTH	V1	V2	MODEL DEPTH(M)
2	0.28500E+02	0.14175E+01	0.00000E+00	90
3	0.21000E+02	0.12107E+02	0.00000E+00	162
4	0.19000E+02	0.12209E+02	0.39263E+01	450
5	0.12500E+02	0.12831E+01	-0.46778E+01	900
6	0.11500E+02	0.84049E+01	0.78001E+00	1080
7	0.75000E+01	-0.54945E+01	0.34386E+01	900
8	0.65000E+01	-0.64503E+01	0.12990E+01	540
9	0.20000E+01	-0.11061E+02	0.00000E+00	157

MODEL BOUNDARY U (INTERPOLATED) VELOCITIES			
POINT	DIST(KM) FROM SOUTH	V1	V2
65	0.32000E+02	0.59060E+00	0.00000E+00
64	0.31500E+02	0.70873E+00	0.00000E+00
63	0.31000E+02	0.82685E+00	0.00000E+00
62	0.30500E+02	0.94497E+00	0.00000E+00
61	0.30000E+02	0.10631E+01	0.00000E+00
60	0.29500E+02	0.11812E+01	0.00000E+00
59	0.29000E+02	0.12993E+01	0.00000E+00
58	0.28500E+02	0.14175E+01	0.00000E+00
57	0.28000E+02	0.21301E+01	0.00000E+00
56	0.27500E+02	0.28427E+01	0.00000E+00
55	0.27000E+02	0.35554E+01	0.00000E+00
54	0.26500E+02	0.42680E+01	0.00000E+00
53	0.26000E+02	0.49806E+01	0.00000E+00
52	0.25500E+02	0.56933E+01	0.00000E+00
51	0.25000E+02	0.64059E+01	0.00000E+00
50	0.24500E+02	0.71185E+01	0.00000E+00
49	0.24000E+02	0.78312E+01	0.00000E+00
48	0.23500E+02	0.85438E+01	0.00000E+00
47	0.23000E+02	0.92565E+01	0.00000E+00
46	0.22500E+02	0.99691E+01	0.00000E+00

45	0.22000E+02	0.10682E+02	0.00000E+00
44	0.21500E+02	0.11394E+02	0.00000E+00
43	0.21000E+02	0.12107E+02	0.00000E+00
42	0.20500E+02	0.12132E+02	0.98157E+00
41	0.20000E+02	0.12158E+02	0.19631E+01
40	0.19500E+02	0.12183E+02	0.29447E+01
39	0.19000E+02	0.12209E+02	0.39263E+01
38	0.18500E+02	0.11368E+02	0.32644E+01
37	0.18000E+02	0.10528E+02	0.26026E+01
36	0.17500E+02	0.96874E+01	0.19407E+01
35	0.17000E+02	0.88470E+01	0.12789E+01
34	0.16500E+02	0.80065E+01	0.61703E+00
33	0.16000E+02	0.71661E+01	-0.44824E-01
32	0.15500E+02	0.63257E+01	-0.70668E+00
31	0.15000E+02	0.54853E+01	-0.13685E+01
30	0.14500E+02	0.46448E+01	-0.20304E+01
29	0.14000E+02	0.38044E+01	-0.26922E+01
28	0.13500E+02	0.29640E+01	-0.33541E+01
27	0.13000E+02	0.21236E+01	-0.40159E+01
26	0.12500E+02	0.12831E+01	-0.46778E+01
25	0.12000E+02	0.48440E+01	-0.19489E+01
24	0.11500E+02	0.84049E+01	0.78001E+00
23	0.11000E+02	0.66675E+01	0.11123E+01
22	0.10500E+02	0.49301E+01	0.14446E+01
21	0.10000E+02	0.31926E+01	0.17770E+01
20	0.95000E+01	0.14552E+01	0.21093E+01
19	0.90000E+01	-0.28223E+00	0.24416E+01
18	0.85000E+01	-0.20197E+01	0.27739E+01
17	0.80000E+01	-0.37571E+01	0.31063E+01
16	0.75000E+01	-0.54945E+01	0.34386E+01
15	0.70000E+01	-0.59724E+01	0.23688E+01
14	0.65000E+01	-0.64503E+01	0.12990E+01
13	0.60000E+01	-0.69626E+01	0.11547E+01
12	0.55000E+01	-0.74750E+01	0.10103E+01
11	0.50000E+01	-0.79873E+01	0.86600E+00
10	0.45000E+01	-0.84996E+01	0.72167E+00
9	0.40000E+01	-0.90119E+01	0.57733E+00
8	0.35000E+01	-0.95243E+01	0.43300E+00
7	0.30000E+01	-0.10037E+02	0.28867E+00
6	0.25000E+01	-0.10549E+02	0.14433E+00
5	0.20000E+01	-0.11061E+02	0.00000E+00
4	0.15000E+01	-0.82959E+01	0.00000E+00
3	0.10000E+01	-0.55306E+01	0.00000E+00
2	0.50000E+00	-0.27653E+01	0.00000E+00
1	0.00000E+00	0.00000E+00	0.00000E+00

# DERIVATION OF MASS BALANCED FLOW FIELD

GRID POINT	RAW VALUES (M**2/S)		MASS BALANCED VALUES (M**2/S)	
	V1	V2	V1	V2
1	0.0	0.0	0.0	0.0
3	0.5	0.0	0.3	0.0
5	0.6	0.0	0.4	0.0
7	0.7	0.0	0.5	0.0
9	1.4	0.0	0.9	0.0
11	2.1	0.0	1.4	0.0
13	2.8	0.0	1.8	0.0
15	3.6	0.0	2.4	0.0
17	4.3	0.0	2.8	0.0
19	5.0	0.0	3.3	0.0
21	5.7	0.0	3.7	0.0
23	6.1	0.0	4.0	0.0
25	6.1	4.9	4.0	3.6
27	5.7	11.0	3.7	8.1
29	4.8	9.6	3.1	7.1
31	4.0	3.9	2.6	2.9
33	3.2	-5.4	2.1	-7.9
35	2.3	-16.0	1.5	-23.4
37	1.5	-26.0	1.0	-38.0
39	0.6	-40.0	0.4	-58.4
41	4.2	7.4	2.8	5.5
43	2.5	16.0	1.6	11.8
45	0.7	26.0	0.5	19.2
47	-1.0	34.0	-1.5	25.2
49	-2.7	40.0	-4.2	29.6
51	-3.2	11.0	-4.9	8.1
53	-3.7	5.1	-5.7	3.8
55	-4.2	2.5	-6.5	1.8
57	-4.8	0.9	-7.4	0.6
59	-5.3	0.3	-8.2	0.2
61	-4.1	0.0	-6.3	0.0
63	0.0	0.0	0.0	0.0
NET TRANSPORT	39.4	85.1	0.0	0.0

## LINEAR CORRECTION COEFFICIENTS APPLIED TO:

NEGATIVE V1 VALUES = 1.5450  
 POSITIVE V1 VALUES = 0.6550  
 NEGATIVE V2 VALUES = 1.4605  
 POSITIVE V2 VALUES = 0.7399

# MODEL BATHYMETRY ALONG OPEN BOUNDARY

DISTANCE(KM) FROM SOUTH	MODEL DEPTH (M)
31.5	90.0
31.0	90.0
30.5	90.0
30.0	90.0
29.5	90.0
29.0	90.0
28.5	90.0
28.0	90.0
27.5	90.0
27.0	90.0
26.5	90.0
26.0	90.0
25.5	90.0
25.0	90.0
24.5	90.0
24.0	94.5
23.5	99.0
23.0	103.5
22.5	108.0
22.0	126.0
21.5	144.0
21.0	162.0
20.5	180.0
20.0	270.0
19.5	360.0
19.0	450.0
18.5	540.0
18.0	585.0
17.5	630.0
17.0	675.0
16.5	720.0
16.0	720.0
15.5	720.0
15.0	720.0
14.5	720.0
14.0	765.0
13.5	810.0
13.0	855.0
12.5	900.0
12.0	990.0
11.5	1080.0
11.0	1170.0
10.5	1260.0
10.0	1260.0
9.5	1260.0
9.0	1260.0
8.5	1260.0
8.0	1080.0
7.5	900.0
7.0	720.0
6.5	540.0
6.0	461.2

5.5	382.5
5.0	303.7
4.5	225.0
4.0	213.7
3.5	202.5
3.0	191.2
2.5	180.0
2.0	157.5
1.5	135.0
1.0	112.5
0.5	90.0

## APPENDIX D. MEAN BRUNT-VAISALA FREQUENCIES AND ROSSBY RADII

STATION: 1 LAT: 36 55.2 LON: 122 5.8  
BOTTOM DEPTH = 45.5  
MEAN BRUNT-VAISALA FREQ (CPS) = 0.1174E-01  
EXTERNAL ROSSBY RADIUS (KM) = 241.85  
FIRST INTERNAL ROSSBY RADIUS (KM) = 1.95

STATION: 2 LAT: 36 52.8 LON: 122 5.9  
BOTTOM DEPTH = 75.2  
MEAN BRUNT-VAISALA FREQ (CPS) = 0.1063E-01  
EXTERNAL ROSSBY RADIUS (KM) = 311.12  
FIRST INTERNAL ROSSBY RADIUS (KM) = 2.92

STATION: 3 LAT: 36 50.5 LON: 122 5.9  
BOTTOM DEPTH = 91.1  
MEAN BRUNT-VAISALA FREQ (CPS) = 0.9942E-02  
EXTERNAL ROSSBY RADIUS (KM) = 342.38  
FIRST INTERNAL ROSSBY RADIUS (KM) = 3.30

STATION: 4 LAT: 36 48.1 LON: 122 5.8  
BOTTOM DEPTH = 186.3  
MEAN BRUNT-VAISALA FREQ (CPS) = 0.7315E-02  
EXTERNAL ROSSBY RADIUS (KM) = 489.65  
FIRST INTERNAL ROSSBY RADIUS (KM) = 4.97

STATION: 5 LAT: 36 46.8 LON: 122 5.8  
BOTTOM DEPTH = 669.8  
MEAN BRUNT-VAISALA FREQ (CPS) = 0.4895E-02  
EXTERNAL ROSSBY RADIUS (KM) = 928.38  
FIRST INTERNAL ROSSBY RADIUS (KM) = 11.96

STATION: 6 LAT: 36 45.5 LON: 122 5.8  
BOTTOM DEPTH = 1023.6  
MEAN BRUNT-VAISALA FREQ (CPS) = 0.4220E-02  
EXTERNAL ROSSBY RADIUS (KM) = 1147.67  
FIRST INTERNAL ROSSBY RADIUS (KM) = 15.76

STATION: 7 LAT: 36 42.3 LON: 122 5.8  
BOTTOM DEPTH = 1582.0  
MEAN BRUNT-VAISALA FREQ (CPS) = 0.3597E-02  
EXTERNAL ROSSBY RADIUS (KM) = 1426.77  
FIRST INTERNAL ROSSBY RADIUS (KM) = 20.76

STATION: 8 LAT: 36 41.1 LON: 122 3.6  
BOTTOM DEPTH = 891.3  
MEAN BRUNT-VAISALA FREQ (CPS) = 0.4457E-02  
EXTERNAL ROSSBY RADIUS (KM) = 1070.94  
FIRST INTERNAL ROSSBY RADIUS (KM) = 14.49

STATION: 9 LAT: 36 40.3 LON: 122 2.1  
BOTTOM DEPTH = 594.6  
MEAN BRUNT-VAISALA FREQ (CPS) = 0.5098E-02  
EXTERNAL ROSSBY RADIUS (KM) = 874.71  
FIRST INTERNAL ROSSBY RADIUS (KM) = 11.06

STATION: 10 LAT: 36 38.8 LON: 121 59.1  
BOTTOM DEPTH = 83.2  
MEAN BRUNT-VAISALA FREQ (CPS) = 0.1041E-01  
EXTERNAL ROSSBY RADIUS (KM) = 327.13  
FIRST INTERNAL ROSSBY RADIUS (KM) = 3.16

STATION: 11 LAT: 36 41.2 LON: 121 58.2  
BOTTOM DEPTH = 93.1  
MEAN BRUNT-VAISALA FREQ (CPS) = 0.1005E-01  
EXTERNAL ROSSBY RADIUS (KM) = 346.09  
FIRST INTERNAL ROSSBY RADIUS (KM) = 3.41

STATION: 12 LAT: 36 43.6 LON: 121 57.4  
BOTTOM DEPTH = 93.1  
MEAN BRUNT-VAISALA FREQ (CPS) = 0.9903E-02  
EXTERNAL ROSSBY RADIUS (KM) = 346.09  
FIRST INTERNAL ROSSBY RADIUS (KM) = 3.36

STATION: 13 LAT: 36 46.1 LON: 121 57.9  
BOTTOM DEPTH = 648.2  
MEAN BRUNT-VAISALA FREQ (CPS) = 0.4821E-02  
EXTERNAL ROSSBY RADIUS (KM) = 913.24  
FIRST INTERNAL ROSSBY RADIUS (KM) = 11.40



STATION: 14 LAT: 36 47.6 LON: 121 58.6  
BOTTOM DEPTH = 297.5  
MEAN BRUNT-VAISALA FREQ (CPS) = 0.5949E-02  
EXTERNAL ROSSBY RADIUS (KM) = 618.68  
FIRST INTERNAL ROSSBY RADIUS (KM) = 6.46

STATION: 15 LAT: 36 49.3 LON: 121 59.1  
BOTTOM DEPTH = 428.2  
MEAN BRUNT-VAISALA FREQ (CPS) = 0.5447E-02  
EXTERNAL ROSSBY RADIUS (KM) = 742.25  
FIRST INTERNAL ROSSBY RADIUS (KM) = 8.51

STATION: 16 LAT: 36 51.9 LON: 121 59.9  
BOTTOM DEPTH = 59.4  
MEAN BRUNT-VAISALA FREQ (CPS) = 0.1177E-01  
EXTERNAL ROSSBY RADIUS (KM) = 276.58  
FIRST INTERNAL ROSSBY RADIUS (KM) = 2.55

STATION: 17 LAT: 36 54.1 LON: 122 0.7  
BOTTOM DEPTH = 27.8  
MEAN BRUNT-VAISALA FREQ (CPS) = 0.1490E-01  
EXTERNAL ROSSBY RADIUS (KM) = 189.10  
FIRST INTERNAL ROSSBY RADIUS (KM) = 1.51

## REFERENCES

- Bigelow, H.B., and M. Leslie, 1930: Reconnaissance of the waters and plankton of Monterey Bay, July, 1928., *Bulletin of the Museum of Comparative Zoology, Harvard College*, 70, 427-581.
- Bolin, R.L., and others, 1964: *Hydrographic data from the area of the Monterey Submarine Canyon, 1951-1955.*, Final Report, Hopkins Marine Station, Stanford University, Pacific Grove, Calif., 101 pp.
- Breaker, L.C., and W.W. Broenkow, 1989: *The circulation of Monterey Bay and related processes.* Moss Landing Marine Laboratories, Moss Landing, Calif., Technical Publication, 89-1, 99 pp.
- Breaker, L.C., and C.N.K. Mooers, 1986: Oceanic variability off the central California coast., *Prog. in Oceanogr.*, 17, 61-135.
- Broenkow, W.W., and S.J. McKain, 1972: *Tidal oscillations at the head of Monterey Submarine Canyon and their relation to oceanographic sampling and the circulation of water in Monterey Bay.*, Moss Landing Marine Laboratories, Moss Landing, Calif., Technical Publication 73-3, 336 pp.
- Broenkow, W.W., and W.M. Smethie Jr., 1978: Surface circulation and replacement of water in Monterey Bay., *Estuarine and Coastal Marine Science*, 6, 583-603.
- Bruner, B.L., 1988: *A numerical study of baroclinic circulation in Monterey Bay.*, M.S. thesis, Naval Postgraduate Sch., Monterey, Calif., 40 pp.
- Camerlengo, A., and J.J. O'Brien, 1980: Open boundary conditions in rotating fluids., *J. Comput. Phys.*, 35, 12-35.
- Caster, W.A., 1969: *Near-bottom currents in Monterey Submarine Canyon and on the adjacent shelf*, M.S. thesis, Naval Postgraduate Sch., Monterey, Calif., 201 pp.

- Chelton, D.B., 1984: Seasonal variability of alongshore geostrophic velocity off central California, *J. Geophys. Res.*, 89, 3473-3486.
- Dooley, J.J., 1968: *An investigation of near-bottom currents in the Monterey Submarine Canyon*, M.S. thesis, Naval Postgraduate Sch., Monterey, Calif., 46 pp.
- Engineering Science, Inc., 1978: *Facilities plan for north Monterey County. draft oceanographic pre-design report 1*, Engineering Science, Inc., Berkeley, Calif.
- Garcia, R.A., 1971: *Numerical simulation of currents in Monterey Bay*. M.S. thesis, Naval Postgraduate Sch., Monterey, Calif., 154 pp.
- Gatje, P.H., and D.D. Pizinger, 1965: *Bottom current measurements in the head of Monterey Submarine Canyon*. M.S. thesis, Naval Postgraduate Sch., Monterey, Calif., 43 pp.
- Halliwell, G.R., Jr., and J.S. Allen, 1987: The large-scale coastal wind field along the west coast of North America, 1981-1982., *J. Geophys. Res.*, 92, 1861-1884.
- Hickey, B.M., 1979: The California Current System - hypothesis and facts, *Prog. in Oceanogr.*, 8, 191-279.
- Hollister, J.E., 1975: *Currents in Monterey Submarine Canyon*. M.S. thesis, Naval Postgraduate Sch., Monterey, Calif., 86 pp.
- Hurlburt, H.E., 1974: *The influence of coastline geometry and bottom topography on the eastern ocean circulation*. Ph.D. thesis, Florida State University, 103 pp.
- Huyer, A., 1983: Coastal upwelling in the California Current System., *Prog. Oceanog.*, 12, 259-284.
- Klinck, J.M., 1988: The influence of a narrow, transverse canyon on initially geostrophic flow., *J. Geophys. Res.*, 93, 509-515.

Klinck, J.M., 1989: Geostrophic adjustment over submarine canyons., *J. Geophys. Res.*, 94, 6133-6144.

Kosro, P.M., 1985: *Shipboard Acoustic Doppler Current Profiling during the coastal ocean dynamics experiment.*, Ph.D. Dissertation, SIO Ref. 85-8, Scripps Inst. of Oceanogr., La Jolla, Calif.

Lasley, S.R., 1977: *Hydrographic changes in Monterey Bay surface waters in relation to nearshore circulation*, M.A. thesis, San Jose State University, San Jose, Calif., 75 pp.

McCreary, J.P., P.K. Kundu, and S.Y. Chao, 1987: On the dynamics of the California Current System, *J. Mar. Res.*, 45, 1-32.

Martin, B.D., 1964: *Monterey Submarine Canyon, California: Genesis and relationship to continental geology*, Ph.D. Dissertation, University of Southern California, Los Angeles, Calif., 249 pp.

Mooney, D.H., 1973: *Temperature variations throughout Monterey Bay, September 1971 - October 1972.*, M.S. thesis, Naval Postgraduate Sch., Monterey Calif., 166 pp.

Nelson, C.S., 1976: *Wind stress and wind stress curl over the California Current.*, NOAA Technical Report NMFS SSRF-714, U.S. Department of Commerce, 89 pp.

Njus, I.J., 1968: *An investigation of the environmental factors affecting the near-bottom currents in Monterey Submarine Canyon.*, M.S thesis, Naval Postgraduate Sch., Monterey Calif., 68 pp.

Pickard, P.L., and W.J. Emery, 1982: *Descriptive physical oceanography, an introduction.*, Pergamon Press, New York, 249 pp.

Pirie, D.M., and D.D. Steller, 1974: *California coast nearshore processes study Final Report-ERTS-A.*, Goddard Space Flight Center, Greenbelt, Md., 164 pp.

- Reise, J.A., 1973: *A Drift Bottle study of the southern Monterey Bay*, M.S. thesis, Naval Postgraduate Sch., Monterey Calif., 113 pp.
- Schomaker, C.W., 1983: *A model for tidal circulation adapted to Monterey Bay, California.*, M.S. thesis, Naval Postgraduate Sch., Monterey, Calif., 99 pp.
- Shaw, P.T., and G.T. Csanady, 1983: Self-advection of density perturbations on a sloping continental shelf., *J. Phys. Oceanogr.*, 13, 769-782.
- Shea, R.E., and W.W. Broenkow, 1982: The role of internal tides in the nutrient enrichment of Monterey Bay, California., *Estuarine, Coastal and Shelf Science*, 15, 57-66.
- Shepard, F.P., N.F. Marshall, P.A. McLoughlin, and G.G. Sullivan, 1979: *Currents in submarine canyons and other sea valleys.*, AAPG Studies in Geology No.8, American Association of Petroleum Geologists, Tulsa, Oklahoma, 173 pp.
- Shepard, F.P., and R.F. Dill, 1966: *Submarine Canyons and other Sea Floor Valleys.*, Rand McNally & Company, Chicago, 381 pp.
- Skogsberg, T., 1936: Hydrography of Monterey Bay, California. Thermal Conditions, 1929-1933., *Transactions of the American Philosophical Society*, 29, 152 pp.
- Smethie, W.M., 1973: *Some aspects of temperature, oxygen and nutrient distributions in Monterey Bay, California*, M.A. thesis, Moss Landing Marine Laboratories, Moss Landing, Calif., 97 pp.
- Smith, D.C., IV, and J.J. O'Brien, 1983: The interaction of a two layer isolated mesoscale eddy with topography. *J. Phys. Oceanogr.*, 13, 1681-1697.
- Sverdrup, H.U., 1947: Wind-driven currents in a baroclinic ocean with application to the equatorial currents of the eastern Pacific., *Proceedings of the National Academy of Science*, 33(11), 318-326.

Tisch, T.T., 1990: *Seasonal variability of the baroclinic transport and water mass structure off Point Sur, California.*, M.S. thesis, Naval Postgraduate Sch., Monterey, Calif.

Tracy, D.E., 1990: *Surface circulation of Monterey Bay from AVHRR satellite imagery*, M.S. thesis, Naval Postgraduate Sch., Monterey, Calif.

Wickham, J.B., A.A. Bird, and C.N.K. Mooers, 1987: Mean and variable flow over the central California continental margin, 1978-1980., *Continental Shelf Research*, 7, 827-849.

Winant, C.D. and R.C. Beardsley, 1979: A comparison of some shallow wind-driven currents., *J. Phys. Oceanogr.*, 9, 218-220.

## INITIAL DISTRIBUTION LIST

	No. Copies
1. Defense Technical Information Center Cameron Station Alexandria, VA 22304-6145	2
2. Library, Code 0142 Naval Postgraduate School Monterey, CA 93943-5002	2
3. Chairman (Code 68Co) Department of Oceanography Naval Postgraduate School Monterey, CA 93943-5000	1
4. Chairman (Code 63Rd) Department of Oceanography Naval Postgraduate School Monterey, CA 93943-5000	1
5. Professor Steven R. Ramp (Code 68Ra) Department of Oceanography Naval Postgraduate School Monterey, CA 93943-5000	1
6. Professor David C. Smith IV (Code 68Si) Department of Oceanography Naval Postgraduate School Monterey, CA 93943-5000	1
7. LCDR Kim A. Koehler Naval Oceanography Command Facility Mobile Environmental Team Naval Air Station San Diego, CA 92135	2
8. Director Naval Oceanography Division Naval Observatory 34th and Massachusetts Avenue NW Washington, DC 20390	1
9. Commander Naval Oceanography Command Stennis Space Center Bay St. Louis, MS 39529-5000	1

- |     |  |   |
|-----|--|---|
| 10. | Commanding Officer<br>Naval Oceanographic Office<br>Stennis Space Center<br>Bay St. Louis, MS 39522-5001                               | 1 |
| 11. | Commanding Officer<br>Fleet Numerical Oceanography Center<br>Monterey, CA 93943-5005   | 1 |
| 12. | Commanding Officer<br>Naval Ocean Research and Development<br>Activity<br>Stennis Space Center<br>Bay St. Louis, MS 39529-5004         | 1 |
| 13. | Director<br>Naval Oceanographic and Atmospheric<br>Research Laboratory (West)<br>Monterey, CA 93943-5006                               | 1 |
| 14. | Chairman, Oceanography Department<br>U.S. Naval Academy<br>Annapolis, MD 21402   | 1 |
| 15. | Chief of Naval Research<br>800 N. Quincy Street<br>Arlington, VA 22217   | 1 |
| 16. | Office of Naval Research (Code 420)<br>Naval Ocean Research and Development<br>Activity<br>800 N. Quincy Street<br>Arlington, VA 22217 | 1 |
| 17. | Scientific Liaison Office<br>Office of Naval Research<br>Scripps Institution of Oceanography<br>La Jolla, CA 92037                     | 1 |
| 18. | Library<br>Scripps Institution of Oceanography<br>P.O. Box 2367<br>La Jolla, CA 92037  | 1 |
| 19. | Library<br>Department of Oceanography<br>University of Washington<br>Seattle, WA 98105   | 1 |



- |     |  |   |
|-----|--|---|
| 20. | Library<br>CICESE<br>P.O. Box 4803<br>San Ysidro, CA 92073   | 1 |
| 21. | Library<br>School of Oceanography<br>Oregon State University<br>Corvallis, OR 97331  | 1 |
| 22. | Commander<br>Oceanographic Systems Pacific<br>Box 1390<br>Pearl Harbor, HI 96860   | 1 |
| 23. | Director<br>Monterey Bay Aquarium Research Institute<br>P.O. Box 160<br>Central Avenue<br>Pacific Grove, CA 93950-0020             | 1 |
| 24. | Dr. Leslie Rosenfeld<br>Monterey Bay Aquarium Research Institute<br>P.O. Box 160<br>Central Avenue<br>Pacific Grove, CA 93950-0020 | 1 |
| 25. | Dr. Lex Broenkow<br>Moss Landing Marine Laboratory<br>P.O. Box 223<br>Moss Landing, CA 95039                                       | 1 |
| 26. | Dr. John Martin<br>Moss Landing Marine Laboratory<br>P.O. Box 223<br>Moss Landing, CA 95039  | 1 |
| 27. | Dr. Jon Roughgarden<br>Department of Biological Sciences<br>Herrin Laboratory<br>Stanford University<br>Stanford, CA 94305         | 1 |